



Algorithm Theoretical Basis Document (ATBD)
for the
Conical-Scanning Microwave Imager/Sounder (CMIS)
Environmental Data Records (EDRs)

Volume 17: Temperature Data Record and Sensor Data
Record Algorithms

Version 2.0 – 15 March 2001

Solicitation No. F04701-01-R-0500

Submitted by:
Atmospheric and Environmental Research, Inc.
131 Hartwell Avenue
Lexington, MA 02421-3126

With contributions by:
Michael Plonski, AER, Inc.
Craig Smith, Remote Sensing Systems, Inc.

Prepared for:
Boeing Satellite Systems
919 Imperial Avenue
El Segundo, CA 90245

AER Document P757-TR-I-ATBD-TDR-SDR-20010315

This page intentionally left blank.

REVISION HISTORY

Version	Release Date	POC	Comments
1.0	15 Jan., 2001	Plonski	Initial partial draft release.
1.1	14 Feb., 2001	Plonski	PDR Draft release
2.0	15 March 2001	AER	Multiple revisions; reformatting and cleanup

RELATED CMIS DOCUMENTATION

Government Documents

Title	Version	Authorship	Date
CMIS SRD for NPOESS Spacecraft and Sensors	3.0	Associate Directorate for Acquisition NPOESS IPO	2 March 2001

Boeing Satellite Systems Documents

Title		Covering
ATBD for the CMIS EDRs	Volume 1: Overview	Part 1: Integration Part 2: Spatial Data Processing <ul style="list-style-type: none"> • Footprint Matching and Interpolation • Gridding • Imagery EDR
	Volume 2: Core Physical Inversion Module	
	Volume 3: Water Vapor EDRs	Atmospheric Vertical Moisture Profile EDR Precipitable Water EDR
	Volume 4: Atmospheric Vertical Temperature Profile EDR	
	Volume 5: Precipitation Type and Rate EDR	
	Volume 6: Pressure Profile EDR	
	Volume 7: Cloud EDRs	Part 1: Cloud Ice Water Path EDR
		Part 2: Cloud Liquid Water EDR
		Part 3: Cloud Base Height EDR
	Volume 8: Total Water Content EDR	
	Volume 9: Soil Moisture EDR	
	Volume 10: Snow Cover/Depth EDR	
	Volume 11: Vegetation/Surface Type EDR	
	Volume 12: Ice EDRs	Sea Ice Age and Sea Ice Edge Motion EDR Fresh Water Ice EDR
	Volume 13: Surface Temperature EDRs	Land Surface Temperature EDR Ice Surface Temperature EDR
	Volume 14: Ocean EDR Algorithm Suite	Sea Surface Temperature EDR Sea Surface Wind Speed/Direction EDR Surface Wind Stress EDR
	Volume 15: Test and Validation	All EDRs
	Volume 16: Code Documentation	Part 1: Purpose, Implementation, and Tutorial
		Part 2: Description of Modules
	Volume 17: TDR/SDR Algorithms	

Bold= this document

TABLE OF CONTENTS

REVISION HISTORY	3
TABLE OF CONTENTS	5
LIST OF TABLES	8
LIST OF FIGURES	9
1 Abstract	11
2 Introduction.....	12
2.1 Purpose.....	12
2.2 Document Scope	13
3 Overview and Background Information	14
3.1 Overview of the SDR Processing	14
3.2 Summary of TDR / SDR requirements	14
3.2.1 SSS Requirements.....	14
3.2.2 Requirements interpretations	14
3.2.3 Derived requirements on TDR / SDR Processing.....	15
3.2.4 Range Checking	16
3.3 Historical and background perspective of proposed algorithm	16
3.4 Instrument characteristics and derived sensor requirements.....	17
3.5 Requirements for External Data.....	17
4 Antenna Temperature and Spillover Module	18
4.1 Overview	18
4.2 Physical / Theoretical Basis of Algorithm	18
4.2.1 Two-Point Calibration.....	18
4.2.2 FFT Passband Correction.....	18
4.2.3 Antenna feed corrections for extraneous energy	19
4.3 Antenna Temperature Processing Flow	21
4.4 Mathematical Description of Algorithm	22
4.4.1 Range Checking	22
4.4.2 Cold Load	23
4.4.3 Warm Load.....	23
4.4.4 FFT Corrections to Calibration Counts	24
4.4.5 Antenna Temperature	27
4.4.6 Earth Scene Component of Antenna Temperature	27
4.5 Algorithm inputs	27
4.6 Algorithm Performance against Requirement	27

5	Geolocation.....	28
5.1	Overview of Geolocation.....	28
5.2	Theoretical Basis of Geolocation.....	29
5.3	Algorithm Processing Flow	32
5.4	Mathematical Description of Geolocation.....	33
5.4.1	Coordinate Transformations	33
5.4.2	Scan Timing	34
5.4.3	Earth location of a specific scene station.....	36
5.5	Data Needed for Geolocation.....	36
5.6	Algorithm Performance against Requirements	37
6	The SDR Cross Polarization Correction	38
6.1	Overview	38
6.2	Physical Basis of the SDR Cross Polarization Correction Algorithm	39
6.3	Mathematical Description of the SDR Cross Polarization Correction	42
6.3.1	Symbolic Description of the Algorithm	42
6.3.2	Considerations for the Antenna Cross-Polarization Correction.....	42
6.3.3	Considerations for the Rotation Corrections	47
6.3.4	Final Form of the Cross Polarization Algorithm.....	49
6.3.5	Faraday Rotation.....	49
6.4	Data Needed by the Cross Polarization Correction	50
6.4.1	CMIS Data.....	50
6.4.2	External Data Sources	51
6.5	Requirements Levied on the Cross Polarization Correction.....	51
6.5.1	Introduction.....	51
6.5.2	Faraday Rotation.....	52
6.5.3	Magnitude Requirement on Cross Polarization Matrix.....	52
6.5.4	Cross Polarization Knowledge Requirement	56
6.5.5	CMIS Polarization Rotation Control Error Requirement	66
6.5.6	CMIS Polarization Rotation Knowledge Error Requirement	67
7	Pre-Launch Algorithm Calibration and Validation Requirements	70
7.1	Antenna Range Testing.....	70
7.2	Thermal Vacuum Testing.....	70
8	Post-launch Calibration and Validation.....	71
8.1	Calibration to RTM for bias removal.....	71
8.2	Validation of Geolocation Accuracy.....	78

9	Practical Considerations	79
9.1	Numerical Computation Considerations	79
9.1.1	Calibration.....	79
9.1.2	Geolocation	79
9.2	Programming/Procedure Considerations	79
9.2.1	Calibration.....	79
9.2.2	Geolocation	80
9.3	Computer hardware or software requirements.....	80
9.4	Quality Control and Diagnostics.....	80
9.5	Exception and Error Handling	80
9.6	Special database considerations	80
9.7	Special operator training requirements	80
9.8	Archival requirements.....	80
10	Glossary of Acronyms	81
11	References.....	84
11.1	Government Documents and Communications	84
11.2	BSS Documents	84
11.3	Technical Literature	84
Appendix A: Derivation of the Antenna Temperature Equations for Antenna Cross Polarization.....		85
Appendix B: Representations of the Cross-Polarization Matrix.....		104
Appendix C: Linearity: Planck versus Brightness Temperature		114
Appendix D: Derivation of TDR / SDR equations from calibration budget analysis.....		116
Appendix E: Sensor Constants File		131
Appendix F: Sample Results from Antenna / Timing Analysis.....		132

LIST OF TABLES

Table 3-1 EDR derived accuracies on T_{Bec}	15
Table 3-2 EDR derived Inter-Channel accuracies on T_{Bec}	16
Table 3-3: Temperature Sensors used to support SDR processing.....	16
Table 4-1: Active Scan Antenna Feed Sources List	21
Table 4-2: Components of Cold Temperature (T_{cold}) calculation.....	23
Table 4-3: Nominal energy coupling coefficients for cold reference	23
Table 4-4: Components of Warm Temperature (T_{warm}) calculation	24
Table 4-5: Nominal energy coupling coefficients for warm reference	24
Table 4-6: Components of Spillover during the active scan.	27
Table 4-7: Nominal energy coupling coefficients for spillover terms	27
Table 5-1: Sensor Channel Specification.....	29
Table 5-2: Antenna and Beam position Alignments from PDSR baseline used in geolocation to be stored in sensor constants file	37
Table 5-3: Additional geolocation supporting data in sensor constants file	37
Table 5-4: Geolocation supporting data in RDR packet.....	37
Table 6-1 Expected values of polarization differences over Ocean.....	62
Table 6-2 M-Matrix uncertainty contributing to TB bias is driven by 1 st two columns	62

LIST OF FIGURES

Figure 3-1: Calibration Data Flow.....	14
Figure 4-1: Two-Point Calibration.....	18
Figure 4-2: Energy sources entering feed for a reflector configuration.....	20
Figure 4-3: Energy sources entering feed for a warm load configuration.....	21
Figure 4-4: Antenna Temperature Processing Flow	22
Figure 4-5: FFT Calibration Results using Risk Reduction Hardware	26
Figure 5-1: CMIS Scan Geometry	28
Figure 5-2 Look Down Angle for Low Frequency Channels	30
Figure 5-3: Ground Projections of the individual channel IFOVs.....	31
Figure 5-4 CMIS Scan timing	35
Figure 6-1: Perturbations to the earth scene brightness temperatures from the top of the atmosphere through reception of the radiation by the radiometer. The SDR algorithm undoes each of these perturbations in the reverse order, so the the earth scene brightness temperatures can be found and used in the EDR algorithms. The cross polarization correction of the SDR algorithm undoes the perturbations corresponding to the blue (darkened) arrows.	41
Figure 6-2: Zero error M-matrices computed from antenna design. The assemblage of blue columns for each frequency defines the M-matrices used by the cross polarization correction. The white columns correspond to cross polarization from the polarizations not measured at each frequency; they represent cross polarization from the 3 rd and/or 4 th Stokes parameters that cannot be corrected. The residual cross polarization from these Stokes parameters is approximately that shown in the white columns, as per equation 6-18.....	53
Figure 6-3: Sensitivity Analysis for the Magnitude of the Columns of the M-matrix Eliminated in the Cross Polarization Correction. SST Uncertainty drives the requirement to be set at 0.02, on average, over the all the eliminated columns, 6-36 GHz.	55
Figure 6-4: Bias mode sensitivity analysis for cross polarization knowledge error. The knowledge error realization is “co-pol down, cross-pol up.”	59
Figure 6-5: EDR Sensitivity analysis to cross polarization noise, using the Monte Carlo Mode simulation. Sensitivity of EDR precision is greatly amplified compared to the bias mode simulation. We use this simulation to set the cross polarization knowledge noise requirement (at 0.00025 = -36dB), and leave the cross polarization knowledge bias requirement at that value found in the bias mode simulation (0.001).	60
Figure 6-6: Basic process to calibrate the CMIS sensor to the RTM	64
Figure 6-7: Reduction in EDR sensitivity to cross polarization knowledge bias, after calibration of CMIS measurements to the RTM. Calibration to RTM simulated by removing mean TQ bias, using mean TQ over test data sets.	65
Figure 6-8: EDR sensitivity to CMIS polarization rotation control error. This is a Monte Carlo mode simulation where the rotation angle is different fro each observation in the test data sets.....	67

Figure 6-9: Ocean EDR sensitivity to CMIS polarization rotation knowledge error. Knowledge error Monte Carlo for each observation of each run using a zero mean Gaussian distribution with known sigma (x-axis) for each run.69

1 Abstract

The Conical Microwave Imager Sounder (CMIS) Temperature Data Record/Sensor Data Record (TDR/SDR) Algorithm translates the counts from the sensor Raw Data Records (RDRs) into earth located, calibrated earth scene brightness temperatures. The TDR/SDR algorithm consist of 3 main parts; Antenna Temperature computation, Geo-location and Cross-Polarization Corrections. The Antenna Temperature computation first calculates the total temperature at the antenna feed (T_A), and then the earth scene component of the antenna temperature (T_A'). T_A is output as the Temperature Data Record (TDR) value along with the results of any checks for bad or out of range data. T_A' , is computed from T_A by correcting for antenna spillover and any stray energy that may be incident on the antenna aperture and feed. The earth location portion of the SDR algorithm provides a latitude and longitude for each scene station as well as the radiometer look angles relative to the earth. The cross-polarization algorithm computes the earth scene brightness temperature (T_B), by using the look angles to correct T_A' for polarization rotations in the sensor and atmosphere. The calibration equations used in the TDR/SDR processing are derived from the sensor calibration analysis. Post-Launch analysis is used to determine static bias corrections for calibration and polarization errors. These corrections are applied as part of the SDR process and in the EDR pre-processing.

2 Introduction

2.1 Purpose

The CMIS sensor will fly on the National Polar Orbiting Environmental Satellite System (NPOESS) and provides raw sensor data that can be used to generate a variety of Environmental Data Records (EDRs). The first step in generating the EDRs is to convert the sensor RDRs that are received on the ground into SDRs that can be processed into EDRs using specialized algorithms that are described in the additional CMIS Algorithm Theoretical Basis Documents (ATBDs). This SDR ATBD describes the processing algorithms used to generate the SDRs from the RDRs, as well as the TDRs, which are output as an intermediate product. The TDR file replicates any necessary information from the RDR file so that the SDRs can be computed solely from the TDR file. The SDR processing is broken down into 3 main sections: Antenna Temperature Computation, Geolocation, and Cross-Polarization.

Section 3 summarizes the TDR / SDR requirements specified in the CMIS System/Subsystem Specification (SSS). This section presents the historical background and physical basis for the proposed algorithm, and it describes the instrument characteristics and data from all sources necessary to meet NPOESS requirements. Derived requirements from the SSS are also presented here.

Section 4 describes the Antenna Temperature portion of the SDR processing. This portion of the algorithm starts with the raw counts and converts them into the antenna temperature at the feed (T_A), which is output as the TDR. The earth scene component of the antenna temperature (T_A') is then computed by correcting for stray energy that enters the feed. Checks for bad data ranges are also performed in this step.

Section 4.6 describes the Geolocation portion of the algorithm. Each scene station is mapped to a latitude / longitude (lat/lon) on the earth. The Earth Incidence Angle (EIA) and other sensor looks angles are also generated.

Section 6 describes the Cross Polarization correction portion of the SDR algorithm. The earth scene brightness temperature (T_B) is computed from T_A' by correcting the antenna temperature for cross-polarization effects and polarization rotations that occur in the atmosphere and sensor.

Section 7 describes the Pre and Post Launch Calibration and Validation activities. The Pre-launch activities include antenna range testing to compute parameters used in the sensor calibration and thermal vacuum activities (TV) used to validate the calibration performance. Post-Launch activities consist of calibration bias removal and validation of the earth location accuracy.

Section 9 describes practical considerations for the SDR implementation including numerical computation considerations, algorithm quality control and diagnostics, exception and error handling, and archival requirements.

Sections 10 and 11 provide a glossary and reference list, respectively.

Appendices are provided for detailed supporting information. Appendix A show the derivation of the equations used in the Cross polarization correction. Appendix B shows the representations of the cross polarization matrix. Appendix C shows the calibration accuracy budget. Appendix D shows the earth location budget. Appendix E describes the sensor constants file (SCF).

2.2 Document Scope

The *ATBD for the CMIS TDR / SDR* covers algorithm operations beginning with the ingestion of the sensor RDR file and ends with the creation of the SDR file. The TDR file is produced as an intermediate output. The Sensor Constants File (SCF) which is used to support the TDR / SDR processing is also described in this ATBD. The calibration equations used in the TDR / SDR processing are derived from the included calibration analysis which flows directly into the sensor calibration budget. This ATBD discusses the pre-launch validation efforts for calibration in thermal-vacuum (TV) testing and the post-launch calibration / validation efforts to remove static sensors biases in the calibration and cross-polarization. The data quality checks in the TDR algorithm and the earth location algorithm in the SDR processing are also included.

3 Overview and Background Information

3.1 Overview of the SDR Processing

The SDR processing flow is shown in Figure 3-1. The IDPS system provides the Raw Data Record (RDR) data file to the CMIS ground processing software. The radiometer counts are calibrated to the antenna temperature (T_A) at the feed using the warm and cold load references. T_A is output to the Temperature Data Record (TDR) file. The earth scene component of the antenna temperature (T_A') is then computed by removing the stray energy entering the feed and correcting for antenna spillover. The Geolocation module computes the sensor look angles to support the cross polarization correction (X-pol) module and the latitude / longitude (lat/lon) of each pixel. The X-pol module corrects for cross polarization effects and polarization rotations that occur in the atmosphere and sensor. Supporting climatological databases are used to determine the polarization rotation corrections. Data quality checks are performed both at the front end of the antenna temperature and geolocation processing to make sure that all RDR data is within expected ranges. Appropriate data quality flags are included in the TDR and SDR data files. A Sensor Constants File (SCF) is used to provide sensor specific information to all of the processing modules.

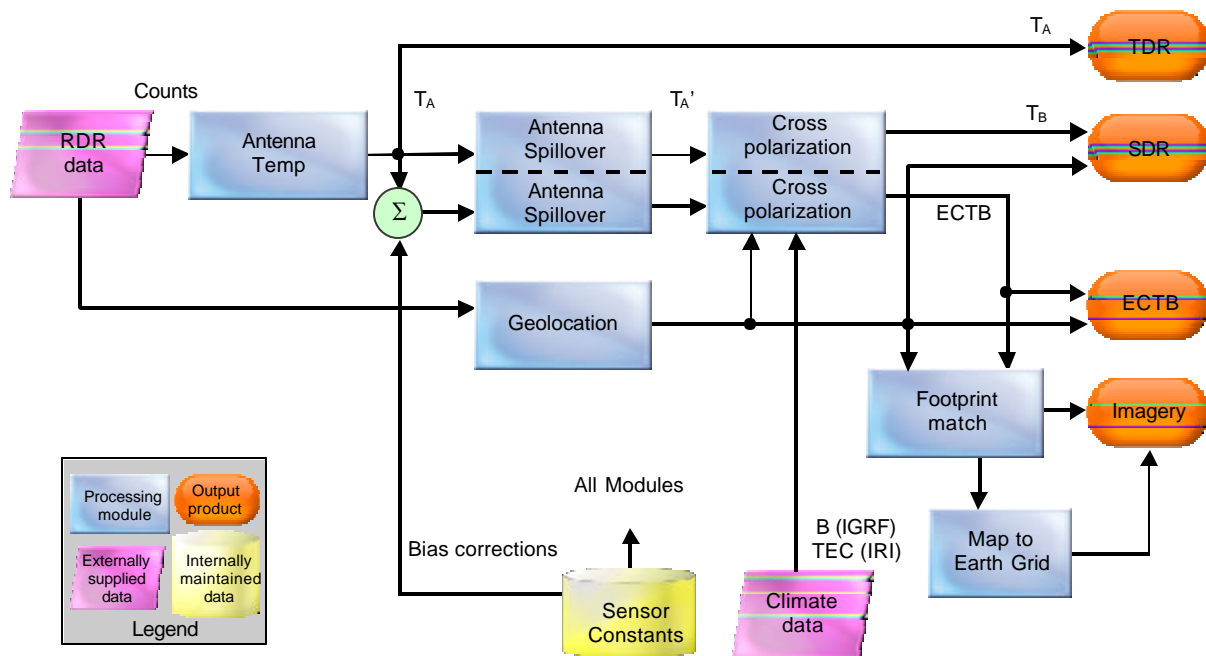


Figure 3-1: Calibration Data Flow

3.2 Summary of TDR / SDR requirements

3.2.1 SSS Requirements

Provided in various sections of the system specification.

3.2.2 Requirements interpretations

To be added later

3.2.3 Derived requirements on TDR / SDR Processing

3.2.3.1 T_{Bec} accuracy derived from EDR Analysis

A portion of the EDR error budget was assigned to absolute accuracy errors on T_{Bec} relative to the RTM and inter-channel accuracy errors as discussed in Volume 1 Overview ATBD Appendix C. A sensitivity analysis was performed to translate the budgeted EDR error to an equivalent accuracy relative to the RTM and the inter-channel accuracy as shown in Table 3-1 and Table 3-2. The inter-channel accuracy is only shown in cases where the sensitivity analysis indicates that the necessary inter-channel accuracy is less than the sum of the absolute accuracy of the two channels. The sum of the absolute accuracy of the two channels being compared provides an upper limit on the absolute accuracy, so it is only necessary to specific values that the sensitivity analysis indicates are below the upper limit. To meet these levels of accuracy, a post-launch calibration activity is required to remove the bias in each of the channels, since the absolute accuracy pre-launch is only specified to be 1.0 K. Section 8.1 describes the post-launch bias correction used to get the required level of accuracy.

Chan.	T_{Bec} Acc. (K)	EDR Driver
6	0.1	Ocean EDRs
10	0.1	Ocean EDRs
18	0.1	AVMP(ice), Ocean EDRs
23	0.1	AVMP(ice), PW(ice), Ocean EDRs
36	0.1	Ocean EDRs
50	0.1	AVTP, IST
89	0.1	AVMP (ocean)
166	0.3	PW (ice)
183	0.3	AVMP

Note: Ocean EDRs assume a constant bias error across all channels

Table 3-1 EDR derived accuracies on T_{Bec}

Chan 1	Chan 2	Inter. Chan (K)	EDR Driver
18V	18H	0.14	SST
23V	23H	0.2	PW (land), PW (ice)
36V	36H	0.4	AVMP (land), PW (ice)
89V	89H	0.2	PW (ice)
50.3	52	0.18	LST
183+-7	183+-3	0.24	AVMP (land)
183+-7	183+-1	0.22	AVMP (land)
10	18	0.1	SST
18	23	0.12	AVMP (ice)
18	36	0.14	AVMP (ice)
23	36	0.12	PW (ice)
23	183	0.1	PW (ice)
36	50	0.12	PW (ice)
50	89	0.18	AVTP (ocean)
89	166	0.2	PW (ice)

166	183	0.2	AVMP (land)
Any 6-36	Any 6-36	0.04	Overly tight for Ocean EDRs – Relax in EMD

Table 3-2 EDR derived Inter-Channel accuracies on T_{Bec}

3.2.3.2 Sun / Satellite angles needed for cross-polarization processing

The cross-polarization correction needs a number of sun-satellite angles from the TDR/SDR algorithms. These angles are computed as part of the geolocation process included in the SDR processing as shown in Section 5.

3.2.3.3 Temperature sensors to support SDR processing

The SDR processing as discussed in Section 4 utilizes a number of temperature sensors to make various corrections to the measured temperatures. In addition to these sensors an assumption is made as to the value of the cosmic temperature (T_{cos}). Note that we currently show the use of a spacecraft temperature sensor. If one is not available then the spacecraft temperature is assumed to be the same as the Sensor temperature. This assumption only adds a negligible effect to the calibration process, since the correction terms are not very dependant on the spacecraft temperature.

Usage	Temperature	Description
Cold	T_{cr}	Cold Reflector Temperature
Cold, Spillover	T_s	Sensor Temperature
Cold, Spillover	T_{sc}	Spacecraft Temperature (use T_s if not available)
Warm	T_{ws}	Sensor Temperature (including internal) seen by warm load
Warm	T_{prt}	Warm Load PRTs
Spillover	T_r	Reflector Temperature (one each for Primary and Auxiliary)

Table 3-3: Temperature Sensors used to support SDR processing

3.2.4 Range Checking

Range checking is used at the front end of the TDR data processing to identify any anomalous readings. These are only meant to be gross checks for software or data transmission errors and should be set in general to 10x the normal variation expected so that noise does not trigger a range check error.

The geolocation output can also be used to perform range checking. The easiest way to identify errors is to check that the satellite sub-point moves in a monotonic fashion (special care must be taken around the poles) and that it does not take any discontinuous jumps. The specifics of these checks will be provided in the next phase and may depend if a NPOESS wide approach to geolocation is taken, rather than a sensor specific geolocation approach.

3.3 Historical and background perspective of proposed algorithm

The two-point calibration method for radiometric calibration is widely used for all virtually all current and proposed space-based microwave radiometers. It has proved to be extremely reliable and can easily provide the 1.0 K absolute accuracy that is required at the sensor level as shown in

the CMIS calibration plan. The 2 point calibration approach with the external cold / warm loads is also extremely stable since any drifts in system gain are seen by both calibration targets and are effectively removed. An analysis of SSM/I data over the 10-year period from 1987 – 1997 has indicated an inter-sensor SSM/I consistency in the order of 0.3 K (Colton 98).

The geo-location algorithm borrows from the MODIS geo-location (SDST-092), which is based on the Patt and Greg algorithm (Patt 94). The Patt & Gregg algorithm is used as the basis for many other geolocation implementations, such as the AFWA Cloud Depiction and Forecast System II and AFWA Combat Mission Needs System, since it provides an efficient closed form solution to the generic earth location problem.

3.4 Instrument characteristics and derived sensor requirements

An absolute sensor calibration of 1.0 K is required as a starting point for the post-launch calibration to the RTM to meet the necessary accuracy levels. This is based on RSS experience with post launch corrections of TMI and SSM/I data.

3.5 Requirements for External Data

The Antenna Temperature and geo-location algorithms only require the RDR data packet and the sensor constant file (SCF). The Cross-Polarization Algorithm requires several supporting databases that are listed in Section 6.4.

4 Antenna Temperature and Spillover Module

4.1 Overview

The antenna temperature and spillover module takes the RDR counts as an input and produces both the total antenna temperature at the feed (T_A) and the earth scene component of the antenna temperature (T_A'). The first step is to check that all values are within expected ranges. This includes checks for both the absolute value of the counts and the maximum change in calibration values from one scan line to the next. The calibration of the counts into antenna temperatures can be broken into three components; a two-point calibration based on a warm/cold calibration target, a correction for a non-uniform FFT passband, and a correction for the antenna spillover.

4.2 Physical / Theoretical Basis of Algorithm

4.2.1 Two-Point Calibration

The two-point calibration method uses a warm and cold calibration reference to interpolate the radiance values over the measurement range as shown in Figure 4-1. The warm reference temperature is computed from a series of PRTs mounted in the calibration target. The cold load temperature is computed from the cosmic sky background temperature. Corrections for stray energy entering the feed are applied to both the PRT temperatures and the cosmic background temperature to compute the reference T_{Warm} and T_{Cold} , respectively. The temperatures are converted to radiance space prior to the two-point calibration via the Planck function. Appendix C discusses the errors that would be introduced if the two-point calibration were done strictly in temperature, without transforming to radiance first. The counts are measured when the radiometer feed passes under the warm load (C_{Warm}) or the cold sky reflector (C_{Cold}). The active scene radiance (R_A) is computed from the counts measured at the active scene station (C_A) using a linear transformation based on the warm and cold references. The active scene radiance is converted to the active scene temperature (T_A) via the inverse plank function. Any non-linearities in the receiver are accounted for in the calibration budget.

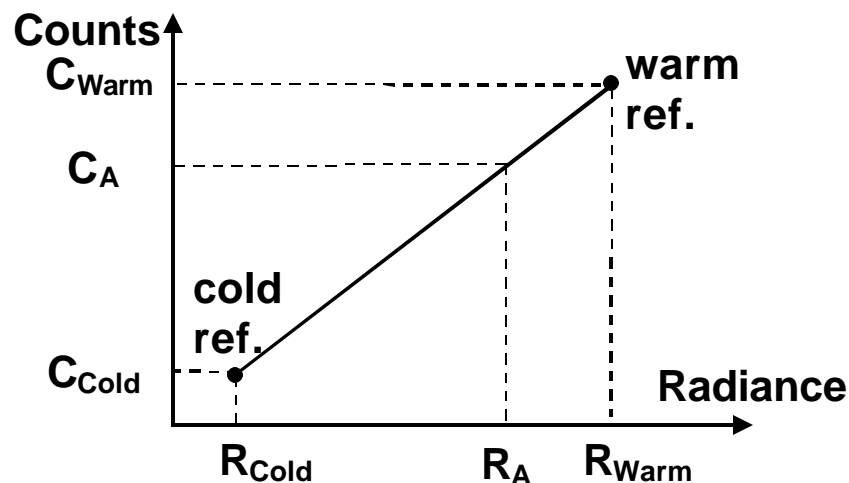


Figure 4-1: Two-Point Calibration

4.2.2 FFT Passband Correction

In the case of the FFT channels, the Noise Equivalent Delta Temperature (NEDT) for each individual bin can be quite large due to the narrow bandwidth. This can introduce a potentially large error for the hot and cold calibration count at each bin. In order to reduce the effective

noise, the calibration target counts from all bins are used to compute the calibration count for each bin. The different calibration for each bin is due to the filtering applied prior to the FFT. If the filter passband characteristics can be precisely measured, then the effects of the filtering can be compensated for. The filter passband characteristics are measured by collecting a large number of samples of the calibration target measurements. The filter characteristic only needs to be determined once and the use of a large number of samples reduces the effective NEDT in each bin by a factor of square root of the number of samples, if one assumes the samples are independent. The use of 10000 samples would reduce the NEDT by a factor of 100 and would require several orbits of data. The computation of the filter passband can be computed both prior to launch and after the sensor is on orbit, to check for any drifts in the filter function.

4.2.3 Antenna feed corrections for extraneous energy

The antenna reflector does not fully subtend the view of the antenna feed, introducing a reduction to the earth scene brightness temperature that enters the feed. In addition, stray energy that does not come from the earth scene also enters the feed, and introduces errors into the antenna feed temperature. Figure 4-2 shows a drawing of all the energy sources that enter the feed when a reflector is used. This figure applies to both the primary / secondary reflector, as well as the cold sky reflector. Only source 1 represents the desired reflected energy along the boresight of the reflector, which corresponds to the earth scene during the primary/secondary reflector active scan and cold sky during the cold calibration measurement interval. In the case of the active scan, the extraneous energy must be subtracted from the antenna temperature (T_A) to get the earth scene component of the antenna temperature (T_A'). In the case of the cold calibration load, the extraneous energy must be added to the estimate of cosmic temperature (T_{cos}) to produce the estimate of T_{cold} used in the two point calibration.

Table 4-1 identifies all of the energy sources by number that are shown in Figure 4-2. The calibration budget in Appendix D shows the derivation and identification of all terms in Table 4-1.

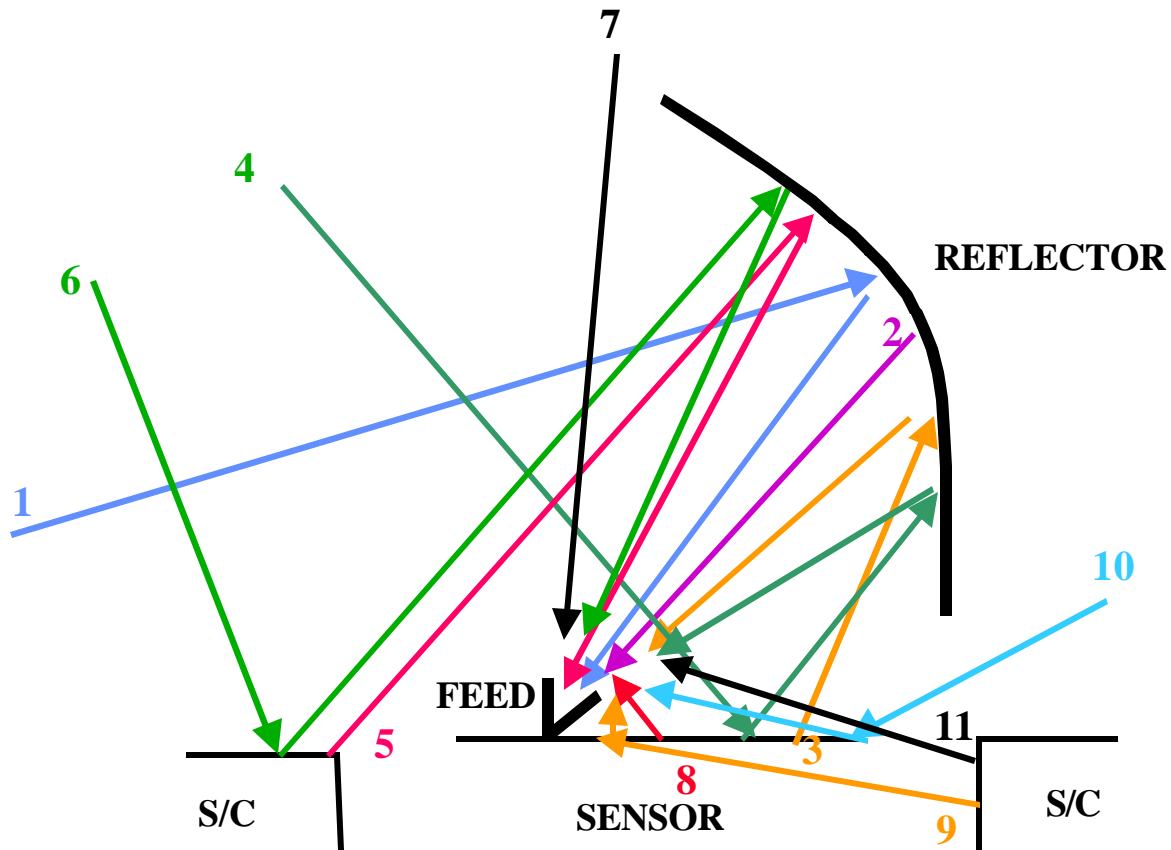


Figure 4-2: Energy sources entering feed for a reflector configuration

If one only considers the active scan scenario presented in Table 4-1, with nominal values for all terms and an earth scene temperature of 300 K, the temperature of the antenna feed would 290.71 K, computed as follows:

$$T_A = A_1 T_1 + A_2 T_2 + A_3 T_3 + A_4 T_4 + A_5 T_5 + A_6 T_5 + A_7 T_7 + A_8 T_8 + A_9 T_9 + A_{10} T_{10} + A_{11} T_{11} = 290.71 \text{ O K}$$

The A coefficients, listed in Table 4-1, represent the percent of the energy source that is coupled into the feed. The purpose of the spillover correction is to correctly compute the earth scene component of 300 K from the measured value of 290.71 K by correcting for all of the terms in Table 4-1. The process to perform these corrections is shown in section 4.4.

i	A_i (sum to 1)	T_i	$A_i T_i$ ($^{\circ}\text{K}$)	Subscene description
1	$Fr*(1-Er)*(1-Vs-Vsc)$	Te	290.185	Earth scene Component
2	$Fr*Er$	Tr	0.09157	Reflector emission
3	$Fr*(1-Er)*Vs*Evs$	Tvs	0.02906	Sensor emission viewed through reflector
4	$Fr*(1-Er)*Vs(1-Evs)$	$Tcos$	0.00235	Sensor reflection viewed through reflector
5	$Fr*(1-Er)*Vsc*Evsc$	$Tvsc$	0.07265	Spacecraft emission viewed through reflector
6	$Fr*(1-Er)*Vsc*(1-Evsc)$	$Tcos$	0.00065	Spacecraft reflection viewed through reflector
7	$(1-Fr)*(1-Ss-Ssc)$	$Tcos$	0.06654	Spillover directly from space
8	$(1-Fr)*Ss*Ess$	Tss	0.186	Spillover emission from sensor
9	$(1-Fr)*Ss*(1-Ess)*Qsc$	$Tqsc$	0.01674	Spillover reflected off sensor from spacecraft
10	$(1-Fr)*Ss*(1-Ess)*(1-Qsc)$	$Tcos$	0.01491	Spillover reflected off sensor from space
11	$(1-Fr)*Ssc$	$Tssc$	0.0465	Spillover emission from spacecraft

Table 4-1: Active Scan Antenna Feed Sources List

There is a similar set of erroneous error sources that enter the feed when the warm load is viewed as shown in Figure 4-3. Appendix D shows the identification and analysis of all energy sources that are present in this figure. Section 4.4.3 shows how the TDR algorithm corrects for all of these extraneous sources in the warm load.

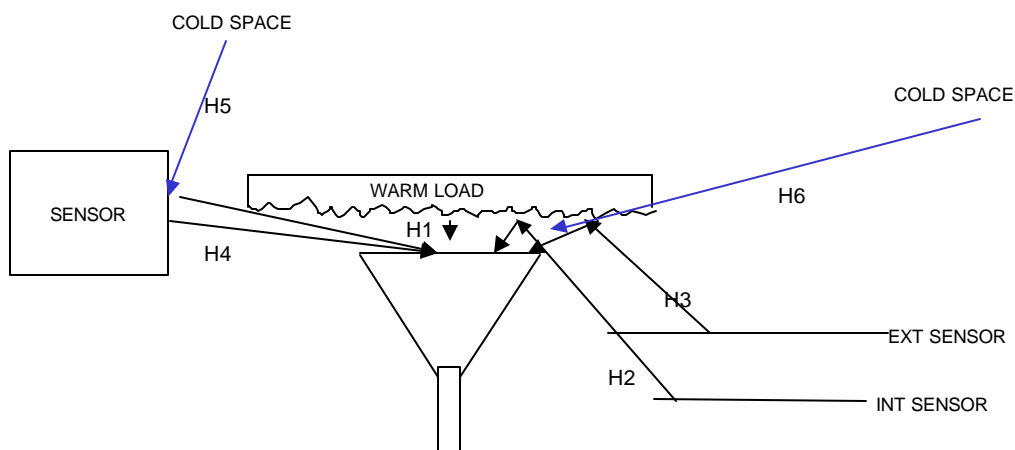


Figure 4-3: Energy sources entering feed for a warm load configuration

4.3 Antenna Temperature Processing Flow

The processing flow for the antenna temperature is shown in Figure 4-4. The inputs are shown on the left side of the figure and the outputs are shown on the right side of the figure. The

system requires the raw counts for each of the scene stations in the calibration warm load, cold load and active scan. The cosmic temperature and warm load PRT temperatures are corrected based on parameters stored in the sensor constants file (SCF) and other Thermocouples (TC) placed on the satellite, sensor and reflectors. During the calibration scan, there are 4 to 16 views of the warm / cold loads, depending on the channel, that can be averaged to reduce noise within a scan. The warm load target also has several PRTs that can be averaged within a scan. In addition, 8 scan lines are averaged to further reduce the noise in the warm / cold calibration counts.

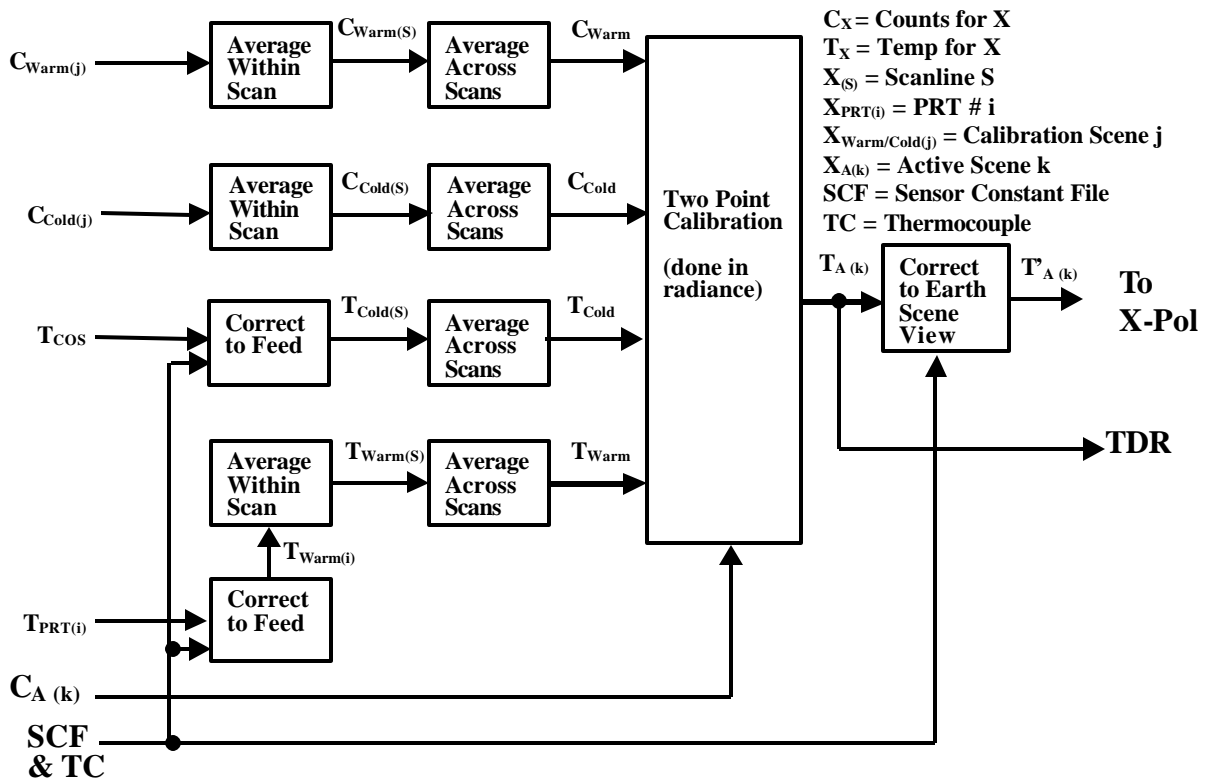


Figure 4-4: Antenna Temperature Processing Flow

4.4 Mathematical Description of Algorithm

4.4.1 Range Checking

The first step in the processing is the identification of potentially bad data by range checking.

Absolute range checks are performed on warm, cold and active scan counts to make sure they are within a physical range. The absolute range checks should be set to the maximum expected range (to be determined from thermal analysis in the next phase) plus 10 x the NEDT for the channel. In addition the warm target should utilize dynamic range checks, since it should only have a very small variation on a scan line by scan line basis. In general the thermal variation on a scan line is less than the NEDT, so the scan line to scan line dynamic range check should be set to 10x the NEDT. The warm load PRTs can be inter-compared and any PRT that is inconsistent with the others can be removed from the PRT averaging process. The specific settings and algorithm for the range checking algorithms will be provided in the next phase, based on measurements and analysis of the flight hardware

4.4.2 Cold Load

The cold target temperature is computed by applying corrections to the cosmic temperatures for extraneous energy that enters the feed. The basic equation for the correction is shown below and Table 4-2 shows the descriptions of all of the terms. Appendix D has a complete derivation of the terms and was used to compute Table 4-3 which shows the nominal values of the energy coupling coefficients. As is expected the vast majority of the energy coupled in comes from the cosmic background, which is assumed to be 2.7 K. The magnitude of the correction varies from 0.25 K for the 6 GHz channel to almost 0.8 K for the 183 GHz channel, with the largest contribution coming from emissions from the cold reflector. Note that the sensor temperature can be used as an estimate of the spacecraft temperature if a separate spacecraft temperature is not available.

$$T_{\text{cold}} = C_{\text{cos}} T_{\text{cos}} + C_{\text{cr}} T_{\text{cr}} + C_{\text{s}} T_{\text{s}} + C_{\text{sc}} T_{\text{sc}}$$

Coupling Coefficient	Description		Energy Source	Description
Ccr	Cold reflector coefficient		Tcr	Cold Reflector Temperature
Cs	Sensor coefficient		Ts	Average Sensor Temperature
Csc	Spacecraft coefficient		Tsc	Average Spacecraft temperature
Ccos	Cosmic background coefficient		Tcos	Cosmic Temperature

Table 4-2: Components of Cold Temperature (Tcold) calculation

	6 GHz	10	18	23	36	50-60	89	166	183
Ccr	0.000268	0.00036	0.00046671	0.0005289	0.000659	0.0008492	0.001	0.0013986	0.00149
Cs	0.000259	0.00013	0.000219403	8.987E-05	0.00018	0.0001697	9.99E-06	4.993E-05	4.99E-05
Csc	0.000259	0.00006	0.000409613	0.000253	0.000702	0.0007504	4.995E-05	0.0001514	0.00015
Ccos	0.999213	0.99891	0.998904274	0.9991282	0.99846	0.9982307	0.9989401	0.9984	0.998

Table 4-3: Nominal energy coupling coefficients for cold reference

The cold reference counts are also averaged both within a scan and across 8 scans, 4 preceding and 4 after the current scan. This reduces the effective noise in the cold calibration reference.

4.4.3 Warm Load

The warm target temperature is computed by applying corrections to the PRT temperatures for extraneous energy that enters the feed. The basic equation for the correction is shown below and Table 4-4 shows the descriptions of all of the terms. Appendix D has a complete derivation of the terms and was used to compute Table 4-5, which shows the nominal values of the energy coupling coefficients. As is expected the vast majority of the energy coupled in comes from the warm target. The front/back delta temperature has a nominal value of 0.2 degrees. The extraneous energy effects for the 18 GHz and above frequencies are negligible due to the low spillover at these frequencies and the high emissivity of the target.

$$T_{\text{warm}} = W_{\text{load}} (T_{\text{prt}} + dT_{\text{prt}}) + W_{\text{ws}} T_{\text{ws}} + W_{\text{cos}} T_{\text{cos}}$$

Coupling Coefficient	Description		Energy Source	Description
Wload	Warm load coefficient		Tprt + dTpri	PRT temperature + front/back delta temperature
Wws	Sensor Coefficient		Tws	Average temperature of sensor seen by warm load
Wcos	Cosmic Background coefficient		Tcos	Cosmic temperature

Table 4-4: Components of Warm Temperature (Twarm) calculation

	6 GHZ	10	18	23	36	50-60	89	166	183
Wload	0.997002	0.994901	0.9989	0.9989	0.9989	0.9989	0.9989	0.9989	0.9989
Wws	0.001018	0.000149	0.00011	0.00011	0.00011	0.00011	0.00011	0.00011	0.00011
Wcos	0.00198	0.00495	0.00099	0.00099	0.00099	0.00099	0.00099	0.00099	0.00099

Table 4-5: Nominal energy coupling coefficients for warm reference

The warm reference counts and PRT temperatures are also averaged both within a scan and across 8 scans, 4 preceding and 4 after the current scan. This reduces the effective noise in the warm calibration reference.

4.4.4 FFT Corrections to Calibration Counts

The noise in the warm load and cold load calibration counts for the FFT bins can be reduced by using all of the bins to compute the average count and then applying this average count to the FFT filter passband. The shape of the filter passband determines the relative amplitude in each bin and is not dependent on the actual calibration target temperature. The effects of the calibration target varying over the course of the measurements can be removed by normalizing the value in each bin by dividing by the weighted average value across all bins for each measurement sample. In computing the average value across all bins, each bin is weighted by the frequency width of the bin, so that the average represents the average across the frequency range of the FFT and is not dependent on the frequency width assigned to each bin. The normalized value for each bin can then be averaged across the number of measurement samples.

The A/D has sufficient range to measure the calibration accurately, without saturating, however, the noise level in each bin however is fairly high due to the narrow bandwidth (250 KHz). The difficulty is in determining the best estimate of the hot and cold load counts in the presence of this noise. The main issue is the difference in system gain for each of the bins across the 20 MHz bandwidth, due primarily to variations in the anti-aliasing filter. The assumption is that the true hot and cold count across the 20 MHz bandwidth is constant, but that the variations in system passband prevent one from using a simple average of the hot / cold counts across all bins. By knowing the passband as a function of bin (P_i), one can then use all bins to estimate the hot/cold counts. This computation of the passband can be computed on orbit and has been validated with the risk reduction hardware. The basic FFT calibration process is as follows:

- 1) Average bin count across center group (nominally bins 32 to 96) of bins:

$$\overline{C_{bin}} = \frac{\sum_i BW_i C_{bin(i)}}{\sum_i BW_i} \quad \text{Eq. 4-1}$$

2) Normalize each bin by the average bin count for this calibration view:

$$CN_{bin(i)} = \frac{BW_i C_{bin(i)}}{\overline{C_{bin}}} \quad \text{Eq. 4-2}$$

3) Determine the passband function from m (typically 1000's) views of hot/cold load readings on orbit:

$$P_i = \left(\frac{1}{m} \right) \sum_{j=1}^m CN_{bin(i)} \quad \text{Eq. 4-3}$$

Once the FFT filter passband has been determined, the corrected count at each bin ($\hat{C}_{bin(i)}$) can be computed from the weighted average count ($\overline{C_{bin}}$) for each new calibration view and the bin Passband Filter Coefficient (P_i). $\overline{C_{bin}}$ is computed by weighting the raw counts by the frequency bandwidth of each bin (BW_i) as shown below. We carry the bandwidth in the equation since some of the bins may be combined prior to inclusion in the RDR packet.

4) Average bin count for a particular calibration view as in step 1):

$$\overline{C_{bin}} = \frac{\sum_i BW_i C_{bin(i)}}{\sum_i BW_i} \quad \text{Eq. 4-4}$$

5) Once $\overline{C_{bin}}$ is computed for each measurement sample, they can be averaged across all of the scene stations for each calibration target and across multiple scan lines as discussed in section 4.4. For computational efficiency, Eqs. 4-4, 4-5 can be applied after any scene station or scan line averaging is performed on $\overline{C_{bin}}$, rather than applying the scene / scan line averaging directly to $C_{bin(i)}$ for each bin. The corrected bin count for a particular calibration view bin using the pre-computed passband is then computed as follows

$$\hat{C}_{bin(i)} = P_i \overline{C_{bin}} \quad \text{Eq. 4-5}$$

The assumption is that P_i is static and does not vary significantly over time. Since P_i is easy to compute, a quality control / diagnostics effort can be used to compute P_i on a routine basis to identify any drift in the FFT passband over the life of the sensor. Figure 4-5 shows sample graphs of the process from the risk reduction FFT hardware. Figure 4-5a shows the noise on 8 individual measurements. Figure 4-5b shows the computation of P_i is repeatable using a 200 measurement average with 3 different target temperatures. Figure 4-5c shows the corrected counts for each bin from a single measurement. Once the corrected hot / cold calibration FFT count is computed for each bin, the calibration proceeds as normal for a non-FFT band.

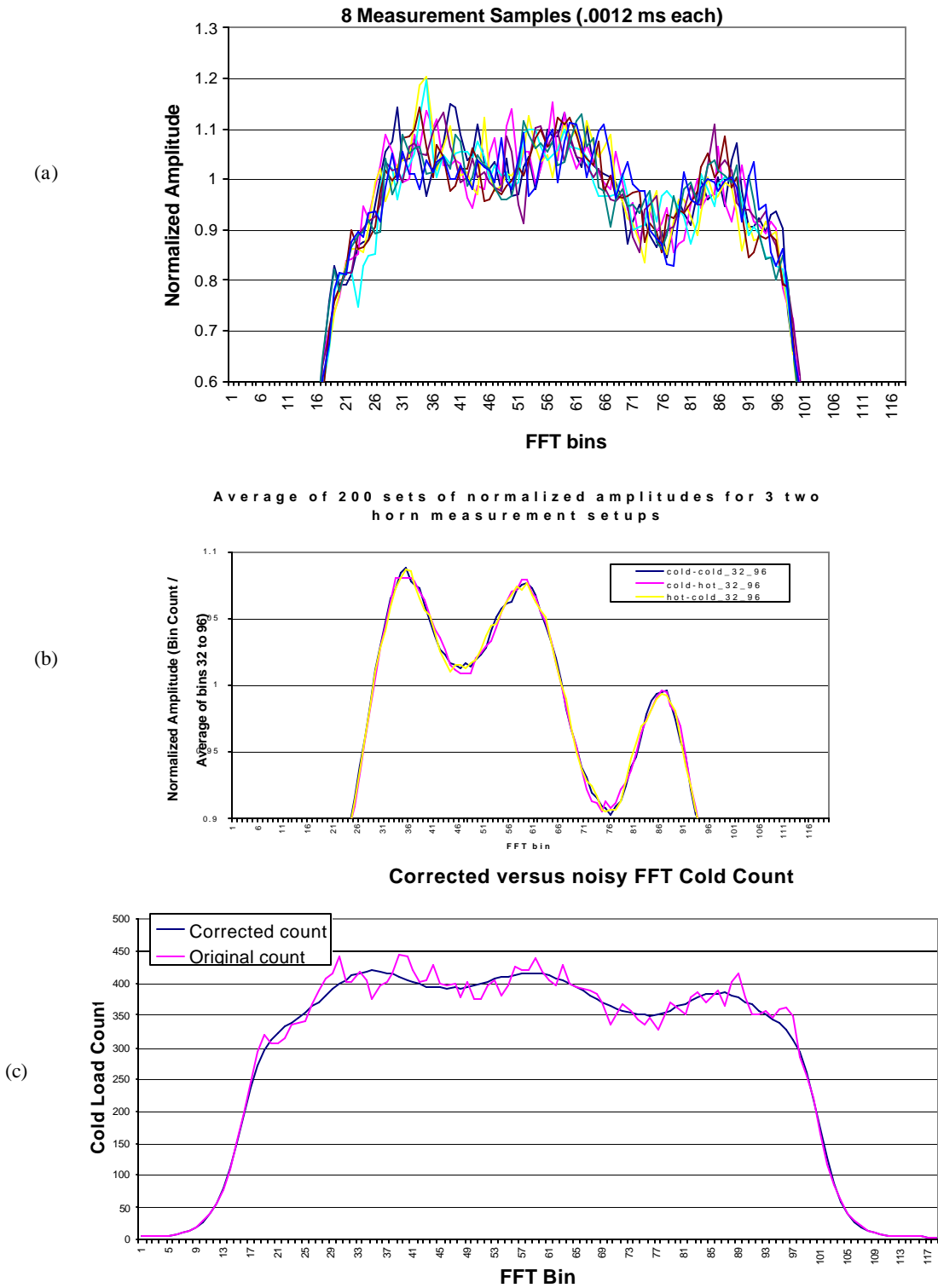


Figure 4-5: FFT Calibration Results using Risk Reduction Hardware

4.4.5 Antenna Temperature

4.4.6 Earth Scene Component of Antenna Temperature

The earth scene component of the antenna temperature can be computed using the following equation. Note that the sensor temperature can be used as an estimate of the spacecraft temperature if a separate spacecraft temperature is not available.

$$TA' = Asp TA - Ar Tr - As Ts - Asc Tsc - Acos Tcos$$

Table 4-6 describes the components of the spillover calculation used to compute T_A' . Table 4-7 shows the nominal values for the energy coupling terms, that are derived in Appendix D.

Coupling Coefficient	Description		Energy Source	Description
Asp	spillover coefficient		Ta	Antenna Temperature
Ar	reflector coefficient		Tr	Reflector Temperature
As	sensor coefficient		Ts	Average Sensor Temperature
Asc	spacecraft coefficient		Tsc	Average Spacecraft temperature
Acos	cosmic background coefficient		Tcos	Cosmic Temperature

Table 4-6: Components of Spillover during the active scan.

	6 GHZ	10	18	23	36	50-60	89	166	183
Asp	1.03492	1.04912	1.01600	1.01022	1.01127	1.00336	1.00250	1.00795	1.00704
Ar	0.00027	0.00036	0.00047	0.00053	0.00066	0.00085	0.00100	0.00140	0.00150
As	0.00068	0.00097	0.00036	0.00027	0.00020	0.00004	0.00002	0.00012	0.00010
Asc	0.00048	0.00058	0.00035	0.00031	0.00032	0.00026	0.00026	0.00029	0.00028
Acos	0.03349	0.04722	0.01481	0.00911	0.01009	0.00220	0.00123	0.00614	0.00515

Table 4-7: Nominal energy coupling coefficients for spillover terms

4.5 Algorithm inputs

The algorithm inputs consist of data from both the RDR data packet and the Sensor Constants Files.

The RDR data packet provides the raw counts from the cold, warm and active scan as well as the on-board temperature measurements listed in Table 3-2. The sensor constants file (SCF) provides all of the coupling coefficients listed in Table 4-3, Table 4-5, and Table 4-7. The SCF also provides the estimate of Tcos and all of the thresholds used for range checking described in Section .

4.6 Algorithm Performance against Requirement

To be completed in EMD phase.

5 Geolocation

5.1 Overview of Geolocation

The geolocation algorithms are used to associated latitude and longitude (lat/lon) points on the ground with sensor scene stations received in the RDR data stream. The lat/lon point represents the intersection of the line of sight (LOS) of the sensor with the Earth as shown in Figure 5-1. The high frequency channels are collected $\frac{1}{2}$ revolution after the low frequency channels, so that the ground tracks overlay. In the case of sounding channels, the soundings are performed along the LOS slant-path and a post-processing operation is used to convert them to vertical profiles.

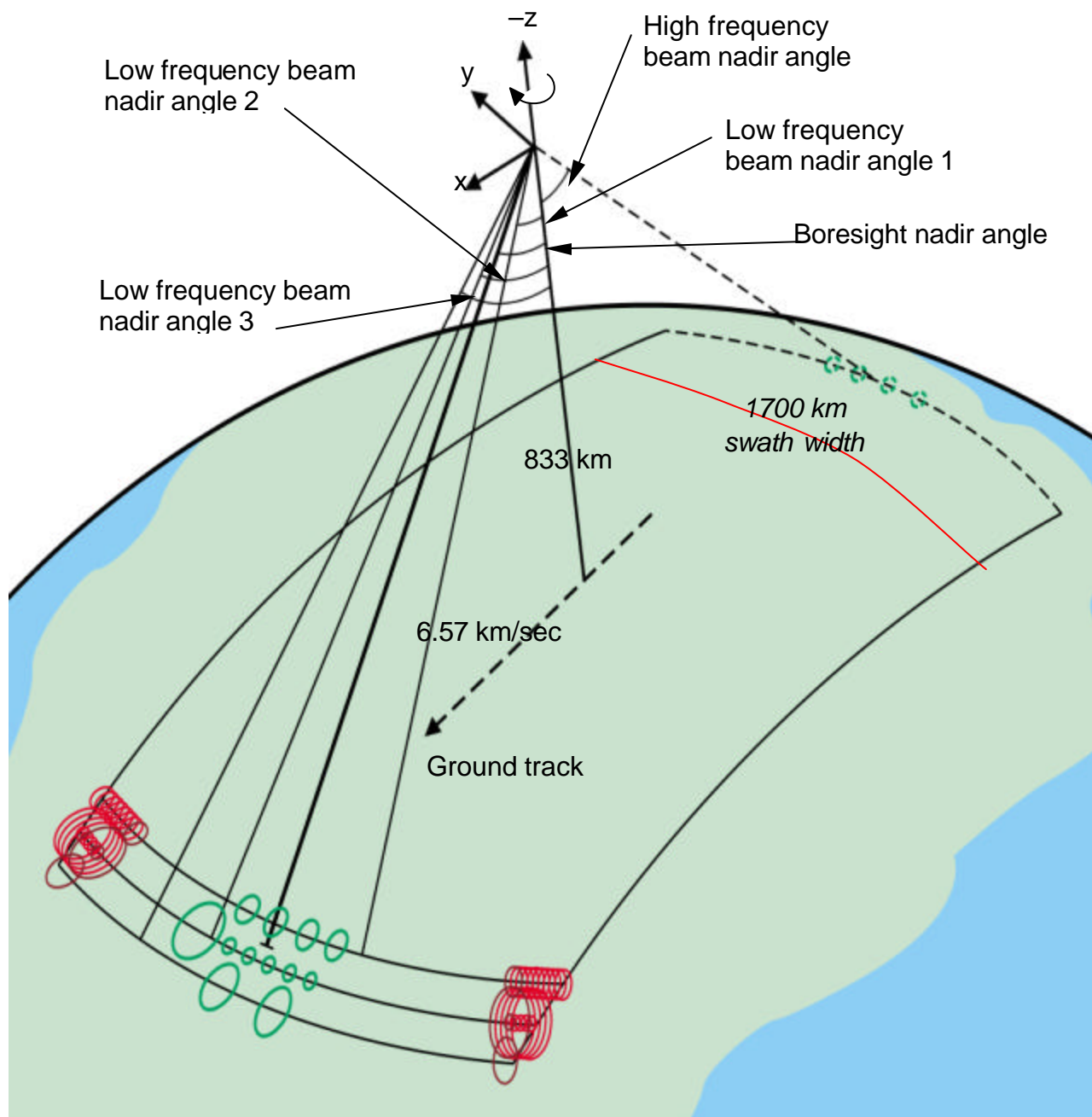


Figure 5-1: CMIS Scan Geometry

5.2 Theoretical Basis of Geolocation

The geolocation algorithm is based on computing the time-varying look angle for each feed and projecting the LOS onto the ground. Geolocation is standard algorithm that is used by many sensors and the physical basis is discussed in detail in the MODIS Level 1A Earth Location Guide (SDST-092). A series of coordinate transformations are used to convert from antenna coordinate system to an Earth Centered Earth Fixed (also called Earth Centered Rotating) coordinate system based on a geocentric earth defined in WGS84. A closed form equation developed by Patt and Gregg (Patt 94) is then used to convert from geocentric to geodetic coordinates in a computationally efficient manner.

The lookdown angles for the conical scan vary by antenna feed orientation as shown in Figure 5-2 and Table 5-1. This produces 4 arcs on the ground where the high frequency arc for the 166 and 183 GHz channels (Arc D in) is designed to overlay the low frequency arc (Arc A in) where co-registration between the high and low frequency channels is most important. Note that while Arcs A & D mostly overlap, they occur $\frac{1}{2}$ scan apart since they come from the two different reflectors. The lookdown angle, and consequentially Earth Incidence Angle (EIA), is adjusted to compensate for the 6.25 km of satellite motion during this $\frac{1}{2}$ scan so that they look at the same point on the ground in the center of the scan.

	Selected Sensor Channel Specifications								
Channel prefix	6	10	18	23	36	60VL	89	166	183V
Channel suffixes	VH	VH, RL	VH, PM, RL	VH	VH, PM	A...V FFT	VH	V	ABC
Frequency range [GHz]	6.45-6.8	10.6-10.7	18.6-18.8	23.6-24.0	36.0-37.0	50-60	87.0-91.0	164.5-167.5	173.4-193.3
Cross-scan EFOV (km)	67.7	45.5	23.5	23.5	16.7	14.9	15.3	14.6	16.1
Along-scan EFOV (km)	39.3	24.8	15.5	15.5	10.3	8.2	8.1	8.8	9.0
Integration time (ms)	5	2.5	1.2	1.2	1.2	1.2	1.2	1.2	1.2
Along-scan sample spacing (km)	16.3	8.78	3.82	3.82	4.08	4.08	4.08	4.05	4.05
Cross-scan IFOV (km)	67.7	45.5	23.4	23.4	16.6	15.0	15.6	14.6	16.1
Along-scan IFOV (km)	37.8	24.2	15.3	15.3	9.9	7.7	7.8	8.4	8.7
Scan arc designation	A	B	C	C	A	A	A	D	D
Lookdown angle	46.98	48.70	45.40	45.40	47.00	47.01	46.99	46.85	46.86
Earth incidence angle	55.76	58.16	53.63	53.63	55.79	55.81	55.77	55.58	55.60
Field of regard (deg)	127	113	145	145	127	127	127	129	129
833 km altitude swath width for sample centers (km)	1760	1754	1745	1745	1750	1751	1750	1751	1754

Table 5-1: Sensor Channel Specification

Figure 5-2 Look Down Angle for Low Frequency Channels

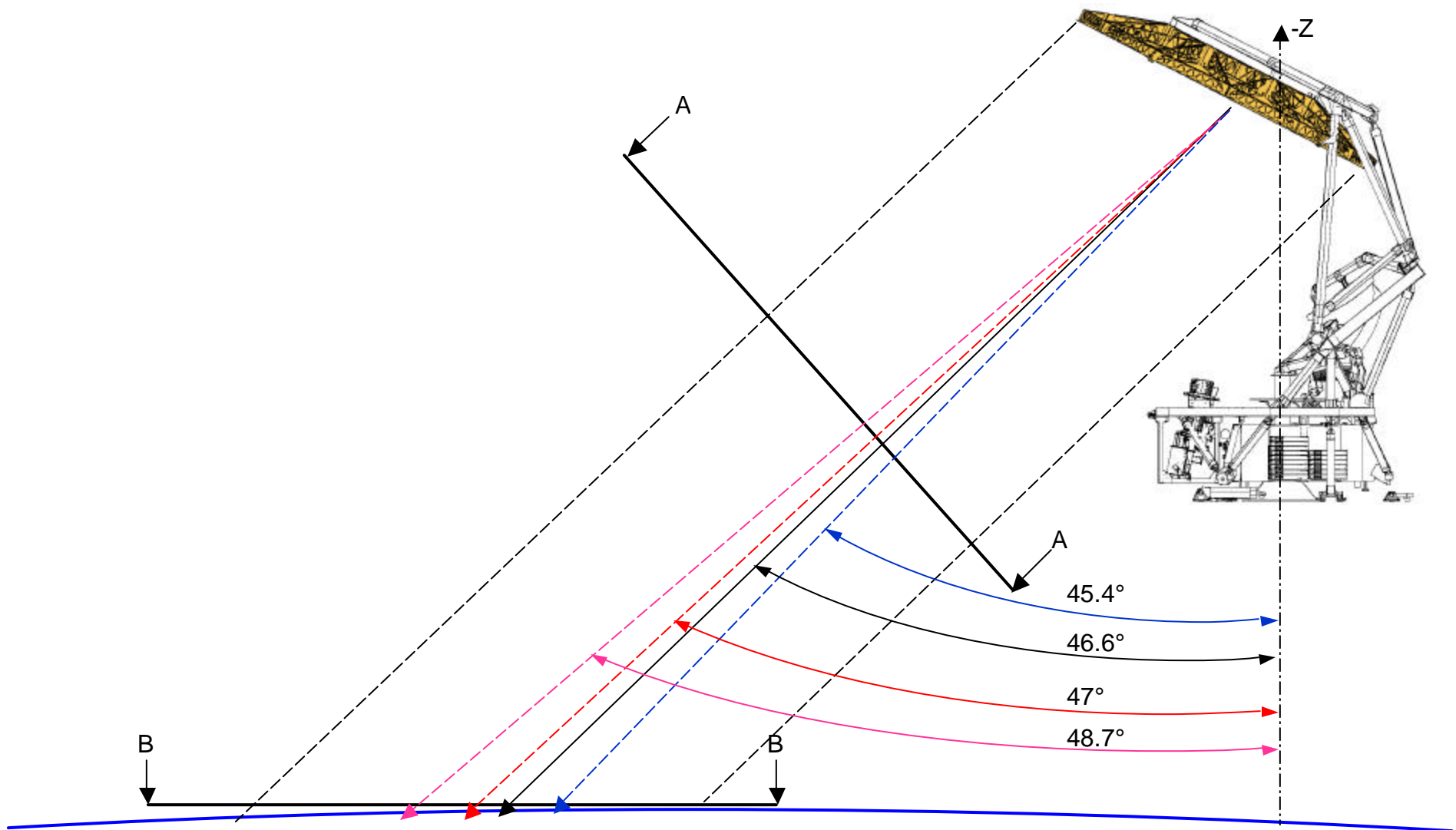
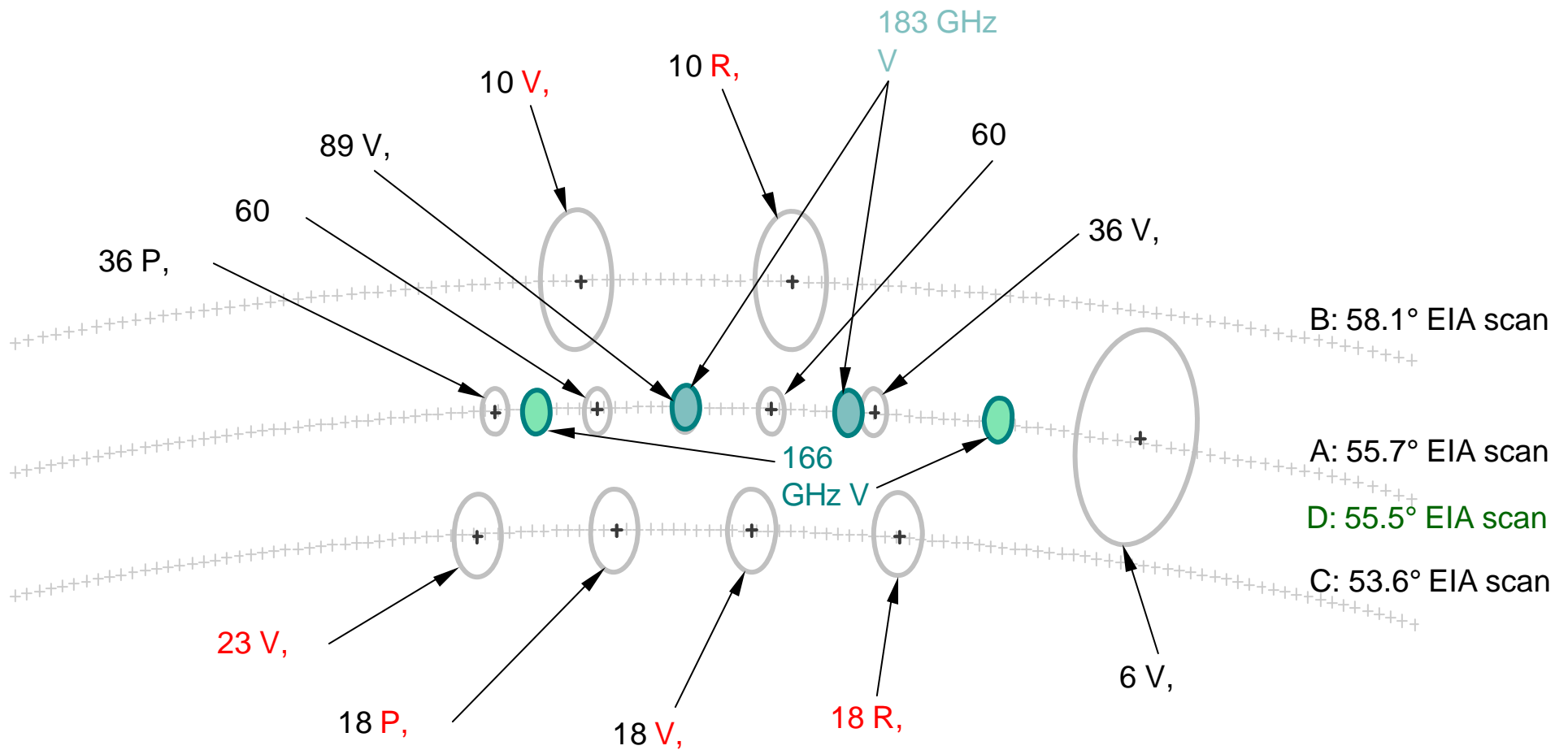


Figure 5-3: Ground Projections of the individual channel IFOVs



The MODIS algorithm approach has 3 basic components of earth location (Sec. 3.1.4.2 of SDST-092):

- 1) Basic Earth Ellipsoid Intersection Algorithm
- 2) Terrain Intersection Algorithm
- 3) Satellite and Sun Viewing Angles

CMIS follows the MODIS approach for the items 1 and 3 with adjustments for the conical scan. The MODIS terrain correction module further refines the latitude and longitude output of the geolocation algorithms for local terrain variation from the geodetic ellipsoid. We have chosen not to follow this approach for CMIS for several reasons, including

- 1) Difference in sensor resolutions – CMIS has Effective Field Of View (EFOV) footprints that vary from 68x40 km for the 6 GHz channel to 9x16 km for the 183 GHz channel (Table 5-1). MODIS has a footprints that range from 250 meters to 1000 meters.
- 2) Difference in sensor earth location requirements – CMIS has an earth location requirement of 3 km, while MODIS has a 2 sigma requirement of 100 meters.
- 3) The footprint matching algorithm discussed in the Vol. 1 Part 2 Overview ATBD assumes that all EFOV footprints from the different channels that overlap lie on the same terrain. This is a by-product of doing the Composite Field Of View (CFOV) footprint matching algorithm based on sensor coordinates, so that a static set of coefficients for the footprint matching across the various channel resolutions can be generated. It would add significant complexity if the relationship between channels in a CFOV was allowed to vary with local terrain.

CMIS footprints are so large that the effects of individual mountains occur at the sub-pixel level and can be ignored. The only local variations for terrain height that should be considered are perhaps for large plateaus where a large region is at a relatively constant terrain height that varies significantly from the geodetic reference. One approach to handling these regions is the use of local Datums that allow the earth eccentricity to vary regional to better fit these regions. This would allow corrections for large regions with significant elevation that can introduce errors in to the CMIS earth location. The efficient Basic Earth Ellipsoid Intersection Algorithm can be used for these Datums as opposed to the computationally expensive ray tracing algorithm in the MODIS Terrain Intersection Algorithm. Care must still be taken as boundary effects can occur where the Datum changes and all local Datums must be converted back to the WGS 84 Datum to be consistent with CMIS requirements. The baseline CMIS algorithms do not currently include any corrections for terrain height variations since inter-sensor (CMIS, VIIRS, CrIS, etc.) earth location consistency may become more important than individual sensor concerns. This issue can be re-investigated in the EMD phase of the program.

5.3 Algorithm Processing Flow

The basic MODIS processing flow (Sec. 3.1.4.2 of SDCT-092) is followed and we try to use the MODIS notation wherever possible. A summary of the Basic Earth Ellipsoid Intercept algorithm is provided below:

- 1) A time varying object viewing vector $u_{Fn/inst}$ is constructed for each of the feed (F_n) lookdown angles in Table 5-1. $u_{Fn/inst}$ represents the conical scan in the instrument coordinate system and any misalignment between the antenna coordinate system and instrument coordinate system is included in $u_{Fn/inst}$.
- 2) The $T_{ecr/inst}$ coordinate transformation is constructed as

$$T_{ecr/inst} = T_{ecr/eci} T_{eci/orb} T_{orb/sc} T_{sc/inst} \quad \text{Eq. 5-1}$$

$T_{ecr/eci}$ performs the Earth Centered Inertial (ECI) to Earth Centered Rotating (ECR) transformation and is a time varying function that depends on the sample time..

$T_{eci/orb}$ converts the satellite ephemeris in the RDR packet to ECI coordinates

$T_{orb/sc}$ corrects for the spacecraft orientation (roll, pitch, yaw) in the RDR packet

$T_{sc/inst}$ corrects for any sensor / spacecraft misalignment

- 3) Transform the object viewing vector and satellite ephemeris to the ECR reference.
- 4) Intersect the ECR earth viewing vector with the WGS84 earth ellipsoid
- 5) Convert the ECR ellipsoid pierce point to geodetic coordinates.

The satellite and solar viewing algorithm flow are not presented here since they are discussed in the MODIS documentation and do not depend on the CMIS instrument, once the earth location and satellite position have been computed from the above process.

5.4 Mathematical Description of Geolocation

The MODIS documentation (Section 3.1.4.2 of SDST-092) provides a complete mathematical description of how earth location is performed. The only portion that is unique to CMIS is the generation of the object viewing vector u_{inst} , however we will start the discussion at the orbit to spacecraft transformation so that we can present where all of the items in the sensor constants file and RDR data stream are utilized. The generation of the satellite and sun viewing angles is not presented here since the MODIS documentation provides a complete description of how to compute these, once the ground pixel location and satellite position are determined.

5.4.1 Coordinate Transformations

The roll, pitch and yaw are all provided in the RDR data stream once per second. The general form for roll, pitch, and yaw presented in Eq. 5-2 is order dependent and will be used for the subsequent transformation where any component that is zero is left out.

$$T_{orb/sc} = \begin{bmatrix} \cos \mathbf{x}_y & -\sin \mathbf{x}_y & 0 \\ \sin \mathbf{x}_y & \cos \mathbf{x}_y & 0 \\ 0 & 0 & 1 \end{bmatrix} \begin{bmatrix} 1 & 0 & 0 \\ 0 & \cos \mathbf{x}_r & -\sin \mathbf{x}_r \\ 0 & \sin \mathbf{x}_r & \cos \mathbf{x}_r \end{bmatrix} \begin{bmatrix} \cos \mathbf{x}_p & 0 & \sin \mathbf{x}_p \\ 0 & 1 & 0 \\ -\sin \mathbf{x}_p & 0 & \cos \mathbf{x}_p \end{bmatrix} \quad \text{Eq. 5-2}$$

where

$$\text{Yaw: } \mathbf{x}_y \quad \text{Roll: } \mathbf{x}_r \quad \text{Pitch: } \mathbf{x}_p$$

A similar formulation can be used for $T_{sc/inst}$, however the nominal design value for this is the unity matrix, if there are no spacecraft / sensor instrument misalignments. $T_{sc/inst}$ will be measured during spacecraft / sensor integration from the offsets between the sensor alignment cube and satellite alignment cubes.

These alignments transformation matrices are combined with the general transformation matrices to convert the sensor instrument coordinate system into an earth centered reference as shown below:

$$T_{ecr/inst} = T_{ecr/eci} T_{eci/orb} T_{orb/sc} T_{sc/inst}$$

Where, the ecr indicates an earth centered reference (sometimes called earth centered earth fixed) and the eci indicates an earth centered inertial frame of reference. Note that both $T_{orb/sc}$ and $T_{ecr/eci}$ are dependent on the absolute time that the pixel is sampled, $T(j, F_n)$ which is computed later in this section.

Two new coordinate frames need to be setup, one for the high frequency antenna and one for the low frequency antenna. $T_{Alf/inst}$ and $T_{Ahf/inst}$ represent the coordinate transformations between the low and high frequency antenna, respectively, and the sensor instrument. In these cases the instrument refers to the CMIS sensor alignment cube and these coordinate transformations will be determined during sensor alignment measurements. The nominal design of the reflectors has a constant elevation offset and scans in azimuth, relative to the sensor coordinate system. This shows up as a constant change in pitch and time varying change in sensor yaw (f_t), as shown below. Appendix F shows the relevant values for the sensor azimuth scan during which each feed is either in the active scan or one of the calibration targets.

$$T_{Alf/inst} = \begin{bmatrix} \cos f_t & -\sin f_t & 0 \\ \sin f_t & \cos f_t & 0 \\ 0 & 0 & 1 \end{bmatrix} \begin{bmatrix} \cos q_{Alf} & 0 & \sin q_{Alf} \\ 0 & 1 & 0 \\ -\sin q_{Alf} & 0 & \cos q_{Alf} \end{bmatrix}$$

The nominal design has the high frequency reflector and low frequency reflector both set at the same boresight look angle. The actual values will come from a table in the sensor constants file as shown in Table 5-2.

$$T_{Ahf/inst} = T_{Alf/inst}$$

Appendix F shows how the feed mounting angles are translated into the effective azimuth and elevation offset in antenna coordinates listed in Table 5-2. Each feed has its own rotation matrix, for Yaw and Pitch offsets due to these angles as shown below for feedhorn n. Table 5-2 shows the values of the azimuth and elevation offset for all feeds from the PDSR material.

$$T_{Alf(Fn)} = \begin{bmatrix} \cos f_{Fn} & -\sin f_{Fn} & 0 \\ \sin f_{Fn} & \cos f_{Fn} & 0 \\ 0 & 0 & 1 \end{bmatrix} \begin{bmatrix} \cos q_{Fn} & 0 & \sin q_{Fn} \\ 0 & 1 & 0 \\ -\sin q_{Fn} & 0 & \cos q_{Fn} \end{bmatrix}$$

where

$$\text{Feed n Yaw: } f_{Fn} \quad \text{Feed n Roll: none} \quad \text{Feed n Pitch: } q_{Fn}$$

Combining the antenna frame of reference with the feed frame of reference yields the viewing vector for feed n (F_n) on the low frequency reflector:

$$U_{inst(Fn)} = T_{Alf(Fn)} T_{Alf/inst}$$

There is a similar formulation for the feeds on the high frequency reflector.

5.4.2 Scan Timing

Figure 5-4 shows the scan timing for the CMIS sensor. Times T1 and T2 are included in the RDR data packet and the physical azimuth angle (f_{sync}) associated with the sync pulse at time T1

is included in the sensor constants file. The baseline approach is to compute the current rotational speed from the time stamps differences on the last few scans, rather than assuming a speed of 31.6 rotations per minute. The current sensor rotational speed can be determined by looking at the time difference between successive sync pulse as shown below:

$$\frac{df_t}{dt} = \frac{k(2p)}{T1_{(i)} - T1_{(i-k)}}$$

where k is the number of scan lines used and $T1_{(i)}$ is the absolute time of the sync pulse on scan i and is not relative to the Master Index Pulse (MIP) as shown in Figure 5-4.

Each sample interval period (τ_T) consist of an Integration Time (τ_i) and a Hold Time (τ_h), which is defined for each channel in Table 3.2.1.3.2-1 of the Performance Specification. A scan consist of 1500 sample periods, which is defined as the shortest sample interval for any channel ($\tau_P = 1.2658$ msec). The scan period is designed for 1.899 secs ($1500 * 1.2658$ msec). Each sample period is further broken down into 24 finer increments allowing the start of a channel scan to be set within 52.7 usecs. Each subsequent sample occurs τ_T later, where τ_T is always a integer multiple of τ_P . τ_T for the 6.8 and 10.7 GHz channels is $4 \tau_P$ (5.0636 msec) and $2 \tau_P$ (2.5318 msec), with all other channels sampling on a $1 \tau_P$ increment. Note that in the current design all channels on the same feed (F_n) use the same timing, so the timing in the following sections is presented as a function of Feed, rather than channel.

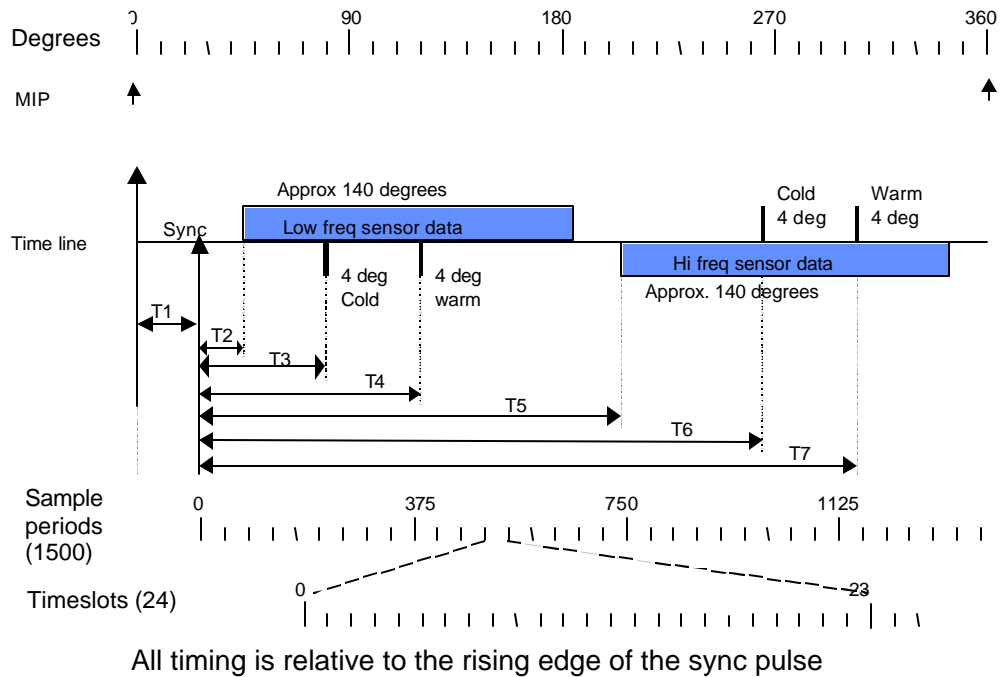


Figure 5-4 CMIS Scan timing

The RDR packet sends down the time of the start time of each channel ($T2$), relative to the sync pulse ($T1$). The earth location for a pixel is set based on the midpoint of the integration period. This means that the time and angle for a given scene station j on Feed n (F_n) is given by:

$$\mathbf{q}_s(j, Fn) = \mathbf{q}_{sync} + (T2_{Fn} + j\mathbf{t}_{T,Fn} + \mathbf{t}_{i,Fn}/2) \frac{d\mathbf{f}_t}{dt}$$

$$T(j, Fn) = T1 + (T2_{Fn} + j\mathbf{t}_{T,Fn} + \mathbf{t}_{i,Fn}/2)$$

5.4.3 Earth location of a specific scene station

Once the antenna scan rotation, $\mathbf{q}_s(j, Fn)$, and time, $T(j, Fn)$, for a particular scene station j on feed Fn is known, the scene station can be earth located using the coordinate transformation matrices. The satellite position $[\mathbf{P}_{eci}(t)]$ and roll, pitch, yaw [contained in $T_{orb/sc}(t)$] are downlinked in the ephemeris portion of RDR packet. Ephemeris information is provide once per second and each RDR packet, which contains approximately 1.9 secs of data for one scan, is designed to provide two ephemeris points that can be used to interpolate the ephemeris to the designed time within the scan. The spacecraft position $[\mathbf{P}_{eci}(t)]$, orientation $[T_{orb/sc}]$, and ecr transformation $[T_{ecr/eci}]$ can all be interpolated to the time of scene station j on feed Fn $[T(j, Fn)]$.

The viewing vector for a particular feed and spacecraft position can then be translated into ecr coordinates:

$$\mathbf{U}_{ecr(Fn)} = \mathbf{T}_{ecr/inst} \mathbf{U}_{inst(Fn)}$$

$$\mathbf{P}_{ecr} = \mathbf{T}_{ecr/eci} \mathbf{P}_{eci}$$

Once these two terms have been computed, steps 3 and 4 in Section 3.1.4.2 of the MODIS documentation provides the detailed equations to compute the latitude and longitude. Section 3.1.4.2 of the MODIS documentation also explains how to compute the satellite and solar viewing angles from this information. Note that the satellite view zenith angles can provide an more accurate estimate of EIA (necessary to support Ocean EDRs) on a pixel basis that includes that variations due to the oblate spheroid earth model. The satellite view azimuth can be used to support the wind direction EDR which needs to know the local viewing geometry of the scene. In addition the MODIS documentation provides information on computing lunar viewing angles if one wanted to compute the lunar illumination of either the ground pixel or satellite.

5.5 Data Needed for Geolocation

The data needed for the earth location includes all of the feed alignments and antenna boresight alignments as shown in the following tables.

Horn	Freq. (GHz)	EL Antenna Boresight($\mathbf{q}_{Alf}, \mathbf{q}_{Ahf}$)		AZ Beam Position (\mathbf{f}_{Fi})	EL Beam Position (\mathbf{q}_{Fi})
1	6.63	Low Freq. (θ_{Alf})	46.6	6.05	0.08
2	10.70		46.6	1.41	2.06
3	10.70		46.6	-1.46	2.06
4	18.70		46.6	2.82	-1.26
6A	18.70		46.6	0.90	-1.20
6B	18.70		46.6	-0.90	-1.20

5	23.50	High Freq. (θ_{Ant})	46.6	-2.77	-1.23
7	37.00		46.6	2.55	0.32
8	37.00		46.6	-2.55	0.32
9A	56.90		46.6	1.18	0.36
9B	56.90		46.6	-1.18	0.36
10	89.00		46.6	0.00	0.36
13	166		46.6	-3.10	0.10
14	166		46.6	3.10	0.10
15	183		46.6	-1.13	0.17
17	183		46.6	1.13	0.17

Table 5-2: Antenna and Beam position Alignments from PDSR baseline used in geolocation to be stored in sensor constants file

Sensor / Satellite Alignment	Roll, Pitch, Yaw from spacecraft integration
Sync angle	f_{sync}
Timing constants by channel	τ_T, τ_i

Table 5-3: Additional geolocation supporting data in sensor constants file

Satellite ephemeris	Position, Roll, Pitch, Yaw, timestamp, once per second
Scan Times and start of Active Scan by channel	T1 and T2 (by channel)

Table 5-4: Geolocation supporting data in RDR packet

5.6 Algorithm Performance against Requirements

To be completed in EMD phase

6 The SDR Cross Polarization Correction

6.1 Overview

The cross-polarization correction algorithm takes spillover corrected, single observation, collocated *antenna temperatures* (TAs) for all polarizations of a given frequency as input, and produces the final SDR *brightness temperature* (TB) product. Observations for each frequency are processed sequentially. The cross polarization correction algorithm actually consists of three corrections; an antenna cross-polarization correction, a polarization basis correction, and a Faraday rotation correction.

The antenna cross-polarization correction is critical to the performance of some of the EDR algorithms, especially sea surface temperature (SST) and wind direction, and for the accuracy of the SDR brightness temperature products in general. Therefore instead of simply designing a single algorithm, we coded and tested three alternative algorithms, which differ in the representation of the antenna cross-polarization matrix or “M-matrix.”

We selected for the final algorithm the antenna cross-polarization correction that uses the M-matrix in the “channel basis,” i.e., uses TAs from individual polarizations (channels) as input, and outputs scene TBs for individual polarizations. We selected this algorithm because it allows for optimal SST EDR performance; it minimizes the correlation of the noise between the TBs of different polarizations (to which the SST algorithm is sensitive). We also find this correction the most robust of those examined with respect to single channel degradation or failure.

The polarization basis of the radiometer is chosen to match the earth scene polarization basis (the local vertical, horizontal polarization vectors for a spherical earth) when the spacecraft has the nominal attitude, and the CMIS instrument is aligned absolutely with the spacecraft. Spacecraft attitude and CMIS-to-spacecraft alignment errors cause the radiometer polarization basis to be rotated with respect to the earth scene polarization basis. All algorithms downstream expect brightness temperatures measured in the earth scene polarization basis, and so a rotation correction is applied following the antenna cross-polarization correction.

The Faraday rotation (FR) correction is last, and is important for SST performance (mainly retrieval accuracy), wind direction performance (precision), and for the accuracy of the SDR TB products. (Since the polarimetric channel configuration was changed to replace the +/- 45 degree channels with circularly polarized channels at 10 GHz, the FR correction has become a bit less critical for the wind direction algorithm, but is still important around the time of solar maximum, when FR reaches a maximum.)

It is important to set requirements on the knowledge of the M-matrix, polarization rotation, and Faraday rotation which allow the EDR retrieval errors to meet the EDR requirements in the CMIS Sensor Requirements Document (SRD). We use sensitivity analyses of the EDR retrieval errors with respect to each knowledge error to derive the requirements. To perform these analyses, we developed an end to end simulation of the sensor errors and SDR cross polarization algorithm: that is, we take the simulated TBs for testing the algorithms (see Ocean EDR Algorithm ATBD, Section 5), and transform them according to the equations describing FR, polarization rotation, and antenna cross-polarization, to obtain simulated scene TAs; we then add knowledge error to the truth values of FR and the sensor errors, and use the perturbed values of these parameters and the simulated TAs in SDR cross polarization correction to obtain simulated SDR TBs; the simulated SDR TBs are then used in the EDR algorithms.

We set the requirement on M-matrix knowledge at 0.001 per element—the limit to state of the art in antenna measurement—but find that this may not be sufficient to keep the SST and wind direction errors within the SRD thresholds when the SDR TB products are used directly by the ocean EDR algorithms. However, we find that, when we simulate the effect of an on-orbit calibration of the CMIS SDR TB product to the radiative transfer model (RTM) used to generate the algorithms, the requirement is sufficient to allow SST and wind direction errors to meet the required performance.

The accuracy error in the absolute TA calibration of radiometer measurements is generally larger than the errors in the SDR TB product due to sensor and FR knowledge errors alone. Therefore, such a calibration is required for the CMIS ocean algorithms. Because this calibration removes the total bias with respect to the RTM (including the component due to sensor errors), we show how such a calibration limits the effect of sensor knowledge errors on the SDR TB product.

As will be shown, it is not possible to correct the cross polarization from TBs whose polarizations correspond to TAs that are not measured by the instrument. Therefore we set a requirement on the cross polarization from these unmeasured polarizations; the requirement is found to be that the cross polarization from unmeasured polarizations be less than 0.02, on average, over the 6-36 GHz frequencies.

A similar situation arises in the rotation corrections for frequencies where the +/-45 polarizations are not measured. Because the rotation corrections for the v and h polarized channels involve the +/- 45 channels, the rotation correction is approximate for frequencies where they are not measured. We derive a top-level requirement of 0.6 deg RMS on the CMIS polarization rotation, corresponding to the point where the SST accuracy error becomes large enough to influence the measurement uncertainty. We also derive a top-level knowledge error requirement of 0.05 deg. We have set the requirement on Faraday rotation knowledge at 0.2 deg, allowing the SST and wind direction algorithms to perform within the EDR error thresholds. In turn, we selected external data sources for determining determine FR that allow us to meet the 0.2 deg requirement in the absence of magnetic storms.

6.2 Physical Basis of the SDR Cross Polarization Correction Algorithm

Figure 6-1 shows the perturbations to the earth scene radiation from the top of the atmosphere (TOA) through the radiometer antenna. The TOA radiation can be described in terms of the TBs for the earth scene polarizations, which are points along the TB *polarization ellipse*. First the radiation encounters the ionosphere, where the magnetic field and electron density conspire to rotate the polarization ellipse, i.e. the polarization basis vectors, while maintaining the brightness temperatures at the original values in the rotated basis. Alternately, as used here, one can describe effect of the rotation on magnitude of the TBs for fixed earth scene polarization basis using a rotation matrix.

Let the vector T_B describe the polarization state of the earth scene radiation in the observation footprint at some frequency. T_B can be a 6-vector of earth scene TOA TBs, or of the 4 corresponding Stokes parameters. Let T_B' be a similar vector describing the polarization state in the earth scene polarization basis, but after undergoing Faraday rotation. Then the effect of the Faraday rotation can be described by the equation

$$\bar{T}'_B = R(\mathbf{j}_{FR})\bar{T}_B \quad (6-1)$$

where ϕ_{FR} is the magnitude of the FR. The R-matrix is square, and will be specified later.

The polarization basis of the radiometer is chosen to match the earth scene polarization basis (defined by the local vertical, horizontal polarization vectors for a spherical earth) when the spacecraft has the nominal attitude, and the CMIS instrument is aligned absolutely with the spacecraft. Spacecraft attitude and CMIS alignment errors cause the radiometer polarization basis to be rotated with respect to the earth scene polarization basis. The cross-polarization correction operates on measurements in the radiometer polarization basis, so one must transform the earth scene, Faraday rotated TBs in the earth scene polarization basis to those the radiometer basis using another rotation matrix (same form as for Faraday rotation, but the argument is different). If \bar{T}''_B represents the polarization state of the radiation in the radiometer basis then,

$$\bar{T}''_B = R(\mathbf{j}_{CMIS})\bar{T}'_B \quad (6-2)$$

where ϕ_{CMIS} represents the rotation between the radiometer and earth scene polarization bases.

The radiation then encounters the offset parabolic reflector of the CMIS antenna. The radiation for each polarization induces surface currents in the reflector, which, due to the curvature of the reflector, result in radiation not just of the input polarization but also for the orthogonal polarization. The reflector also adds a phase to the radiation, which differs for the two orthogonal components of the reflected radiation. This is the first source of antenna cross-polarization.

The reflected radiation is focused onto the feed farm. Due to the finite directionality of the feeds, each feed collects radiation for not only the antenna but the surroundings as well, i.e., “spillover.” The feed is connected to two ports which isolate two orthogonal polarization of the radiation. But, the isolation is not perfect, and so the feeds themselves introduce some cross-polarization as well. The temperature of the radiation collected by the feed for a given polarization is the antenna temperature (T_A) for that polarization. The temperature of the radiation collected by the feed from the earth scene is called the scene component of the antenna temperature (“scene T_A ” for short).

Letting the vector T_A' represent the scene T_A s, the antenna cross-polarization can be expressed as

$$\bar{T}'_A = M\bar{T}''_B \quad (6-3)$$

where M is the cross-polarization matrix, describing the contribution of each polarized brightness temperature into each polarized antenna temperature. Finally, since the spillover in the feed for polarization p results in a fraction δ_p of the input radiation coming from the surrounds and a fraction $1-\delta_p$ from the earth scene, the temperature of the radiation received by the p -polarized channel of the antenna can be expressed as

$$T_{Ap} = (1 - \mathbf{d}_p)T'_{Ap} + \mathbf{d}_p T_{eff,p} \quad (6-4)$$

Equation 6-4 is inverted to obtain the scene TAs in the antenna illumination correction algorithm that precedes the cross polarization correction. Putting together the equations 6-1 to 6-3 gives an expression for the scene TAs in terms of the scene TBs in the earth polarization basis:

The EDR algorithms require as input the scene TBs in the earth polarization basis. Therefore, the purpose of the SDR algorithm is to accept the scene TAs and undo each of the perturbations just discussed, in the reverse order, until one arrives at the earth scene TBs in the earth polarization basis.

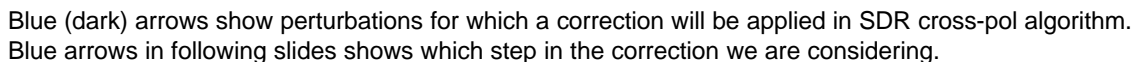


Figure 6-1: Perturbations to the earth scene brightness temperatures from the top of the atmosphere through reception of the radiation by the radiometer. The SDR algorithm undoes each of these perturbations in the reverse order, so the the earth scene brightness temperatures can be found and used in the EDR algorithms. The cross polarization correction of the SDR algorithm undoes the perturbations corresponding to the blue (darkened) arrows.

6.3 Mathematical Description of the SDR Cross Polarization Correction

6.3.1 Symbolic Description of the Algorithm

We can symbolically recover the earth scene TBs from the scene TAs by inverting 6-5:

$$\bar{T}_B = R^{-1}(\mathbf{j}_{FR})R^{-1}(\mathbf{j}_{CMIS})M^{-1}\bar{T}_A' \quad (6-6)$$

At 18 GHz, where all 6 polarizations are measured, this is the expression for the SDR cross polarization correction. However, returning to equation 6-3, if less than 6 polarizations are measured, the M-matrix is not square, and cannot be directly inverted. We show in Section 6.3.2.3 what modification needs to be made to the algorithm when less than 6 polarizations are measured.

6.3.2 Considerations for the Antenna Cross-Polarization Correction

6.3.2.1 Earth Incidence Angle

The WindSat team has set up their antenna cross polarization correction so the M-matrix is computed for each observation using the feed boresight earth incidence angle (EIA) reported for each frequency. Of course the M-matrix must be computed for the nominal EIA at each frequency. But, recomputing it for every observation only makes sense if the M-matrix is sensitive to small departures from the nominal EIA, and therefore needs to be computed for the actual EIA of the measurements. However, our preliminary sensitivity analysis with respect to EIA shows the EIA dependence of the 6 through 36 GHz M-matrices to be extremely weak (10^{-5} per degree, much less than the 10^{-3} knowledge error requirement that will be derived later).

However, if subsequent studies show the sensitivity to EIA is larger, we can compute the M-matrix for each frequency at equal intervals in EIA, store them in a table, and use the EIA reported with the observations to interpolate the M-matrix before application of the correction.

6.3.2.2 Choice of Representation for the M-matrix

We have explored several possibilities for the representation of the M-matrix. Among these are

Channel Representation: The M-matrix is written in terms of the individual polarized TAs and TBs (v,h,+, -,l,r). The rows correspond to the TAs and the columns to the TBs. The matrix then has 6 columns, corresponding to the 6 brightness temperatures, and n rows corresponding to the n antenna temperatures measured. At 18 GHz, where all 6 polarizations are measured, the M-matrix is 6x6; because of this, we tend to call this the 6x6 M-matrix, regardless of the number of polarizations measured.

Stokes Representation: The M-matrix is written in terms of the v,h TAs (T_{Av} , T_{Ah}) as before, but now the difference of the + and - TAs (“ T_{AU} ”), and the difference of the left and right circular TAs (“ T_{A4} ”). The M-matrix is also written in terms of the Stokes parameters for the TBs (T_v, T_h, T_U, T_4). The Stokes representation of the M-matrix is therefore mx4, where m is the

number of “antenna Stokes parameters” and 4 is the number of Stokes parameters for the scene TBs. Because $m=4$ at 18 GHz, we often refer to this as the 4x4 M-matrix.

(One should note that the antenna Stokes parameters are not real Stokes parameters, as they do not follow the algebra of Stokes parameters. But, the label, and symbolism employing the Stokes vector representation (i.e. T_{AU} , T_{A4}) is more convenient than constantly referring to “the difference of the + and – antenna temperatures,” etc.)

Mixed Representation: The M-matrix is written in terms of the individual polarized TAs ($v, h, +, -, l, r$) and the Stokes parameters for the TBs ($v, h, U, 4$). Therefore the M-matrix in the mixed basis is $n \times 4$. Because $n=6$ at 18 GHz, we often refer to this as the 6x4 M-matrix.

In the appendix A, we derive expressions for the unique coefficients of the antenna temperature equations, and then show how the 6x6, 6x4 and 4x4 M-matrices can be computed from these coefficients. There we also discuss in more detail the advantages and disadvantages of each in terms of the performance of the cross-polarization correction.

We have performed simulations of the cross-polarization correction using all three representations of the M-matrix. Based on the results, we have chosen the 6x6 M-matrix for the cross-polarization correction. There are three reasons:

- (1) The SST EDR uncertainty error is the lowest (by 0.02-0.03K depending on true SST) using the 6x6 correction. (This is significant because we are close to the uncertainty threshold requirement for SST). The reason is that the SST retrieval algorithm uses the individual polarized TBs as input (as do all algorithms except wind direction), and not the Stokes parameters; since the output of the 6x4 and 4x4 algorithms are the Stokes parameters, the v and h polarized TBs must be used to convert the Stokes parameters back to the individual polarized TBs. This correlates the noise (resulting from NEDTs) between the TBs, and the SST algorithm does not like correlated noise—it amplifies it.
- (2) The correction based on the 6x6 algorithm is the most robust with respect to single channel degradation and spurious noise; the derived TB for any polarization p depends to a high degree on the scene TA for polarization p , and very little on the other antenna temperatures. This is because the 6x6 M-matrix is nearly diagonal (diagonal elements near one, off diagonal elements are of the order of 10^{-2} to 10^{-5}). Also no conversion of Stokes parameters to obtain the individual polarized TBs is needed. Therefore, only the TB corresponding to a degraded channel would be significantly degraded.
- (3) It is a simple matter to transform the 6x6 matrix to another basis if one channel fails, without significantly affecting the values of the TBs derived for other channels.

These properties do not hold for the cross-polarization correction using the 6x4 or 4x4 M-matrices, as outlined below. A full treatment of the M-matrix in each representation, and the advantages and disadvantages of each representation is the topic of Appendix B.

Inverting the 6x4, as necessary for the correction algorithm, is really a least-squares problem for an overdetermined system (6 TA equations in 4 unknown Stokes parameters at 18 GHz). The least squares solution badly mixes all antenna temperatures measured in the solution for the Stokes parameters. For example, when all 6 polarization are measured, in the absence of cross-polarization (the 6x6 matrix is the identity matrix), the solution for the vertically polarized TB is

$$T_v'' = \frac{2}{3}T_{Av}' - \frac{1}{3}T_{Ah}' + \frac{1}{6}(T_{A+}' + T_{A-}') + \frac{1}{6}(T_{Al}' + T_{Ar}') \quad (6-7)$$

when the simplest solution is just

$$T_v'' = T_{Av}' \quad (6-8)$$

But, least squares always tries to minimize the sum-square of the coefficients to minimize the noise in the product, but does this at the expense of significant mixing of the antenna temperatures in the solution. Spurious noise or degradation in one channel would be propagated to all SDR derived TBs to a significant degree.

In addition, the necessity of using the derived v and h TBs to transform the derived Stokes parameters back to individual polarized scene TBs means that the cross-polarization corrections utilizing the 6x4 or 4x4 M-matrices have an additional problem with respect to spurious noise or degradation of the v,h, antenna temperatures.

Also, if one of the polarimetric channels fails, then the inputs to the cross-pol correction utilizing the 4x4 M-matrix cannot be computed. The algorithm can be modified, but not without knowing the M-matrix in the channel representation (i.e., the 6x6).

6.3.2.3 The Column Elimination Method for Frequencies at which Less Than 6 Polarizations are Measured

As mentioned above, if n polarizations are measured at a given frequency, then the (channel representation) cross polarization matrix for that frequency is nx6. If n<6, the inversion cannot be done directly; the M-matrix is not square.

As an example to motivate what needs to be done, we consider the correction at 10 GHz, where only the vertical (v), horizontal (h), and left (l) and right (r) circular polarizations are measured. We can rewrite equation 6-3 as:

$$\begin{pmatrix} T_{Av}' \\ T_{Ah}' \\ T_{Al}' \\ T_{Ar}' \end{pmatrix} = \begin{pmatrix} M_{vv} & M_{vh} & M_{v+} & M_{v-} & M_{vl} & M_{vr} \\ M_{hv} & M_{hh} & M_{h+} & M_{h-} & M_{hl} & M_{hr} \\ M_{lv} & M_{lh} & M_{l+} & M_{l-} & M_{ll} & M_{lr} \\ M_{rv} & M_{rh} & M_{r+} & M_{r-} & M_{rl} & M_{rr} \end{pmatrix} \begin{pmatrix} T_v'' \\ T_h'' \\ T_+'' \\ T_-'' \\ T_l'' \\ T_r'' \end{pmatrix} \quad (6-9)$$

Since only the v,h,l,r, polarizations are measured, and only 4 parameters can be recovered from the 4 equations uniquely; at most the v,h,l,r, components of the scene TBs can be recovered from these equations.

One solution to the inversion problem is therefore to eliminate those columns from the M-matrix that refer to TBs that we don't hope to recover. This makes the M-matrix square and invertible. One can find the error in the derived TBs using this *column elimination method* in the following

way. First take terms that we don't hope to recover (involving T_+ and T_-) to the left hand side of (6-9):

$$\begin{pmatrix} T'_{Av} - (M_{v+}T''_+ + M_{v-}T''_-) \\ T'_{Ah} - (M_{h+}T''_+ + M_{h-}T''_-) \\ T'_{Al} - (M_{l+}T''_+ + M_{l-}T''_-) \\ T'_{Ar} - (M_{r+}T''_+ + M_{r-}T''_-) \end{pmatrix} = \begin{pmatrix} M_{vv} & M_{vh} & M_{vl} & M_{vr} \\ M_{hv} & M_{hh} & M_{hl} & M_{hr} \\ M_{lv} & M_{lh} & M_{ll} & M_{lr} \\ M_{rv} & M_{rh} & M_{rl} & M_{rr} \end{pmatrix} \begin{pmatrix} T''_v \\ T''_h \\ T''_l \\ T''_r \end{pmatrix} \quad (6-10).$$

Now the system of equations can be directly inverted to yield

$$\begin{pmatrix} T''_v \\ T''_h \\ T''_l \\ T''_r \end{pmatrix} = M_{elim}^{-1} \begin{pmatrix} T'_{Av} - (M_{v+}T''_+ + M_{v-}T''_-) \\ T'_{Ah} - (M_{h+}T''_+ + M_{h-}T''_-) \\ T'_{Al} - (M_{l+}T''_+ + M_{l-}T''_-) \\ T'_{Ar} - (M_{r+}T''_+ + M_{r-}T''_-) \end{pmatrix} \quad (6-11),$$

where

$$M_{elim} = \begin{pmatrix} M_{vv} & M_{vh} & M_{vl} & M_{vr} \\ M_{hv} & M_{hh} & M_{hl} & M_{hr} \\ M_{lv} & M_{lh} & M_{ll} & M_{lr} \\ M_{rv} & M_{rh} & M_{rl} & M_{rr} \end{pmatrix} \quad (6-12).$$

We now need to anticipate two results from Appendix B. The first is that for any measured polarization p and its orthogonal polarization q (which is always measured)

$$M_{pp} + M_{pq} = 1 \quad (6-13)$$

The M -matrices computed from antenna design will show that at each frequency $M_{pp'}$ is much smaller than 1 for p' not equal to p (e.g. Figure 6-2). Therefore the column-eliminated matrix is nearly the identity matrix.

The second result is that the off diagonal elements are not all independent, and in fact

$$M_{pU} \equiv M_{p-} = -M_{p+} \text{ for } p = v, h, l, r \quad (6-14)$$

Putting this together with the fact that the difference of the $+$ and $-$ TB is the third Stokes parameter T_U , we can rewrite equations 6-11 and 6-12 as

$$\begin{pmatrix} T''_v \\ T''_h \\ T''_l \\ T''_r \end{pmatrix}_{Exact} = M_{elim}^{-1} \begin{pmatrix} T'_{Av} - (M_{vU}T'_U) \\ T'_{Ah} - (M_{hU}T'_U) \\ T'_{Al} - (M_{lU}T'_U) \\ T'_{Ar} - (M_{rU}T'_U) \end{pmatrix} \quad (6-15)$$

where

$$M_{elim} = \begin{pmatrix} 1 - M_{vh} & M_{vh} & M_{vl} & M_{vr} \\ M_{hv} & 1 - M_{hv} & M_{hl} & M_{hr} \\ M_{lv} & M_{lh} & 1 - M_{lr} & M_{lr} \\ M_{rv} & M_{rh} & M_{rl} & 1 - M_{rl} \end{pmatrix} \quad (6-16)$$

In 6-16, we have written the column eliminated matrix in terms of the small (10^{-2} to 10^{-5}) matrix elements to emphasize that it is nearly the identity matrix.

On the other hand, the SDR result that we would obtain from the column elimination on the M-matrix would be

$$\begin{pmatrix} T_v'' \\ T_h'' \\ T_l'' \\ T_r'' \end{pmatrix}_{SDR} = M_{elim}^{-1} \begin{pmatrix} T_{Av}' \\ T_{Ah}' \\ T_{Al}' \\ T_{Ar}' \end{pmatrix} \quad (6-17)$$

The difference between these two solutions is

$$\begin{pmatrix} T_v'' \\ T_h'' \\ T_l'' \\ T_r'' \end{pmatrix}_{SDR} - \begin{pmatrix} T_v'' \\ T_h'' \\ T_l'' \\ T_r'' \end{pmatrix}_{Exact} = M_{elim}^{-1} \begin{pmatrix} M_{vU} \\ M_{hU} \\ M_{lU} \\ M_{rU} \end{pmatrix} T_U'' \approx \begin{pmatrix} M_{vU} \\ M_{hU} \\ M_{lU} \\ M_{rU} \end{pmatrix} T_U'' \quad (6-18)$$

The approximation at the end of equation 6-18 results from the fact that M_{elim} is nearly the identity matrix. This equation says that the error in the cross-polarization correction due to not measuring the + and – channels at 10 GHz is approximately equal to the magnitude of the corresponding columns of the M-matrix, times the corresponding Stokes parameter for the scene.

The error in the cross-polarization correction at 37 GHz, where we do not measure the l and r polarizations, can be found by making the substitutions U to 4, l to +, r to – in equations 6-16 and 6-18.

In the case of 6 and 23 GHz, where neither the + and - nor the l and r polarizations are measured, the error in the cross polarization correction is

$$\begin{pmatrix} T_v'' \\ T_h'' \end{pmatrix}_{SDR} - \begin{pmatrix} T_v'' \\ T_h'' \end{pmatrix}_{Exact} = M_{elim}^{-1} \left[\begin{pmatrix} M_{vU} \\ M_{hU} \end{pmatrix} T_U'' + \begin{pmatrix} M_{v4} \\ M_{h4} \end{pmatrix} T_4'' \right] \quad (6-19)$$

where

$$M_{elim} = \begin{pmatrix} 1 - M_{vh} & M_{vh} \\ M_{hv} & 1 - M_{hv} \end{pmatrix} \quad (6-20)$$

Again, the TB error in equation 6-19 can be approximated as

$$\Delta \begin{pmatrix} T_v'' \\ T_h'' \end{pmatrix} \approx \begin{pmatrix} M_{vU} \\ M_{hU} \end{pmatrix} T_U'' + \begin{pmatrix} M_{v4} \\ M_{h4} \end{pmatrix} T_4'' \quad (6-21)$$

It is important to recognize that this error in the SDR solution for the TBs is a result of not measuring the all 6 polarizations, and not a result of any approximation within the algorithm; there is simply no other way to handle the fact that some polarizations are not measured at all frequencies except 18 GHz. In fact, the inversion of M_{elim} for the 6 and 23 GHz corresponds to the conventional cross polarization correction for a dual-polarized radiometer.

The magnitude of T_U and T_4 for ocean scenes is generally on the order of a few Kelvin or less. Therefore, one must put a constraint (a requirement) on the magnitude of the matrix elements in the columns to be eliminated before the inversion. Later, we will use EDR retrieval sensitivity analyses, where we vary of the magnitude of the matrix elements in the columns to be eliminated, to set this requirement.

6.3.3 Considerations for the Rotation Corrections

The rotation correction could also use 6x6 rotation matrices, for the same reasons as the M-matrix:

$$\bar{T}_B = R_{66}^{-1}(\mathbf{j}_{FR}) R_{66}^{-1}(\mathbf{j}_{CMIS}) \bar{T}_B'' \quad (6-22)$$

where

$$R_{66} = \begin{pmatrix} \cos^2 \mathbf{j} & \sin^2 \mathbf{j} & \sin \mathbf{j} \cos \mathbf{j} & -\sin \mathbf{j} \cos \mathbf{j} & 0 & 0 \\ \sin^2 \mathbf{j} & \cos^2 \mathbf{j} & -\sin \mathbf{j} \cos \mathbf{j} & \sin \mathbf{j} \cos \mathbf{j} & 0 & 0 \\ -\sin \mathbf{j} \cos \mathbf{j} & \sin \mathbf{j} \cos \mathbf{j} & \cos^2 \mathbf{j} & \sin^2 \mathbf{j} & 0 & 0 \\ \sin \mathbf{j} \cos \mathbf{j} & -\sin \mathbf{j} \cos \mathbf{j} & \sin^2 \mathbf{j} & \cos^2 \mathbf{j} & 0 & 0 \\ 0 & 0 & 0 & 0 & 1 & 0 \\ 0 & 0 & 0 & 0 & 0 & 1 \end{pmatrix} \quad (6-23)$$

But, first, the circular polarizations are not affected by rotation, and do not enter into the correction for other polarizations. Second, the rotation equations are most simply expressed in terms of the Stokes parameters

$$\begin{aligned} T_Q &= T_v - T_h \\ T_U &= T_+ - T_- \end{aligned} \quad (6-24)$$

with the relations for a single rotation being

$$\begin{aligned} T'_Q &= T_Q \cos 2j + T_U \sin 2j \\ T'_U &= -T_Q \sin 2j + T_U \cos 2j \end{aligned} \quad (6-25)$$

or

$$\begin{pmatrix} T'_Q \\ T'_U \end{pmatrix} = \begin{pmatrix} \cos 2j & \sin 2j \\ -\sin 2j & \cos 2j \end{pmatrix} \begin{pmatrix} T_Q \\ T_U \end{pmatrix} \quad (6-26)$$

Third, as the matrix in equation 6-26 is a standard rotation matrix for vectors (but with the argument double the spatial rotation angle). Therefore, the two rotations can be combined, since the sequential rotation by two angles equals a rotation by the sum of the two angles.

Fourth, there are two relationships among the TBs (that didn't apply to TAs, so we couldn't use them in the antenna cross-polarization correction), that allows us to work in the Stokes basis, while preserving the robustness of the algorithm with respect to single channel degradation and spurious noise:

$$\begin{aligned} I &= T_v + T_h = T_+ + T_- \quad (\text{primed or unprimed}), \text{ and} \\ I' &= I \quad (I \text{ unaffected by rotation}) \end{aligned} \quad (6-27)$$

Fifth, we must handle that fact that + and – polarizations are not measured at some frequencies, by eliminating the T_U equation and the T_U terms in remaining equation 6-25, analogous to what we did with the M-matrix, i.e.

$$T'_Q = T_Q \cos 2j \quad (\text{in absence of } +, - \text{ channel measurements}) \quad (6-28)$$

Putting all this together, the rotation correction is performed using the sum of the Faraday and polarization rotation, using the following algorithm (Fortran assignments).

$$\begin{aligned} j &= j_{FR} + j_{CMIS} \\ I'' &= T''_v + T''_h, \quad I''_{45} = T''_+ + T''_-, \quad Q'' = T''_v - T''_h, \quad U'' = T''_+ - T''_- \end{aligned}$$

$$I = I'' \quad I_{45} = I''_{45}$$

If have +, – channels at this frequency :

$$Q = Q'' \cos 2j - U'' \sin 2j$$

$$U = Q'' \sin 2j + U'' \cos 2j$$

If not, then : $Q = Q'' / \cos 2j$

$$T_v = \frac{I + Q}{2}, \quad T_h = \frac{I - Q}{2}, \quad T_+ = \frac{I_{45} + U}{2}, \quad T_- = \frac{I_{45} - U}{2}$$

$$T_l = T''_l \quad T_r = T''_r$$

This can be shown to be identical to the rotation correction of equation 6-22; the reason this is equivalent is the use of I_{45} , which keeps the mixing of the v and h polarizations out of the transformation of the 3rd Stokes parameter back to the individual + and – polarized TBs.

6.3.4 Final Form of the Cross Polarization Algorithm

The final cross-polarization correction algorithm for given frequency can be expressed as follows:

- (1) Interpolate the M-matrix to the EIA for that frequency (if necessary)
- (2) Eliminate columns corresponding to polarizations not measured at that frequency
- (3) Invert the column eliminated M-matrix
- (4) Multiply the vector of spillover corrected (scene component of) antenna temperatures by the inverted, column eliminated M-matrix on the left to obtain the (Faraday and polarization) rotated scene brightness temperatures
- (5) Compute the Faraday rotation for the look direction, and add it to the CMIS rotation around the feed boresight (CMIS rotation will not change significantly as each feed for a given frequency observes the same spot on the earth).
- (6) Use the algorithm of the last section to compute the earth scene TBs from the rotated TBs.

6.3.5 Faraday Rotation

6.3.5.1 Background

Faraday rotation is a result of the dispersion relationship for circularly polarized radiation passing through a plasma with non-zero magnetic field. That is, left and right circularly polarized radiation of the same frequency have different wavelengths, leading to a differential phase between the left and right circularly polarized radiation traveling the same distance and direction through the plasma. It is an elementary result of EM theory that linearly polarized radiation with known polarization vector can be decomposed into left and right circularly polarized radiation. The decomposition, propagation, and recombination as linearly polarized radiation shows that the differential phase results in a rotation of the linear polarization vector by the Faraday rotation angle (Rybicki, 1979).

Let the radiation travel along the look direction \hat{l} . We have verified the result of Wu (1977) that the Faraday rotation angle is defined by

$$\phi_{FR} = \frac{135}{\nu^2} \int_{look} n_e \vec{B} \cdot d\vec{l} \quad (6-29)$$

where n_e is the electron density [m^{-3}], B is the magnetic field [gauss], ν is the frequency [s^{-1}], and l is the path [m], and ϕ_{FR} is the rotation angle [deg]. The limits of integration are from the spacecraft to the bottom of the ionosphere. A negative FR indicates a left-handed (counter-clockwise) rotation when looking down from CMIS, while a positive FR indicates a right-handed rotation.

6.3.5.2 Computing Faraday Rotation

There are several choices as to how to evaluate equation 6-29, depending on the data sources available for n_e and B . If n_e and B are available everywhere through the ionosphere, then one can attempt direct integration of the above equation. But, computing the position of each point along the path and accessing the n_e and B values can be very time consuming; given the error n_e in the available sources, approximations to (6-29) are of interest.

A reasonable approximation is to consider the ionosphere as a thin shell (delta function) at the height of the peak of the ionosphere, with a total density equal to the electron density along the look direction. Then equation 6-29 simplifies to

$$j_{FR} \approx \frac{1.35}{n^2} TEC_{path} * [B \cos q_{Btol}] \Big|_{ionospheremax} \quad (\text{thin shell approximation}) \quad (6-30)$$

where we have taken the liberty to express the *total electron content* (TEC) along the look direction in units of TECU [10^{16}m^{-2}] and the frequency in terms of GHz.

One must use a climatology for the TEC if real time observations are not used. Most climatologies can yield the vertically integrated TEC (hereinafter denoted simply TEC). In that case, the thin shell approximation is used with planar assumption to approximate the TEC along the path as

$$TEC_{path} = TEC \sec q_{ion} \quad (6-31)$$

where θ_{ion} is the incidence angle of the look direction onto the thin shell. Equation 6-31 is valid out to about 60 degrees.

θ_{ion} is computed from the law of sines

$$\frac{R_E + H_{SC}}{\sin q_n} = \frac{R_E + H_{ion}}{\sin q_{ion}} \quad (6-32)$$

where R_E is the earth radius, H_{SC} is the spacecraft altitude, and H_{ion} is the altitude of the ionospheric peak, and θ_n is the nadir angle of the CMIS observation.

Therefore, the simplest and least computationally intensive approximation to FR is given by

$$j_{FR} \approx \frac{1.35}{n^2} \frac{TEC}{\cos q_{ion}} * [B \cos q_{Btol}] \Big|_{ionospheremax} \quad (6-33)$$

6.4 Data Needed by the Cross Polarization Correction

6.4.1 CMIS Data

The following table shows the CMIS data needed for the cross polarization correction. The earth incidence angle is used to interpolate the M-matrix (if needed).

The CMIS latitude and longitude, scan azimuth, and nadir angle for the observations of a given frequency are used to compute the geographic location of the intersection of the look direction with a shell of altitude H_{ion} , and incidence angle θ_{ion} at that position. The intersection point used find the magnetic field B and the TEC from the external data sources. The angle between the look direction and the B field is then computed, completing the data needed for the FR computation in (6-33).

Data	Symbol (Units)	Source	Use
Earth scene component of antenna temperatures	T'_A (K)	SDR spillover correction	SDR Cross-pol algorithm
Earth Incidence Angle	θ_{EIA} (deg)	SDR Geolocation Algorithm	Interpolate M-matrix
CMIS rotation angle around antenna boresight	ϕ_{CMIS} (deg)	SDR Geolocation Algorithm	Rotation correction
CMIS latitude, longitude	Lat (deg), Long (deg)	SDR Geolocation Algorithm	Faraday Rotation computation
Radiometer look direction	ϕ_{scan} (deg) scan azimuth from N θ_n (deg) observation nadir angle	SDR Geolocation algorithm	Faraday rotation computation

6.4.2 External Data Sources

External data is used to compute Faraday rotation for the rotation correction. There are two main components to this computation, the magnetic field at the intersection of the peak of the ionosphere (taken to be 400 km), and the total electron content of the ionosphere.

The total electron content is found using the International Reference Ionosphere (IRI) (IRI 1995) as a function of the latitude and longitude, date and time. The IRI is the most advanced model for the ionosphere we found in the available data sources. Several improved editions have been released over a 20 year time period and the database is updated yearly.

For the magnetic field at the intersection of the look direction and the ionospheric peak, we use the International Geomagnetic Reference Field (IGRF).

Given that both IRI and IGRF are climatologies, and the files and data acquisition programs for both will be kept with the SDR algorithm, there is no chance of losing an external data source.

6.5 Requirements Levied on the Cross Polarization Correction

6.5.1 Introduction

In this section, we will discuss the requirements levied on the contributors to cross polarization error. The following sections discuss the contributions from Faraday Rotation, components of the full 6x6 cross polarization matrix that are not measured, knowledge error on the components in the matrix that are measured, and control error on the polarization rotation.

6.5.2 Faraday Rotation

Faraday rotation (FR) as defined in Eq. 6-33 can reach 0.6 degrees around solar max in ascending orbits. IRI simulations showed 0.4 deg (see IDR slide 10c-117 for histograms), but IRI is known to underestimate FR where it is greatest by factor of up to 1/3. The Ocean EDR sensitivity starts at a residual FR of 0.2 degrees, referenced to 10.7 GHz. This implies that the fractional requirement on FR knowledge is 1/3 as shown below in Eq. 6-34

$$\frac{\Delta j_{FR}}{j_{FR}} \leq \frac{0.2}{0.6} = \frac{1}{3} \quad (6-34)$$

This will provide a FR knowledge $\ll 0.2$ deg away from solar max, or away from geomagnetic equator, or for descending orbits.

The IRI database has a TEC of $\frac{\Delta TEC}{TEC} \leq \frac{1}{3}$ under typical conditions.

It is important that knowledge of B and θ do not add significantly to FR knowledge error, i.e.,

$$\frac{\Delta B}{B} \leq 1 \text{ or } 2\% \quad \Delta q_{B \text{ to Look Dir}} \leq 1 \text{ or } 2 \text{ deg}$$

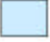
The IGRF B and θ meet these requirements in absence of magnetic storms.

6.5.3 Magnitude Requirement on Cross Polarization Matrix

In Section 6.3.2.3, we discussed the form of the cross-polarization correction for frequencies where less than all 6 polarizations are measured. We found that, in order to obtain a system of equations that could be inverted for the TBs corresponding to antenna temperatures that are measured, we needed to eliminate columns of the M-matrix corresponding to the polarizations that are not measured. When we did that, we found the error in the antenna cross-polarization correction was approximated by the odd columns that we eliminated, times the corresponding scene Stokes parameter (e.g. equation 6-18).

To elucidate this further, we return to the 10 GHz example of that section. At 10 GHz, we do not measure the + and – polarizations. The “+” column of the 10 GHz M-matrix shows that the cross polarization from the + and – polarizations into the v,h,l, and r polarizations is .88%, .85%, .024% and .0042%, respectively as shown in Figure 6-2; equation 6-18 states that the *residual* cross polarization from the third Stokes parameter, U, into the SDR derived TBs for the v,h,l, and r polarizations will then be approximately .88%, .85%, .024% and .0042%, respectively. This is what we mean when we say that one cannot correct for the cross-polarization from polarizations not measured; if a pair of orthogonal polarizations corresponding to the nth Stokes parameter are not measured, then the residual cross polarization in the SDR TB product from the nth Stokes parameter will be approximately the same as that in the original antenna temperatures. n is always 3 or 4, since at all frequencies the v and h polarizations are measured.

6.8 GHz	v	h	+	-	l	r
v _{ant}	0.995960	0.004040	0.015037	-0.015037	0.000122	-0.000122
h _{ant}	0.004064	0.995936	-0.015183	0.015183	-0.000057	0.000057
10.7 GHz	v	h	+	-	l	r
v _{ant}	0.995940	0.004060	0.008793	-0.008793	-0.000047	0.000047
h _{ant}	0.004213	0.995787	-0.008515	0.008515	0.000028	-0.000028
l _{ant}	0.000067	-0.000067	-0.000239	0.000239	0.999440	0.000560
r _{ant}	0.000207	-0.000207	-0.000042	0.000042	0.000561	0.999439
18.7 GHz	v	h	+	-	l	r
v _{ant}	0.996780	0.003220	-0.004918	0.004918	-0.000010	0.000010
h _{ant}	0.003031	0.996969	0.004999	-0.004999	0.000006	-0.000006
+ _{ant}	0.002095	-0.002095	0.996922	0.003078	0.000012	-0.000012
- _{ant}	-0.001863	0.001863	0.003133	0.996867	-0.000009	0.000009
l _{ant}	-0.000089	0.000089	0.000176	-0.000176	0.998484	0.001516
r _{ant}	-0.000183	0.000183	0.000094	-0.000094	0.001515	0.998485
23.5 GHz	v	h	+	-	l	r
v _{ant}	0.997194	0.002806	0.023023	-0.023023	0.000021	-0.000021
h _{ant}	0.002761	0.997239	-0.023190	0.023190	-0.000020	0.000020
37 GHz	v	h	+	-	l	r
v _{ant}	0.997992	0.002008	0.001088	-0.001088	0.000005	-0.000005
h _{ant}	0.002027	0.997973	-0.001120	0.001120	-0.000001	0.000001
+ _{ant}	0.001097	-0.001097	0.997972	0.002028	-0.000003	0.000003
- _{ant}	-0.001110	0.001110	0.002008	0.997992	-0.000001	0.000001

 In optimized channel set

Derived Requirement:

Not in channel set (white):
Effective average cross-pol contribution ≤ 0.02

White columns cannot be used in cross-pol correction (these columns are "eliminated"). That is, blue (dark) defines the square matrices used in the cross-pol correction.

Figure 6-2: Zero error M-matrices computed from antenna design. The assemblage of blue columns for each frequency defines the M-matrices used by the cross polarization correction. The white columns correspond to cross polarization from the polarizations not measured at each frequency; they represent cross polarization from the 3rd and/or 4th Stokes parameters that cannot be corrected. The residual cross polarization from these Stokes parameters is approximately that shown in the white columns, as per equation 6-18.

One can therefore read directly from the white columns of the M-matrix in Figure 6-2 what the residual cross polarization will be in the SDR TB product. For example, at 6 GHz, the SDR TB product for the v polarization will contain a residual cross polarization of 1.5% from the 3rd Stokes parameter, and 0.012% from the 4th Stokes parameter; the SDR TB product for the 6 GHz h polarization will contain 1.5% residual cross polarization from U and 0.0057% from the 4th Stokes parameter.

6.5.3.1 Need for Requirement

The residual cross polarization in the SDR produced TBs due to not measuring certain polarizations at some frequencies is always proportional to either the 3rd or 4th Stokes parameters, which are small for ocean scenes (a few K or less). Never the less, we need to insure that the residual cross polarization is small enough that the performance of the EDR algorithms is not significantly affected. Therefore, we perform a sensitivity analysis to residual cross polarization, which in this context, is really a sensitivity analysis to the magnitude of the elements in the white columns of the M-matrices shown in Figure 6-2.

6.5.3.2 Sensitivity Analysis and Requirement Value

To place a requirement on the magnitude of the columns of the M-matrix, we perform a sensitivity analysis using the ocean EDR algorithms. For this purpose, we use the radiosonde test data sets for the SST and wind EDR algorithms described in the Ocean EDR ATBD, Section 5. The sensitivity analysis consists of 4 steps. In the first step, spillover corrected antenna temperatures for each measured polarization are simulated; these simulated antenna temperatures contain the cross polarization defined by the zero error M-matrices. To do this we simulate

ocean scene TBs for all 6 polarizations, and then multiply the vector of 6 TBs by the M-matrices. The full M-matrices are used. In the second step, NEDTs are simulated and added to the antenna temperatures. The third step is to apply the cross polarization correction to the simulated antenna temperatures, using the columns in blue of Figure 6-2, to simulate the SDR TB product. The fourth step is to use the ocean EDR retrieval algorithms on the simulated SDR TB product, and collect the error statistics.

The M-matrices used in the first and third steps are those of Figure 6-2 ; however, the magnitude of the white columns are altered in magnitude (but not in sign) to a constant value for single run through all the test data. This constant value is stepped through values ranging from 0 to 0.06 in increments of 0.005 over the 13 runs comprising the sensitivity analysis. Recalling equation 6-18, this value roughly corresponds to the residual cross polarization in the SDR TBs from the Stokes parameters corresponding to the polarizations not measured at a given frequency.

The results of the sensitivity analysis are shown in Figure 6-3. We show the bias and standard deviation error (precision) for each ocean algorithm (except SST, where only the RMS error or uncertainty is shown). The requirement of 0.02 is set based on the SST uncertainty, which is the only EDR error showing sizable sensitivity.

The seemingly anomalous lack of sensitivity in the warmest SST bin is actually a result of the SST test data set, which has a low range of wind speeds at the highest SSTs; since the residual cross polarization in the 6 GHz SDR TBs results from the 3rd and 4th Stokes parameters, and these are increasing functions of wind speed, the residual cross polarization has little effect on the SDR TBs at high SST. Wind direction precision is not significantly affected the residual cross polarization (i.e. magnitude of the matrix elements in the white columns). However, the fact that the (residual cross polarization from the) 3rd or 4th Stokes parameters is correlated with the true wind direction means that the wind direction bias is affected, although the sensitivity is not large enough to cause the performance to exceed the accuracy requirement at the largest magnitude value in the sensitivity analysis.

In the sensitivity analysis we replaced each element in the white columns with a constant magnitude for each run. As shown in Figure 6-2, in reality these matrix elements are not similar in magnitude. Therefore, the sensitivity analysis is really with respect to the average value of the magnitude of the matrix elements in the white columns. This is why we state the requirement as “effective magnitude of the white columns, averaged over all elements, less than or equal to 0.02.”

EDR Sensitivity to Magnitude of Eliminated M-Matrix Columns

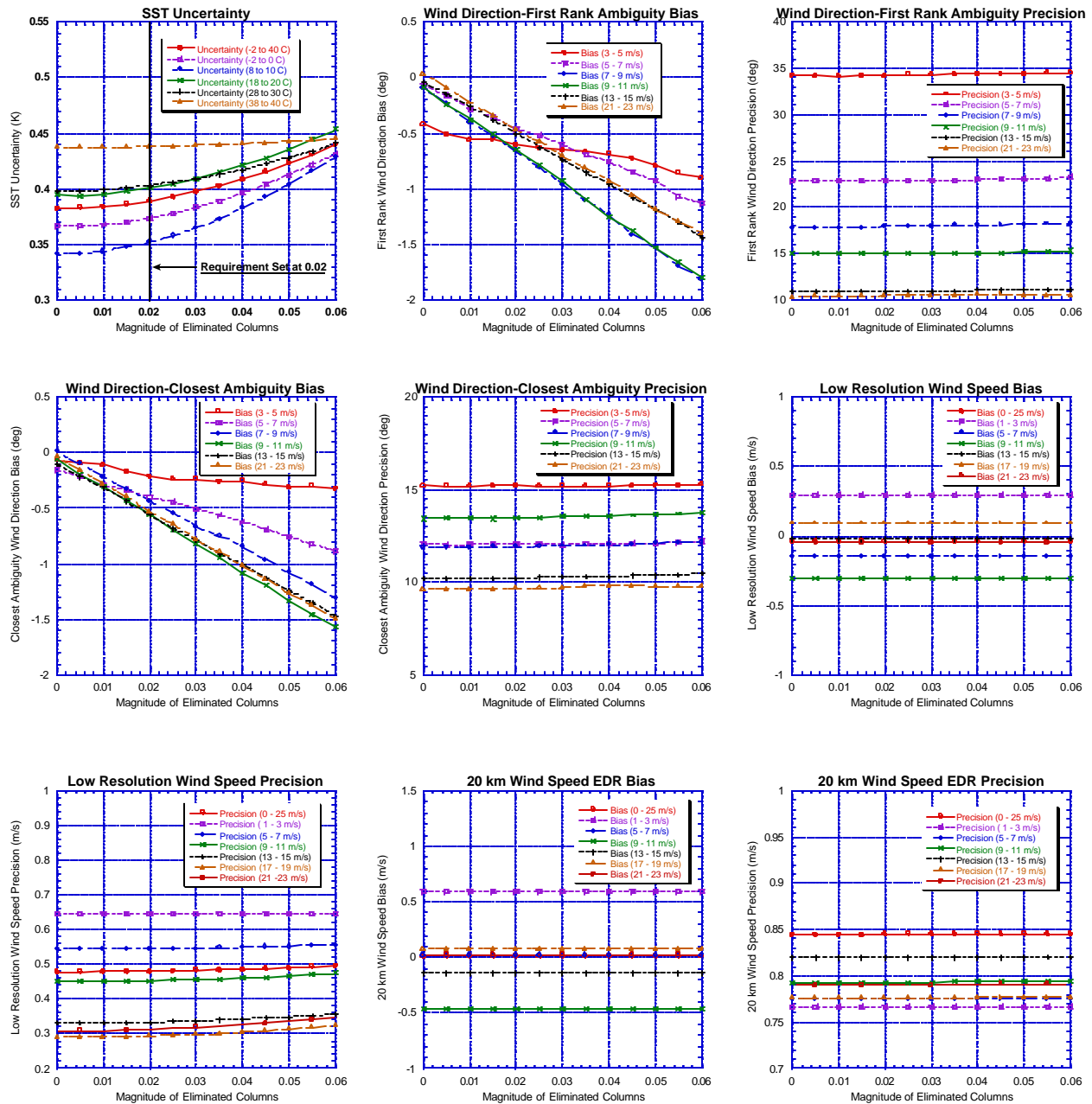


Figure 6-3: Sensitivity Analysis for the Magnitude of the Columns of the M-matrix Eliminated in the Cross Polarization Correction. SST Uncertainty drives the requirement to be set at 0.02, on average, over the all the eliminated columns, 6-36 GHz.

In each sensitivity analysis that follows, we will be showing a matrix of sensitivity plots analogous to Figure 6-3. In each we will be signifying the EDR errors that drive the setting of a requirement using a vertical line drawn at the requirement value in the corresponding plot. We generally only label the requirement in the first instance of a vertical line. We do not put this vertical line in EDR errors plots where, even at the maximum sensor error value shown in the plot (usually 2 or 4 times the requirement value), we do not reach an EDR error threshold. For

example, even though wind direction accuracy shows some sensitivity to the magnitude of the elements in the white columns of the M-matrices, we do not show the requirement in those plots, because the sensitivity is not strong enough to be of concern, even at the maximum x-axis value shown in the plots.

6.5.4 Cross Polarization Knowledge Requirement

6.5.4.1 The Nature of Cross Polarization Knowledge Error

By *knowledge error*, we mean the difference between a measured or computed value of a sensor parameter, and that parameter's true value. To understand the nature of the cross polarization knowledge error, it is important to understand its source. The M-matrices that are used in the antenna cross polarization correction will be computed from range measurements of the antenna gain patterns and phases. These range measurements are imperfect, due to many factors that are included in the antenna range error budget. Some of these include imperfections in the antenna range, test probe to CMIS alignment, and noise in the measurement process.

The knowledge error in the M-matrices is due to the errors in the range measurements. State of the art range measurements produce a 0.001 knowledge error in the M-matrices computed from them.

The cross polarization knowledge error is relatively constant over CMIS observations. That is, the knowledge error is mostly bias and little noise. For observations at a constant EIA, the M-matrices used in the cross polarization correction are fixed (constant). Furthermore, the fixed geometry of the feed/reflector system keeps the cross polarization (i.e. true M-matrix) constant. Therefore the knowledge error is almost completely dominated by a bias, not noise.

Now consider the case where the EIA varies between the observations, as we know it will for an oblate earth. The variation of the M-matrices with EIA is rather weak (2×10^{-5} /degree), about 50 times smaller than the knowledge error bias component, per degree of EIA change.

The only other source that could cause the true antenna cross polarization, and therefore the knowledge error, to vary would be motion of the antenna relative to the feeds, i.e. vibrational modes of the antenna. The amplitudes of the modes are small, and initial computations with theoretical gain patterns and phases taken at different points in the major modes show that the variation of the M-matrices is exceedingly small.

Now, sensor knowledge error biases tend to cause biases in the EDRs, whereas knowledge noise tends to affect EDR precision. Therefore, it is worth performing a two sensor error sensitivity analyses, one with cross polarization knowledge treated as constant (a bias), and another where the knowledge error is Monte Carloed for each observation (i.e., treated as noise).

6.5.4.2 Sensitivity Analysis

We use another end-to-end simulation to determine the EDR sensitivity to the cross polarization knowledge error. Again, the test data sets for the SST and wind algorithms serve as the starting point for the analysis. The first step is to simulate antenna temperatures for each measured polarization. This is accomplished as described in section 6.5.3.2; now the zero error M-matrices of Figure 6-2 are used as the "truth M-matrices." We then add a realization of the cross polarization knowledge error to the truth M-matrices, and use them in the cross polarization

correction to produce simulated SDR TB products. The simulated SDR TB products are then input to the EDR algorithms, and error statistics are collected.

There are two possibilities for how the realization of the cross polarization knowledge error is treated. We could select a knowledge error realization—that is select a knowledge error for each element of each M-matrix—and hold it fixed (constant) for all observations in the simulated data set. This method corresponds to the fact that the knowledge error is a constant (i.e., a bias). Therefore we call this mode of simulating the cross polarization knowledge the “bias mode”.

The other possibility is that we could choose a new realization for the knowledge error for each simulated observation—i.e., the knowledge error for each matrix element changes from observation to observation. The realizations are most easily generated by Monte Carloing the knowledge error for each matrix element for each observation. We therefore call this mode of simulating cross polarization knowledge the “Monte Carlo mode.”

There are advantages and disadvantages to each mode of simulating the knowledge error. The bias mode duplicates what we know about the M-matrix knowledge error—that it is constant over the retrievals. The drawback is that one is forced to choose a single knowledge error realization. The EDR error statistic may depend on the realization, and the chosen realization is unlikely (given there are 54 independent elements in the knowledge errors for the 6-36 GHz M-matrices) to represent the actual knowledge error in each element.

On the other hand, the Monte Carlo mode avoids the dependence of the EDR errors on a particular choice of the realization of the knowledge error, given that the realization is changed for each simulated observation. On the other hand, it turns what we know is a bias into noise, which increases the EDR precision error sensitivity to the knowledge error.

Since neither mode of simulation exactly represents the physical situation, we perform the sensitivity analysis both ways—bias mode and Monte Carlo mode. We take care of two problems at once with the Monte Carlo mode simulation; we avoid reliance on a particular realization of the knowledge error, and at the same time, this simulation method doubles as the sensitivity analysis to any variation of the M-matrix knowledge, and allows us to set a requirement on the variation of the knowledge error (due to EIA variability or vibrational modes of the antenna relative to the feeds).

6.5.4.2.1 Bias Mode Simulation

We begin with the sensitivity analysis using the bias mode for M-matrix knowledge error simulation. As mentioned above, we must choose a particular realization of the knowledge error for each element of the M-matrix. We chose a realization that, physically, makes the most sense. That is we assume that the effect of the range errors in the measurement of the antenna gain functions and phase act so as to reduce the polarization purity and increase the cross polarization in the M-matrices computed from the range measurements. In practice, this means that the knowledge error in diagonal elements formed by the blue columns in Figure 6-2 is negative; the knowledge error in all other elements is determine so that the magnitude of the cross polarization is increased, while preserving the sign of the matrix elements. We call this the “co-pol down, cross-pol up” realization, because it simulates the case where the co-pol elements are smaller and the cross-pol elements are larger in the measured M-matrix (the one used in the correction) as compared to the true M-matrices.

The magnitude (but not the sign) of the knowledge error for each M-matrix element is the same. Thus there is one parameter that governs the cross polarization realization for each run in the

sensitivity analysis. This parameter is stepped from 0 to 0.004 in increments of 0.0005 or 0.001 between each pass over the test data set.

The results, shown in Figure 6-4, show that all EDR error statistics are affected by cross polarization knowledge error, when treated as a constant bias. The greatest sensitivity, in terms of creating EDRs errors that approach or exceed those specified in the SRD, is in the SST EDR. That is the SST EDR errors drive the requirement to be set as low as 0.001. However, the first rank wind direction biases, as a function of wind direction bins, are also very sensitive to this error. While the SRD wind direction accuracy error requirements are phrased in terms of wind direction bins (i.e include all wind directions), and the wind direction accuracy over all wind direction bins (i.e. unbinned in wind direction) remains near zero for all wind speeds (not shown), it makes us uncomfortable to allow the accuracy errors in each wind direction bin to approach the 10 deg requirement. Therefore, first rank wind direction bias is also shown as a driver in setting the requirement, although, considering this error alone, the requirement would not have to be set as low as 0.001.

We also show first rank and closest ambiguity wind direction precision as drivers in setting this requirement, due to the sensitivity of the first rank precision, and the fact that, if we did not constrain the cross polarization knowledge error to less than the maximum value shown in the plots, the closest ambiguity wind direction precision would exceed the 20 degree requirement.

EDR Sensitivity to M-Matrix (Cross Polarization) Knowledge Bias

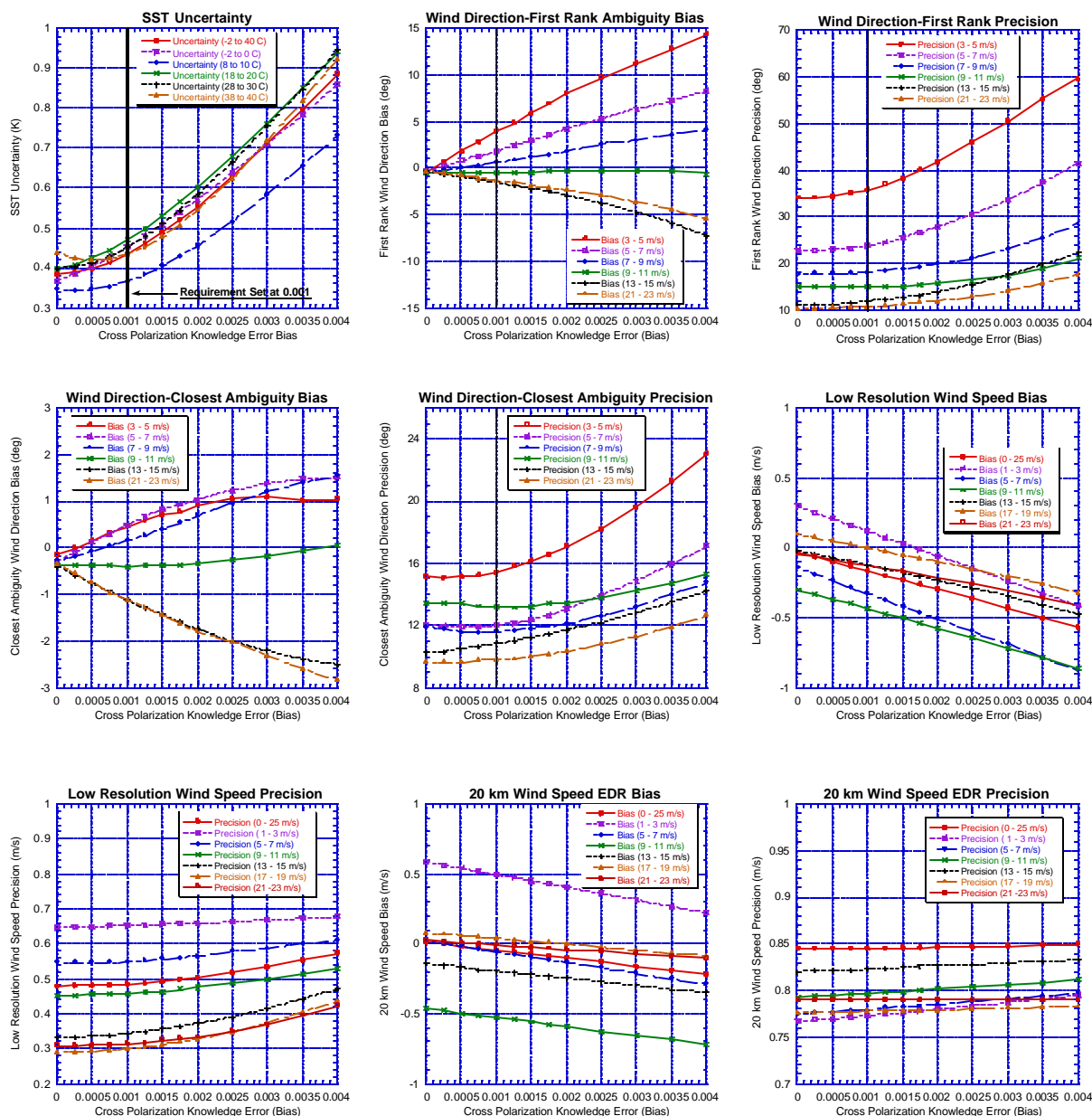


Figure 6-4: Bias mode sensitivity analysis for cross polarization knowledge error. The knowledge error realization is “co-pol down, cross-pol up.”

6.5.4.2.2 Monte Carlo Mode Simulation

For this mode, we chose the knowledge error realization for the 54 independent knowledge error terms in the 6-36 GHz M-matrices by selecting them from a Gaussian distribution with known sigma and zero mean. Thus, the 1-sigma of the Gaussian distribution is the parameter that is varied between each pass through the test data set. The results are shown in Figure 6-5 (note the x-axis scale change to 1/2 of what is was in Figure 6-4). The fact that the knowledge error realization is changed every observation in a run means that the effect of the knowledge error is

to create noise the simulated SDR TB product. That is, the effect of the knowledge errors on the SDR TBs is not unlike the NEDTs. As TB noise tends to affect the EDR precision errors, while leaving the EDR bias errors alone, we expect the sensitivity to be in EDR precision (and SST uncertainty), and not in the EDR biases, which is borne out by the figure.

EDR Sensitivity to M-Matrix (Cross Polarization) Knowledge Noise

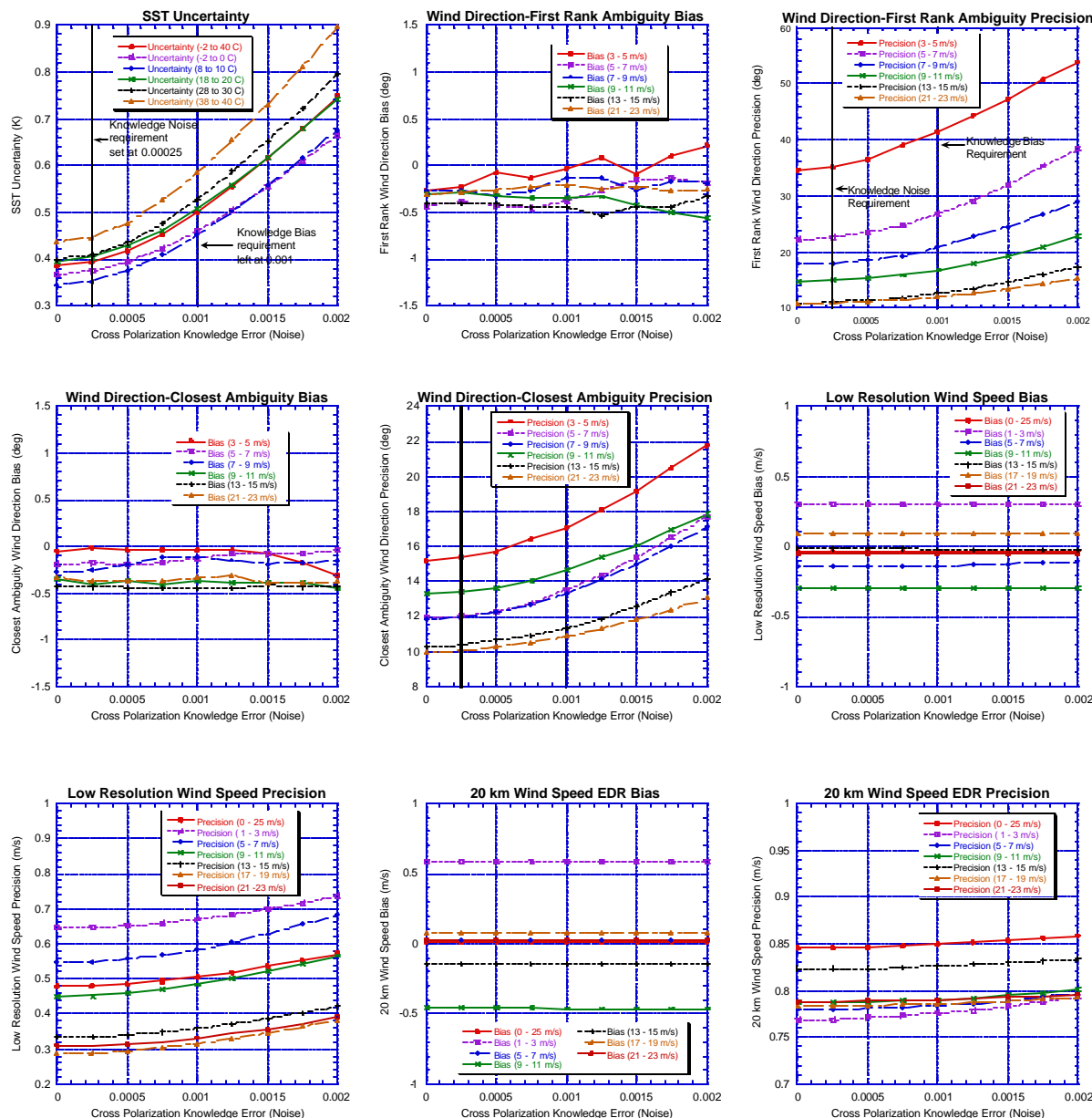


Figure 6-5: EDR Sensitivity analysis to cross polarization noise, using the Monte Carlo Mode simulation. Sensitivity of EDR precision is greatly amplified compared to the bias mode simulation. We use this simulation to set the cross polarization knowledge noise requirement (at 0.00025 = -36dB), and leave the cross polarization knowledge bias requirement at that value found in the bias mode simulation (0.001).

However, due to using a Gaussian distribution for the knowledge error, there are many cases in which the knowledge error in individual matrix elements is much larger than the 1-sigma value,

so the sensitivity to the knowledge error simulated in Monte Carlo mode tends to be more pronounced than that seen in the bias mode simulations, for the same value of the x-axis. This increased sensitivity gives us pause when considering setting a requirement on the M-matrix knowledge bias using the Monte Carlo mode analysis. We also know that state of the art range measurements yield a 0.001 knowledge bias in the M-matrices, so there is no point in setting the requirement lower. (In any case, in the next few sections we identify the mechanism for EDR sensitivity, and show that the on-orbit calibration of the CMIS measurements to the RTM will greatly reduce the influence of cross polarization knowledge on the EDR errors.) We therefore retain the 0.001 cross polarization knowledge bias requirement, derived from the bias mode simulations.

However, as mentioned before, the Monte Carlo mode simulations double as the sensitivity analysis to variation of the cross polarization knowledge (i.e. “knowledge noise”) over the CMIS observations. This variation should be much smaller than the knowledge bias, for reasons outlined in Section 6.5.4.1 (mainly that the reflector-feed geometry is fixed, up to the vibrational modes). But, not wanting to leave any aspect of the cross polarization problem unconstrained, we derive a requirement for the cross polarization knowledge noise component using the sensitivity analysis of Figure 6-5. We therefore reproduce the knowledge bias requirement from Figure 6-4 in Figure 6-5, and also show the requirement for the knowledge noise component.

The requirement for the noise component must be set much smaller than the knowledge bias component, due to the increased sensitivity. Again it is the SST EDR errors that drive the requirement to the value set. The wind direction precision for both first ranked and closest ambiguities show intermediate sensitivity, and the closest ambiguity precision for the 3-5 m/s bin would be larger than 20 degrees if we didn’t set a requirement lower than the maximum knowledge noise shown in the plots; while the first ranked ambiguity has no SRD requirement, we consider a precision error of 50 degrees in the 3-5 m/s bin an indication that the first rank ambiguity is losing its usefulness as a retrieved parameter. Therefore, both first rank and closest ambiguity precision are drivers in setting the requirement, although the requirement would be set somewhat looser if these were the only EDRs to consider. We therefore set a requirement of 0.00025 (-36 dB) on the cross polarization knowledge noise component so that the SST uncertainty errors are not greatly increased.

6.5.4.3 Mechanism of EDR Sensitivity

The EDRs are sensitive to errors in their M-matrix knowledge $\Delta M = M_{\text{meas}} - M_{\text{true}}$. The residual error in the matrix multiplication of M can be expressed by $\Delta M' = M_{\text{meas}}^{-1} M_{\text{true}} - I$, where for small ΔM , $\Delta M' \approx -\Delta M$.

The following definitions are used to combine the differences of the various polarizations:

$$T_Q = T_v - T_h ; T_U = T_+ - T_- ; T_4 = T_l - T_r$$

The error in the SDR brightness temperature for p-polarization can then be expressed as:

$$\Delta T_p = \Delta M'_{pv} T_Q + \Delta M'_{p+} T_U + \Delta M'_{pl} T_4 \quad (6-35)$$

which can be broken down into a bias and noise component

$$\text{bias: } \langle \Delta T_p \rangle = \Delta M'_{pv} \langle T_Q \rangle + \Delta M'_{p+} \langle T_U \rangle + \Delta M'_{pl} \langle T_4 \rangle \quad (6-36)$$

$$\text{noise: } \mathbf{s}_{\Delta T_p}^2 = \Delta M_{pv}'^2 \mathbf{s}_{T_Q}^2 + \Delta M_{p+}'^2 \mathbf{s}_{T_U}^2 + \Delta M_{pl}'^2 \mathbf{s}_{T_4}^2 \quad (6-37)$$

Table 6-1 shows the expected values of the bias and random polarization difference components for a Rayleigh distribution of wind speeds over the ocean. From this table and Eqs. 6-36 and 6-37, it is clear that the TB error is mainly a bias resulting from a large value of $\langle T_Q \rangle$, called the “ T_Q bias”. A large $\langle T_Q \rangle$, σ_Q for ocean scenes implies first two cols of the M-matrix uncertainty, shown in Table 6-2, have greatest impact on SDR TB error. Setting the requirement for $\Delta M = 0.001$, which is achievable for state of the art range measurements yields a TB bias of ± 0.04 to 0.09 K in SDR derived ocean scene TBs, with even less bias for polarized scenes. The TB noise is very small ranging from 0.006 to 0.014 K.

Freq	$\langle T_Q \rangle$	$\langle T_U \rangle$	$\langle T_4 \rangle$	σ_{TQ}	σ_{TU}	σ_{T4}
6.8	86	0	0	6	0.7	0.3
10.7	91	0	0	7	1.1	0.5
18.7	62	0	0	9	0.9	0.4
23.5	43	0	0	14	0.7	0.3
37	55	0	0	11	0.8	0.3

Table 6-1 Expected values of polarization differences over Ocean

6.8 GHz	v	h	+	-	l	r
v,ant	0.995960	0.004040	0.015037	-0.015037	0.000122	-0.000122
h,ant	0.004064	0.995936	-0.015183	0.015183	-0.000057	0.000057
10.7 GHz	v	h	+	-	l	r
v,ant	0.995940	0.004060	0.008793	-0.008793	-0.000047	0.000047
h,ant	0.004213	0.995787	-0.008515	0.008515	0.000028	-0.000028
l,ant	0.000067	-0.000067	-0.000239	0.000239	0.999440	0.000560
r,ant	0.000207	-0.000207	-0.000042	0.000042	0.000561	0.999439
18.7 GHz	v	h	+	-	l	r
v,ant	0.996780	0.003220	-0.004918	0.004918	-0.000010	0.000010
h,ant	0.003031	0.996969	0.004999	-0.004999	0.000006	-0.000006
+,ant	0.002095	-0.002095	0.996922	0.003078	0.000012	-0.000012
-,ant	-0.001863	0.001863	0.003133	0.996867	-0.000009	0.000009
l,ant	-0.000089	0.000089	0.000176	-0.000176	0.998484	0.001516
r,ant	-0.000183	0.000183	0.000094	-0.000094	0.001515	0.998485
23.5 GHz	v	h	+	-	l	r
v,ant	0.997194	0.002806	0.023023	-0.023023	0.000021	-0.000021
h,ant	0.002761	0.997239	-0.023190	0.023190	-0.000020	0.000020
37 GHz	v	h	+	-	l	r
v,ant	0.997992	0.002008	0.001088	-0.001088	0.000005	-0.000005
h,ant	0.002027	0.997973	-0.001120	0.001120	-0.000001	0.000001
+,ant	0.001097	-0.001097	0.997972	0.002028	-0.000003	0.000003
-,ant	-0.001110	0.001110	0.002008	0.997992	-0.000001	0.000001

Table 6-2 M-Matrix uncertainty contributing to TB bias is driven by 1st two columns

6.5.4.4 Cal/Val Bias Removal and EDR Sensitivity

The CMIS EDR algorithms are trained or based on a RTM. In some cases the differences between the RTM and truth can overshadow the effects of sensor errors. Ocean emissivity models are not accurate to 0.1% and there are uncertainties in water vapor and oxygen absorption. For this reason, it is necessary to calibrate the CMIS sensor to the RTM, even if there were no sensor errors.

A post launch calibration validation period can be used to collect data to determine the slope and bias between the RTM and the measured TBs. This is especially important for ocean EDRs, which are very sensitive to RTM vs measurement bias. Biases in TBs w/r/t RTM are removed in lump-sum, regardless of source.

This includes biases resulting from knowledge bias of the following sources, in rough order of size:

- Spillover (slope)
- Warm load temp (slope)
- Cross-polarization (constant)
- Earth incidence angle (EIA) (constant)
- CMIS rotation (constant)
-

The knowledge bias of the last 3 sources cause TB noise as well as TB bias, however the TB bias generated is larger than the noise generated by a factor of 3 to 20 (with the exception of EIA bias in 18-36 GHz h-pol). Therefore calibration to the RTM effectively removes the influence of all these knowledge biases on the EDRs. Figure 6-6 shows the basic process to calibrate the CMIS sensor to the RTM.

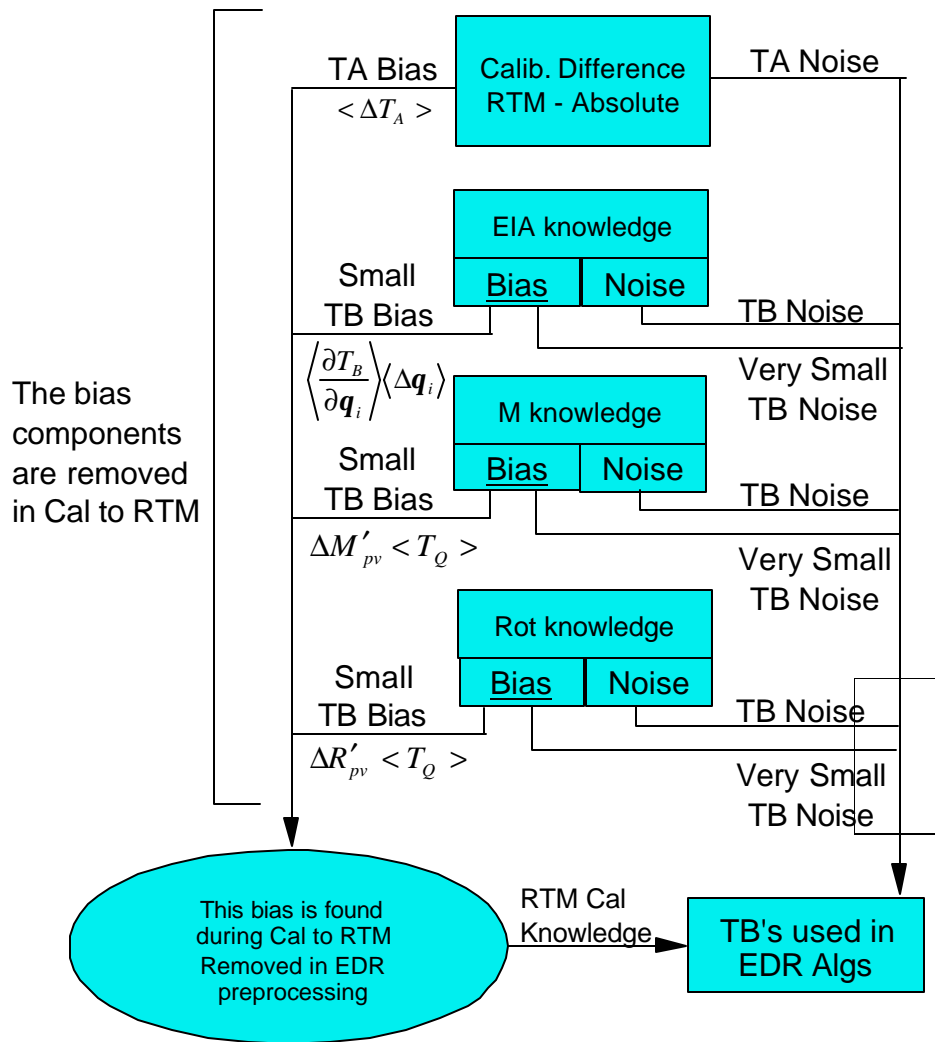


Figure 6-6: Basic process to calibrate the CMIS sensor to the RTM

EDR Sensitivity to Cross Polarization Knowledge Bias, Including Simulation of Calibration of CMIS Measurements to the RTM

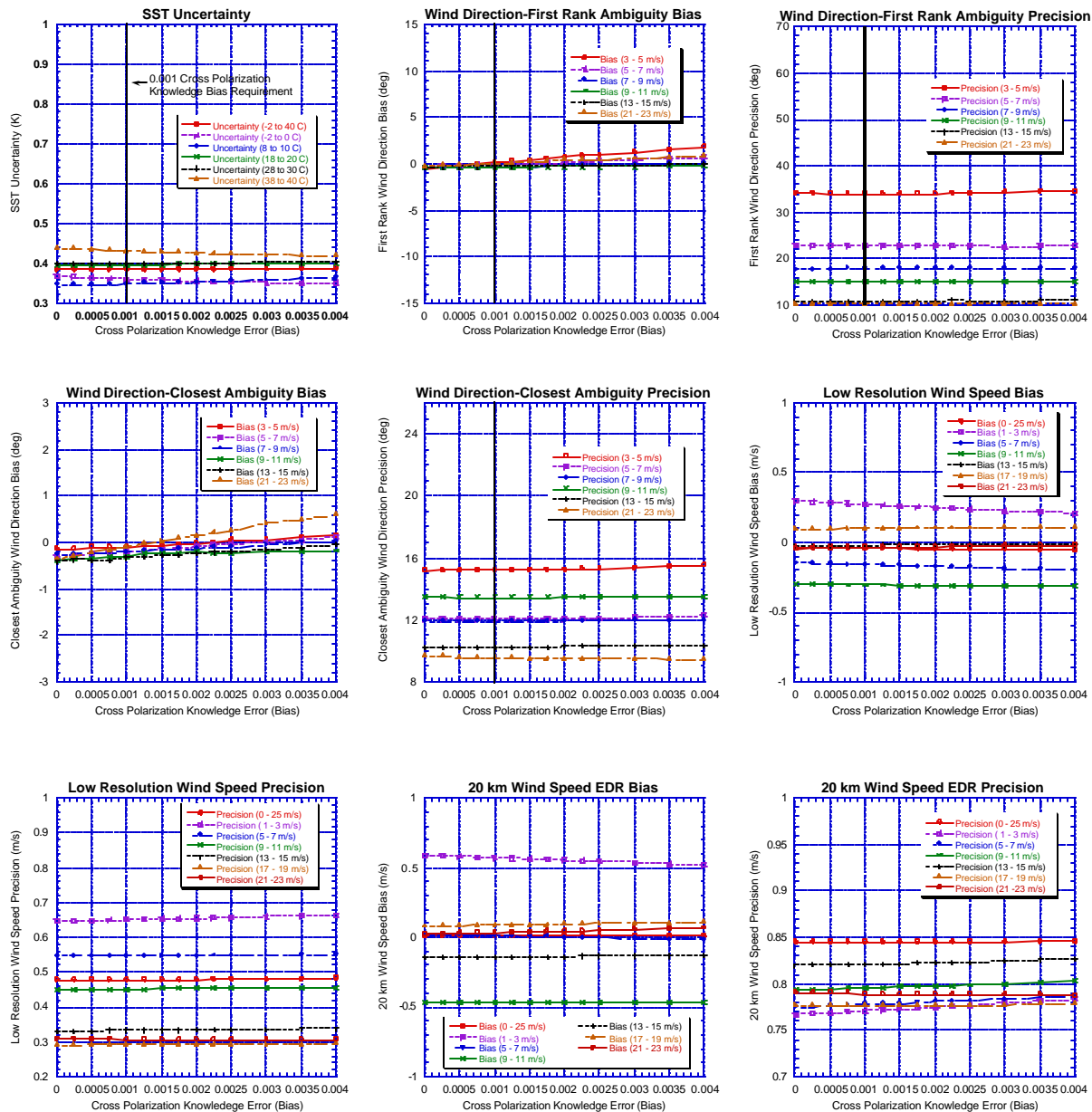


Figure 6-7: Reduction in EDR sensitivity to cross polarization knowledge bias, after calibration of CMIS measurements to the RTM. Calibration to RTM simulated by removing mean TQ bias, using mean TQ over test data sets.

Figure 6-7 shows the result of simulations of the EDR sensitivity to the cross polarization (M-matrix) knowledge errors after the CMIS sensor has been calibrated to the RTM by removing TQ bias. This figure should be compared to Figure 6-4, which shows the same plots prior to the bias removal. Notice how the calibration to the RTM can effectively mitigate the effects of M-matrix knowledge uncertainty, since this uncertainty causes a bias in TB which can be detected and removes. Note that for some knowledge error measurement ranges (e.g. SST 38⁰ to 40⁰ C), the graphs indicate that the EDR uncertainty decreases with increasing bias uncertainty, which is an artifact of the simulation. The bias removal utilizes the entire measurements range (e.g.

SST -2° to 40° C), so the arbitrary binning of sub-ranges for display can show some bins having performance better/worse than the average.

6.5.4.5 Conclusions

The Ocean EDRs are sensitive to errors in the cross-polarization knowledge. Biases in the M-matrix knowledge lead to bias and noise errors in the TB, which in turn effect the EDRs. In general, the M-matrix bias error produces a much larger TB bias error than TB noise error. The EDR sensitivity is driven by the TB bias error, which is dominated by the TQ bias (or bias between the vertical and horizontal polarization). A post-launch calibration of the sensor to the RTM can remove the TQ bias. This greatly reduce the EDR sensitivity to M-matrix knowledge uncertainty

6.5.5 CMIS Polarization Rotation Control Error Requirement

6.5.5.1 Need for Requirement

As shown in section 6.3.3, the + and – polarized antenna temperatures participate in the correction for CMIS and Faraday rotation corrections for the v and h channels. At frequencies where the + and – antenna temperatures are not measured (all frequencies except 18 and 36 GHz), we cannot use them in the derotation for the v and h polarizations. The situation is analogous to that for cross polarization correction; at frequencies where these polarizations are not measured; we cannot correct from cross polarization from the + and – channels when the corresponding antenna temperatures are not measured. In the case of antenna cross polarization, we set a limit on the corresponding columns of the M-matrices. Here, we set a requirement on the magnitude of the + and – columns of the rotation matrices, which is equivalent, via equation 6-x, to setting a requirement on the magnitude of the CMIS polarization rotation control error. The sensitivity of the EDR algorithms to the absence of + and – polarized measurements is included implicitly in the sensitivity analysis for Faraday rotation knowledge; we assumed a 0.6 degree Faraday rotation (at 10.7 GHz), onto which the knowledge error was added in the derotation.

Figure 6-8 shows the sensitivity analysis of each of the ocean EDRs with respect to the CMIS polarization rotation angle. For each run through the test data sets that makes up the sensitivity analysis, the polarization rotation angle is chosen from a Gaussian distribution with zero mean and known, sigma (shown on x-axis). A different rotation angle is chosen for every observation (retrieval) in each run.

A requirement of 0.6 degrees (1-sigma) is placed on the CMIS polarization rotation control error, driven by the SST uncertainty error increase. This is a top-level requirement, including spacecraft attitude, known CMIS misalignments to the spacecraft, any known rotation of the actual earth scene polarization vectors compared to that for a spherical earth.

Given the tight control on the spacecraft attitude and CMIS to spacecraft misalignments, this is a very loose requirement. But, it can be compared with the requirement on the magnitude of the white columns of the M-matrix. Plugging 0.6 deg into the rotation matrix shown earlier shows that this requirement is equivalent to accepting a 0.01 residual cross polarization from the 3rd Stokes parameter into the v and h polarizations ($\sin(0.6)\cos(0.6)=0.01$) after the derotation is done.

EDR Sensitivity to CMIS Polarization Rotation Control Error (Monte Carlo'd as Gaussian Noise, with 1-sigma on x-axis)

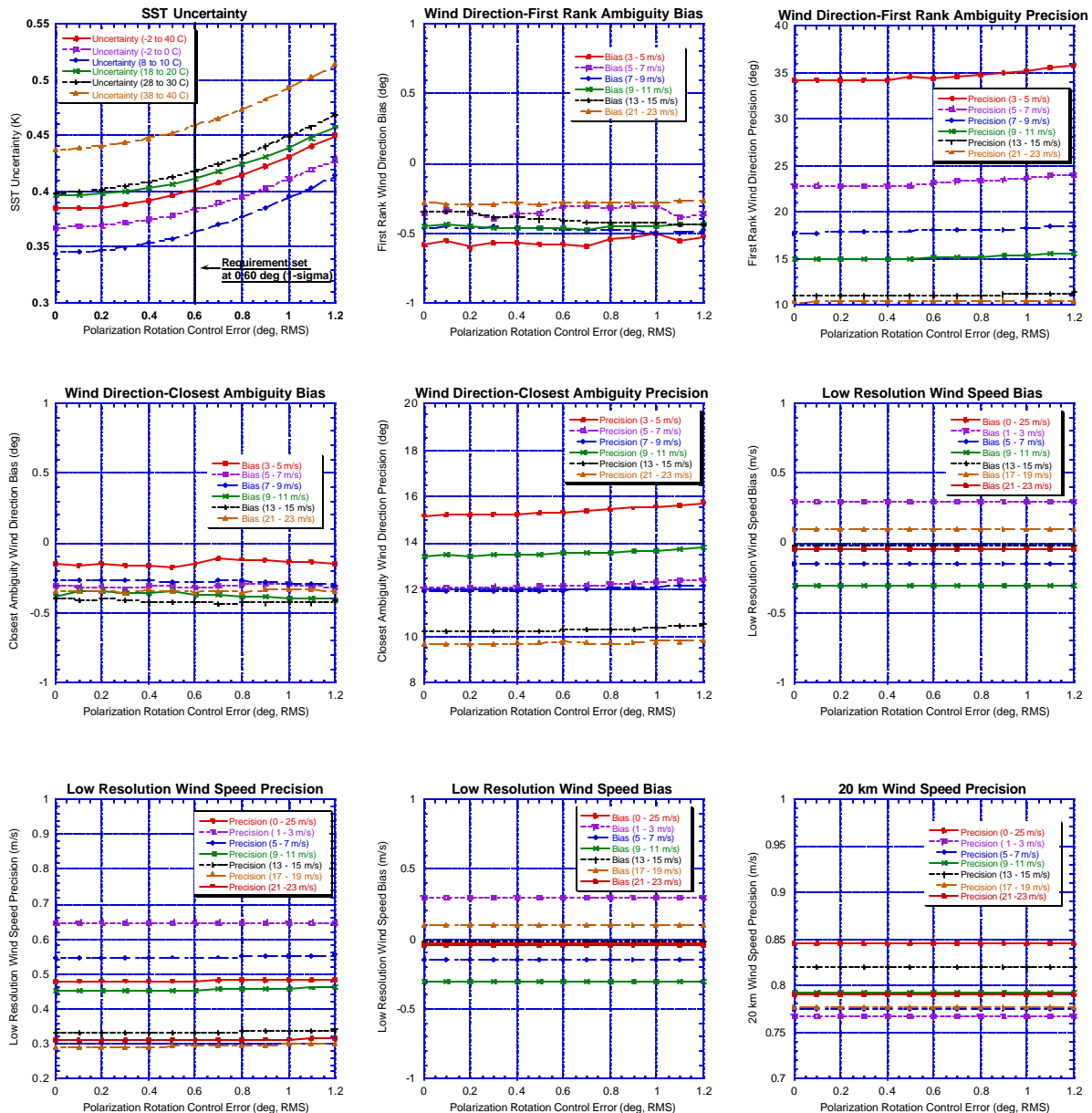


Figure 6-8: EDR sensitivity to CMIS polarization rotation control error. This is a Monte Carlo mode simulation where the rotation angle is different for each observation in the test data sets.

6.5.6 CMIS Polarization Rotation Knowledge Error Requirement

Polarization rotation knowledge is another sensor error that could benefit from considering the bias and noise components separately; analogous to cross polarization knowledge, the bias component causes a bias in the SDR TB product that is proportional to TQ. In fact, one can simply substitute the R matrix for the M-matrix in the discussion of the TB bias caused by M-

matrix knowledge bias, to determine the size of the TB bias due to the bias component of the rotation knowledge error.

The fact that the knowledge bias component causes a bias in the TB product means that the calibration to the RTM will greatly reduce EDR algorithm sensitivity to the knowledge bias, analogous to the situation with the cross polarization knowledge bias. This would allow us to set a looser requirement on the bias component than on the noise component of the polarization rotation knowledge.

However, the sensitivity to polarization rotation knowledge is less than that for cross polarization knowledge, so the benefit to the EDR performance and requirements setting by splitting up the polarization rotation knowledge into bias and noise components is small. Furthermore, we ran short of time to bifurcate this sensitivity analysis.

Therefore, we set a single requirement on the overall RMS (uncertainty, including bias and noise). For the sensitivity analysis, we simulate the entire polarization rotation knowledge error as noise, knowing that this will enhance EDR sensitivity and result in setting a tighter overall uncertainty requirement than if we had considered the bias and noise components separately.. However, BSS pointing error budgets show that the overall uncertainty requirement can be met.

Figure 6-9 shows the sensitivity analysis to polarization rotation knowledge. This is an end to end simulation where the TBs from the test data set are rotated using the full rotation matrix to simulate antenna temperatures, the rotation angle is perturbed by the knowledge error, and then the perturbed rotation angle and the simulated antenna temperatures are sent to the SDR derotation correction to produce the simulated, derotated TBs, which are then used in the EDR algorithms.

We simulate the polarization rotation knowledge error as noise; that is, a different knowledge error is chosen from the parent distribution for each retrieval in a run through the test data sets. The parent distribution is a zero mean Gaussian distribution, with the 1-sigma value shown on the x-axis of Figure 6-9.

The figure shows that all the sensitivity is in the first rank and closest ambiguity wind direction precision; these EDR errors are therefore become de-facto the drivers in setting the requirement, even though the increase in these errors is not sufficient to violate any SRD EDR performance requirement at the high end of the sensor error range considered. Thus, the vertical lines drawn at the requirement value in these two plots.

EDR Sensitivity to CMIS Polarization Rotation Knowledge Error

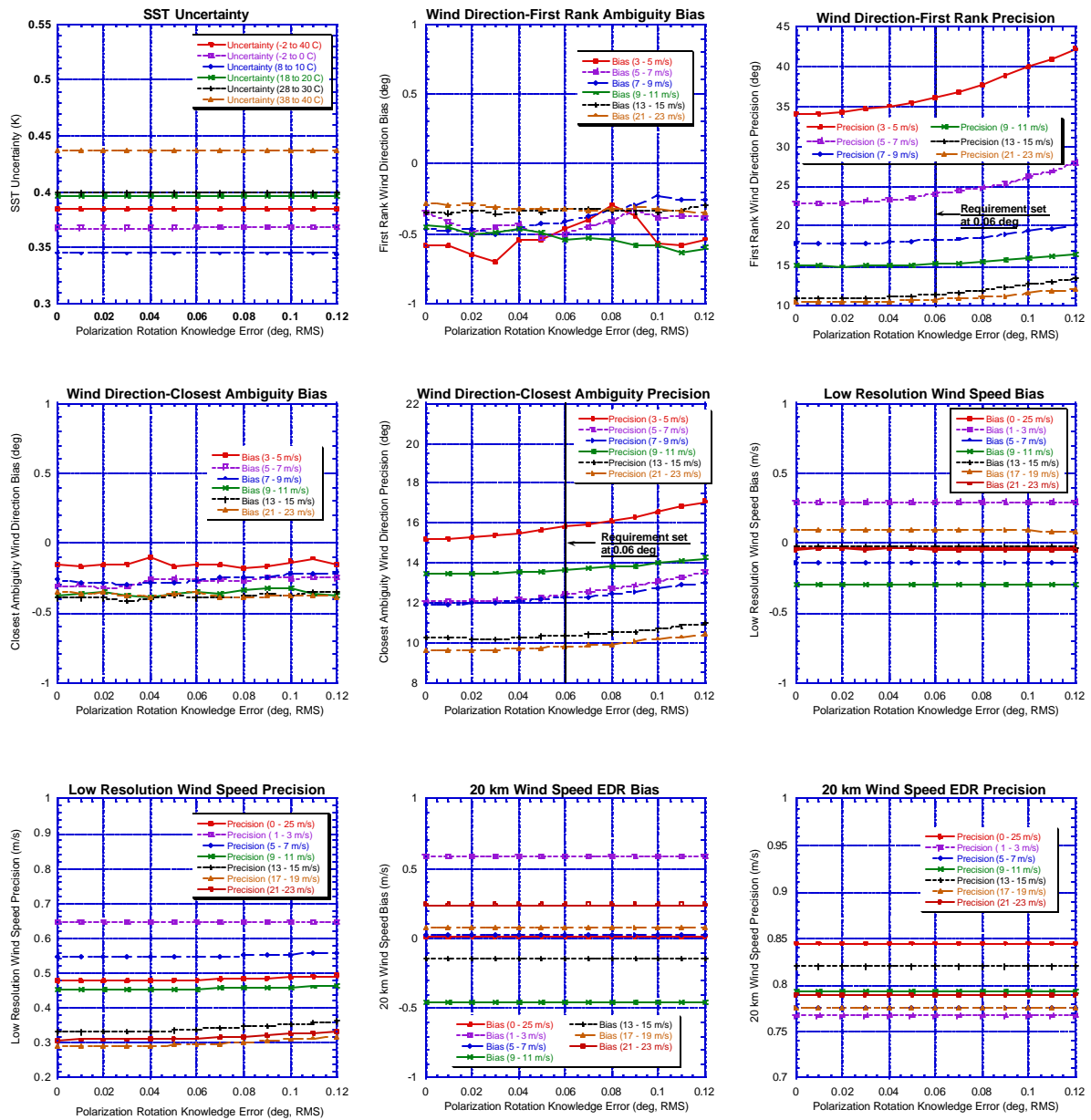


Figure 6-9: Ocean EDR sensitivity to CMIS polarization rotation knowledge error. Knowledge error Monte Carlo for each observation of each run using a zero mean Gaussian distribution with known sigma (x-axis) for each run.

7 Pre-Launch Algorithm Calibration and Validation Requirements

7.1 Antenna Range Testing

To be added

7.2 Thermal Vacuum Testing

To be added

8 Post-launch Calibration and Validation

8.1 Calibration to RTM for bias removal

The calibration to the RTM is currently being carried as a risk item into the EMD phase of CMIS development. This section currently only contains the PDR slides (with minimal reformatting from slides format to text format), as the final algorithms will be completed and documented in the EMD phase.

PDR Slide 3b-16: Post-launch Validation/Calibration

Verify no cross-scan anomalies

On-orbit calibration of CMIS measurements to RTM

Primary method (collocate, simulate and regress)

Collocation sources for calibration of measurements to RTM

Refinement to calibration of CMIS measurements to RTM

Inverse modeling

Conditions for refinement

Resolving the under-determination problem

Results from Calibration of TMI measurements

Calibration of CMIS measurements to RTM during EMD phase

PDR Slide 3b-17: Verify No Along-scan Anomalies

Determine along-scan TA biases, if any

Method I in Wentz, Ashcroft, and Gentemann, "Post Launch Calibration of the TRMM Microwave Imager," IEEE TGRS, 2000

Least squares to find $G(i)$, $B(j)$ where

$$T_{Ap}(i, j) = G(i) + B(j) + \mathbf{e}, \text{ w/constraint } \sum_j B(j) = 0$$

$G(i)$ is the expected mean TA for pixel number i (for $1^\circ \times 1^\circ$ grid on ocean surface)

$B(j)$ is the along-scan bias for scan position j

Eliminates need for assumption that all scan positions should have the same mean TA (may not be true due to geographic sampling)

Does not change overall absolute calibration bias:

Gives TAs from different scan positions a consistent absolute calibration (reduces overall noise in absolute calibration along the scan)

An NPOESS inertial hold maneuver (reflector sees cold space) would be useful in verifying that these are bias and not slope errors, however it is not required

Because we can differentiate bias and slope errors from location where anomalies in $B(j)$ occur in scan, and whether anomalies are positive or negative

Requires no data other than CMIS data

PDR Slide 3b-18: On-orbit Calibration of CMIS TAs to RTM

Background

All calibration done on TAs and not TBs

To enable determination of any slope errors at their likely source before the channel measurements are mixed in SDR cross polarization corrections

Slope errors can result from spillover knowledge error, reflector emissivity knowledge error, warm load temperature bias error, all of which affect TAs directly

Primary method: “collocate, simulate, and regress”

Identify cloudless areas using GOES or by using uncalibrated CMIS integrated CLW retrievals, or collocate CLW from Cal/Val’d radiometer (SSMIS)

Collocate CMIS TAs and:

Vapor, temperature profiles (radiosonde or GCM)

SST, W, WD (buoy, scatterometer, GCM)

Use collocated geophysical parameters and CMIS reported EIA to simulate TBs (all polarizations)

Add measured cross-pol, rotations, and spillover to RTM simulated TBs to obtain RTM simulated TAs (full rotation matrices and M-matrix, involving all polarizations)

Regress CMIS vs RTM simulated antenna temperatures to find overall slope (eta) and bias (beta) for each channel (denoted by p):

$$T_{Ap,RTM} = \mathbf{h}_p T_{Ap,CMIS} + \mathbf{b}_p, \quad p = v, h, +, -, l, r$$

Once found, the eta’s and beta’s for each polarization are used to correct the TAs (via the above formula)

Corrected TAs used as input for generating the ECTBs and imagery products

PDR Slide 3b-19: Collocation Sources for TA Calibration To RTM

For a quick calibration to verify that EDRs can be retrieved with reasonable accuracy/precision

Use GCMs for collocated geophysical parameters

Collocations for all unclouded CMIS retrieval cells

For a detailed calibration, it is necessary to use the same sources that will be used to validate the algorithms

Example: Let’s say we used a source for SST that has a low SST compared to the preferred validation source

Then the calibration will try to make the TAs consistent with the RTM result for the low SST

When the calibrated TAs are used to perform the EDR validation, then the retrieved SST will be low compared to the validation source

Will identify preferred validation sources for each EDR before Cal/Val effort begins

PDR Slide 3b-20: Refinement of TA Calibration of CMIS Measurements to RTM

Method of inverse modeling is used to tune RTM coefficients (discussed in Section 3e, SST Cal/Val)

(Wentz, “Well Calibrated Ocean Algorithm for SSM/I,” JGR, 1997)

Get the lumps out of stratification biases, until they are as close to smooth as at right

Principal conditions: features (lumps) in a single EDR bias as a function of a single strat. param. is governed mainly by 1 or 2 RTM coefficients at a specific frequency

Can also refine slope and bias for each channel using inverse modeling

Different EDRs show differing sensitivity to a given channel

Consider the EDR most sensitive

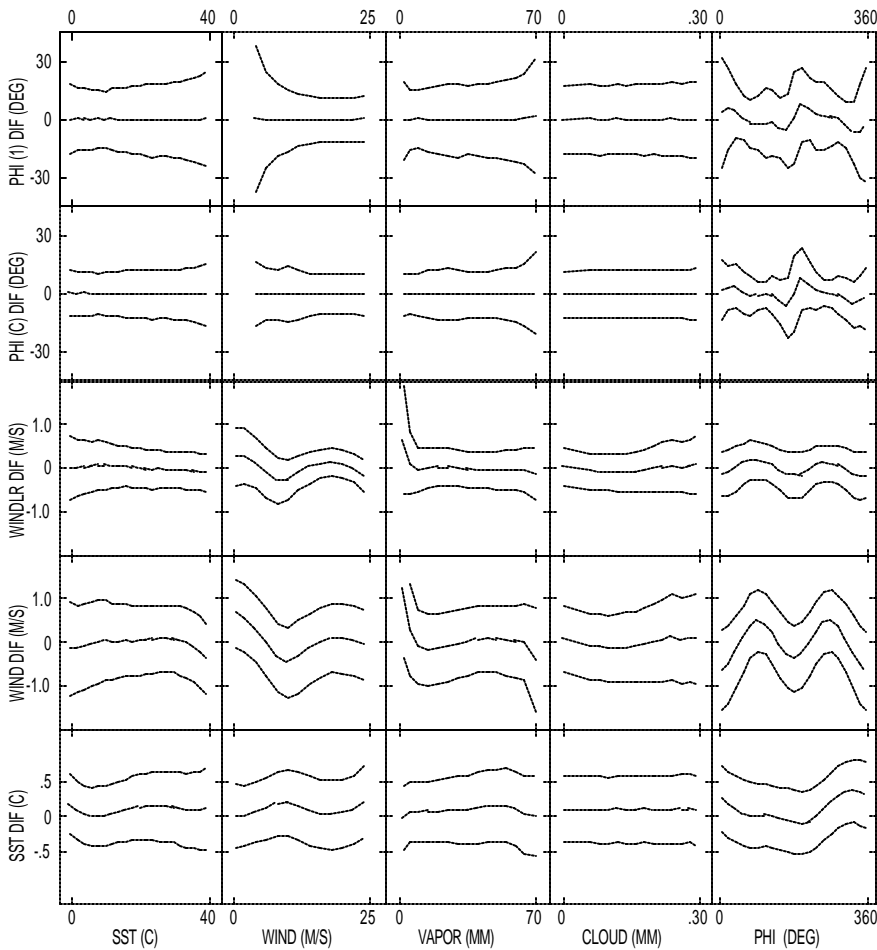
Exclude wind direction for the moment

Slope controls slope and some curvature of EDR bias as a function of one or more of SST, W, V, L

Bias controls overall (unbinned) EDR bias

Matrix of stratification plots showing bias (center line) for all EDRs over ocean that use a given range of frequencies (here 6-36 GHz)
Versus all geophysical parameters (GPPs)

More stratification plots for other EDRs here



PDR Slide 3b-21: Wind Direction and Refinements of TA Calibration to RTM

Because of trigonometric dependence of wind direction signal, slopes, and biases of relevant channels affect *wind direction bias vs wind direction*, not so much overall bias

Lumpiness minimized when slopes and biases set properly

May also affect distribution of retrieved wind directions

Overabundance of retrieved wind directions at extreme values of wind direction signal in channel needing slope/bias adjustment

May be useful in diagnosing small slope/bias errors in 10-36 GHz channels

Prior calibration of RTM to WindSat to minimize the RTM wind direction coefficients' contribution to spikes in histogram, lumpiness in stratification

PDR Slide 3b-22: Conditions for TA Calibration to RTM Refinement

Slopes (η)

Slope of each EDR bias w/r/t stratification variables is minimized

Affected by RTM coefficients, as well as slopes η

Biases (β)

Overall (unbinned) EDR biases = 0

Need 36 conditions to determine 18 bias and slope refinements uniquely (for the eighteen 6-36 GHz channels)

Will likely have fewer conditions

Known conditions (“ $\langle \Delta \text{EDR} \rangle$ ” means unbinned or mean bias over all retrievals)

$\langle \Delta \text{SST} \rangle = 0$ Slope $\Delta \text{SST} = 0$ (vs SST, W, V, L) 6-36 GHz

$\langle \Delta W_{\text{LR}} \rangle = 0$ Slope $\Delta W_{\text{LR}} = 0$ (vs SST, W, V, L) 10-36 GHz

RMS $\Delta \phi_{\text{R}}$ as a function of ϕ_{R} minimized 10-36 GHz

$\langle \Delta W_{20} \rangle = 0$ Slope $\Delta W_{20} = 0$ (vs SST, W, V, L) 18-36 GHz

Problem under-determined

Thought experiment: Suppose we have enough conditions to identify 10-36 GHz η 's and β 's uniquely. Still, we only have one ocean algorithm (SST) using 6 GHz channels

Only 1 condition to constrain solution for β refinement ($\Delta \beta$) for 6V and 6H

Can only solve for $D_{6V}\Delta \beta_{6V} + D_{6H}\Delta \beta_{6H} = \langle \text{remaining } \Delta \text{SST} \rangle$, where $D_i = d\text{SST}/d\text{TB}_i$

PDR Slide 3b-23: Resolving the Under determination Problem in Refinement of TA Calibration to RTM I

When one is left with the choice of altering the bias (slope) for several channels, choose to refine the bias (slope) for the channel that results in minimum change to the TAs

Refine bias (slope) for channel to which the algorithm is most sensitive

“Problem” of sensitivity of EDRs to certain accuracy/interchannel accuracy errors is actually an advantage for this method

Allows us to minimize refinement of the TA biases/slopes found from primary method

Example: Thought experiment utilizing SST

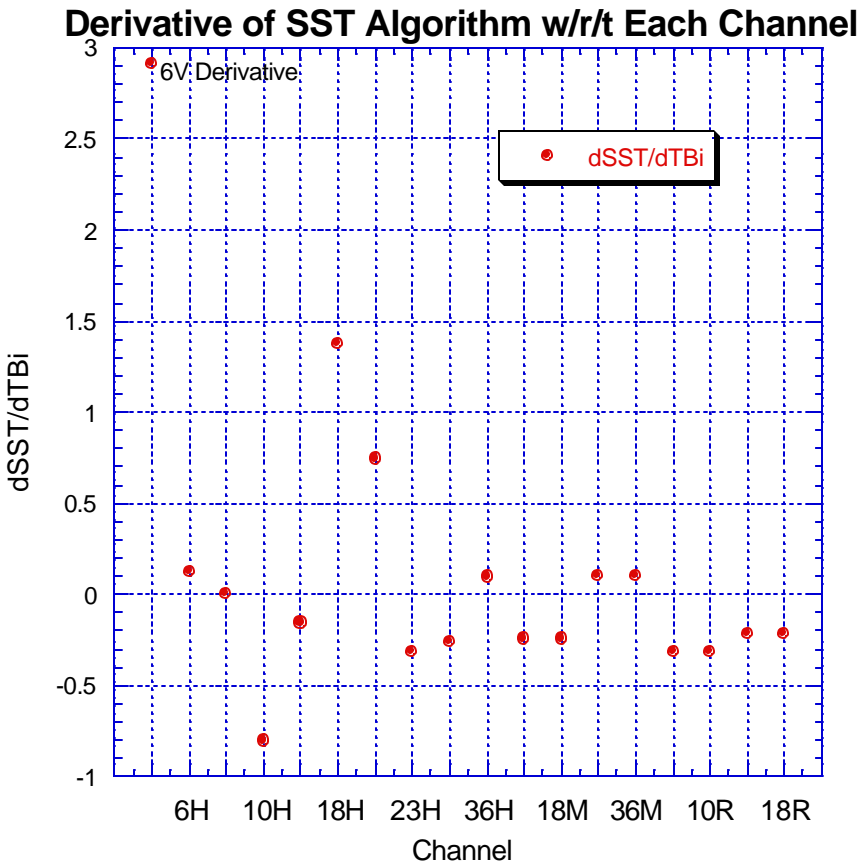
Easy to compute derivative of regression algorithms with respect to TBs

Since 6V derivative is 23X larger than 6H

Minimum adjustment is made using only 6 V

A 0.1K SST bias can be removed by adjusting 6V bias by only 0.034 K

Would have required a 0.79 K bias adjustment to 6H



PDR Slide 3b-24: Resolving the Under determination Problem in Refinement of TA Calibration to RTM II

From the Thought experiment utilizing SST, the full picture of the method emerges:

May not have enough $\langle \Delta EDR \rangle = 0$ and $\text{slope}(\Delta EDR) = 0$ conditions to define the refinements $\Delta \eta, \Delta \beta$ for each channel uniquely

Therefore, add constraints that require the refinements to result in minimum overall change to the TAs while satisfying those conditions

Constraints:

$$\sum_{\substack{\text{all 6-36GHz} \\ \text{channels}}} (\Delta \mathbf{b})^2 \text{ minimized}$$

$$\sum_{\substack{\text{all 6-36GHz} \\ \text{channels}}} (\Delta h \bar{T}_A)^2 \text{ minimized} \quad (\bar{T}_A = \text{average TA for a channel})$$

Will also explore other potential conditions for deriving refinements to slope and bias
Wind direction condition, represented as separate condition on each wind direction bin, represents many more than 1 condition

But some may be degenerate (redundant)

Zero slope & overall bias conditions on atmospheric parameter regressions in WD alg
Up, down atm radiation and transmission at 10, 18, 23, and 36 GHz

Potentially 12 conditions (see 3e-45)

Zero overall bias conditions on TB residual from wind direction physical algorithm

Probably weak conditions: algorithm seems to absorb most of TB bias errors when we did TB accuracy sensitivity analyses

PDR Slide 3b-25: Extra Constraints on Polarimetric Channels

Section 3e Yueh 1999 wind direction signal negligible below ~ 2 m/s

Slopes and biases refined so that mean $T_p = T_m = T_L = T_R$ below 2 m/s, at all SST, V, L

And polarimetric TBs all equal to average of T_v and T_h

Constrains polarimetric inter-channel accuracy errors

Implicitly used in “collocate, simulate, and regress” primary method

Simulated TBs used to produce the simulated TAs satisfy these constraints

PDR Slide 3b-26: Results From Calibration of TMI TAs

Post-launch calibration of TMI TAs using in situ data and comparison to SSM/I

Wentz, Ashcroft, and Gentemann, "Post Launch Calibration of the TRMM Microwave Imager,"
IEEE TGRS, 2000

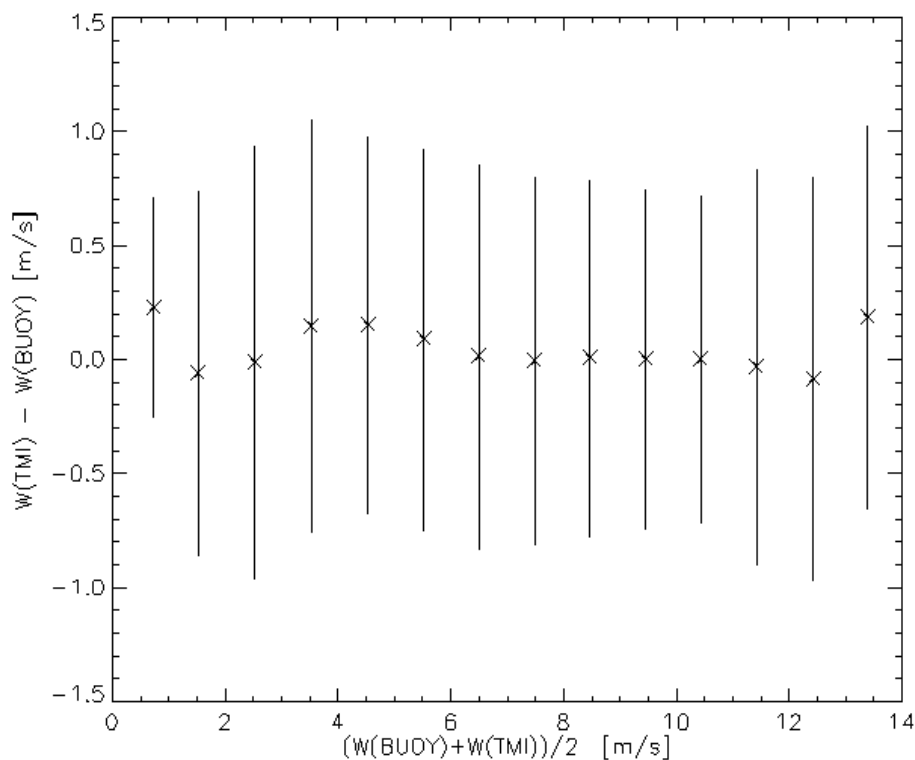
More difficult than "collocate simulate and regress" canonical method for CMIS

Frequency and EIA differences

Wanted comparison with cal'd radiometer due to questions about reflector emissivity

No refinement using inverse modeling – primary method good enough to produce these TMI results

Calibration reduces the mean SST error to 0.03, wind speed error to zero



		Weekly Average TMI – Buoy SST		Weekly Average Reynolds – Buoy SST	
	collocations	Mean Dif.	RMSD	Mean Dif.	RMSD
NDBC	2436	0.24	0.72	0.22	1.03
NDBC*	2295	0.24	0.59	0.09	0.60
TAO	7018	-0.04	0.40	-0.03	0.31
PIRATA	374	0.03	0.35	-0.07	0.32
ALL	9828	0.03	0.50	0.03	0.58
ALL*	9684	0.03	0.45	-0.00	0.40

*Exclude collocations with differences TMI-Buoy or Reynolds-Buoy larger than 2°C; NDBC traditionally excluded from SST bias assessment for IR and microwave SST retrievals (inferior instrument package compared to TAO, PIRATA, and spatial error in coastal regions [high gradients due to currents])

PDR Slide 3b-27: CMIS TA Calibration to RTM During EMD Phase

RSS experience with TMI has validated the proposed method can meet the required accuracy level at 10 to 36 GHz frequencies, V, H polarizations
For wind speed and SST retrievals

Plans for the next phase

Extend and validate the methodology to all CMIS channels

Enhance methodology to make it suitable for automated operation

Long-term stability of the post-launch calibration values

How often do updates need to be computed

Forwarded to the risk management process for mitigation

8.2 Validation of Geolocation Accuracy

To be added.

9 Practical Considerations

9.1 Numerical Computation Considerations

9.1.1 Calibration

The post-launch bias correction for the T_{Bec} calibration to the RTM is currently performed at the T_A level. This is the correct location mathematically for where the bias errors are occurring, however this adds significant computational and storage requirements. The cross-polarization correction has a slight variation with location based on viewing geometry and climate conditions. This changes the static bias correction at T_A into a location and scene dependent correction at T_B . Further analysis may show that the time varying component of this correction is insignificant and that computational complexity and data storage savings can be achieved by assuming that the bias correction is a constant for all locations at the T_B level. This would make $T_{Bec} = T_B + \text{static bias correction}$.

The two-point calibration is currently computed in radiance space. Further investigations can be made into either using look up tables to provide the radiance / temperature conversions or performing the conversions directly in temperature space. Both of these methods would involve a small loss of precision, but would provide some computational benefit. Additionally the current conversion between temperature and radiance is based on an assumption of a single frequency at the center of the passband. Integrating over the entire passband could perform a more precise conversion, at the cost of computational complexity.

9.1.2 Geolocation

There are numerous shortcuts that are commonly used in geolocation algorithms. Frequently one provides only a subset of the pixels as anchor points that are rigorously earth located (using the process described in Section 5). The remaining points are then earth located by interpolation from the anchor points. This can provide a significant computational savings with only minor degradation in earth location accuracy. In addition the computation of solar angles is dependant on the relative location of the Sun with respect to the earth in an inertial coordinate space. Some systems assume that the orientation between the center of the earth and the Sun is constant for some number of minutes, since the rotation of the earth about the sun does not change significantly in this time scale. This only effects the computation of sun viewing angles which general do not have to be as precise as the rest of the earth location process.

Corrections for terrain height variation from a geodetic earth model can be a significant computational burden. This has not been addressed in the risk reduction phase since variations that occur on a scale smaller than CMIS pixels are “averaged” out and the solution for this problem is also highly dependent on how consistent one wants to be across the NPOESS sensors. These variations affect both the geolocation and effective EIA of the land EDRs. Fortunately the Land EDRs are not as sensitive as the Ocean EDRs to variations in EIA. This problem will be further addressed in the next phase.

9.2 Programming/Procedure Considerations

9.2.1 Calibration

The formulation for many of the correction terms in the Section 4 occur on a per scan or per count or per warm load PRT basis. Since many of these terms are aggregated both within a scan and across multiple scans, a mathematically equivalent correction can be applied at the aggregate level rather than for each individual measurement.

9.2.2 Geolocation

The CMIS geolocation procedure have significant overlap with the geolocation procedures required for other sensors and it makes sense that re-use of procedures should be used as much as possible. Not only does this reduce software development cost, but it also ensures consistent earth location results across the sensors. The routines to perform the various coordinate transformations can be common. The IDPS can provide a single routine that provides the spacecraft position and orientation in ecr coordinates for any arbitrary time. This ensures a consistent means of ephemeris interpolation is used for all sensors. Routines to provide sun and satellite viewing angles are not sensor specific once the satellite position and location on the earth have been determined for a specific time.

9.3 Computer hardware or software requirements

9.4 Quality Control and Diagnostics

9.5 Exception and Error Handling

9.6 Special database considerations

N/A

9.7 Special operator training requirements

N/A

9.8 Archival requirements

N/A

10 Glossary of Acronyms

SCF	Sensor Constants File
TV	Thermal Vacuum
T _{Bec}	Empirically Corrected Brightness Temperature (previously ECTB or T _{ECB})
T _A	Antenna Temperature
T _B	Brightness Temperature
IDPS	Integrated Data Processing System

ADD	Algorithm Description Document
AER	Atmospheric and Environment Research
AGL	Above Ground Level
AIRS	Atmospheric InfraRed Sounder
ALFA	AER Local Area Forecast Model
AMS	American Meteorological Society
AMSR	Advanced Microwave Scanning Radiometer
AMSU	Advanced Microwave Sounding Unit
APS	Algorithm Performance Simulation
ARA	Atmospheric Radiation Analysis
ARD	Algorithm Requirements Document
ARM	Atmospheric Radiation Measurement
ASRR	Algorithm System Requirements Review
ATBD	Algorithm Theoretical Basis Document
ATOVs	Advanced TOVS
AVHRR	Advanced Very High Resolution Radiometer
BT	Brightness Temperature
CC	Cloud Clearing
CEPEX	Central Equatorial Pacific Experiment
CF	Central frequency
CHARTS	Code for High resolution Accelerated Radiative Transfer with Scattering
CKD	Clough, Kneizys and Davies
CLW	Cloud Liquid Water
CMIS	Conical Microwave Imaging Sounder
COD	Cloud Optical Depth
CTH	Cloud Top Height
CTP	Cloud Top Pressure
DEM	Digital Elevation Model
DMSP	Defense Meteorological Satellite Program
DoD	Department of Defense
DOE	Department of Energy
ECMWF	European Center for Medium-range Weather Forecasts
EDR	Environmental Data Record
EIA	Earth Incidence Angle
EOF	Empirical Orthogonal Function
EOS	Earth Observing System
ESFT	Exponential Sum Fitting Technique
FFT	Fast Fourier Transform
FIRE	First ISCCP Regional Experiment

FOR	Field Of Regard
FOV	Field Of View
GPS	Global Positioning System
GSFC	Goddard Space Flight Center
HCS	Horizontal Cell Size
HIRS	High-resolution Infrared Sounder
HSB	Humidity Sounder of Brazil
HSR	Horizontal Spatial Resolution
IPO	Integrated Program Office
IPT	Integrated Product Team
ISCCP	International Satellite Cloud Climatology Project
IST	Ice Surface Temperature
IWVC	Integrated Water Vapor Content
JHU	Johns Hopkins University
JPL	Jet Propulsion Laboratory
LA	Lower Atmosphere
LAT	Latitude
LBL	Line By Line
LBLRTM	Line By Line Radiative Transfer Model
LMD	Laboratoire de Météorologie Dynamique
LON	Longitude
LOS	Line Of Sight
LST	Land Surface Temperature
L-V	Levenberg-Marquardt
LVM	Levenberg-Marquardt
MHS	Microwave Humidity Sounder
ML	Maximum Likelihood
MSU	Microwave Sounding Unit
MW	Microwave
NASA	National Aeronautics and Space Administration
NCAR	National Center for Atmospheric Research
NCEP	National Center for Environmental Prediction
NDSI	Normalized Difference Snow Index
NDVI	Normalized Difference Vegetation Index
NEDN	Noise Equivalent Difference
NESDIS	National Environmental Satellite, Data, and Information Service
NN	Neural Network
NOAA	National Oceanic and Atmospheric Administration
NPM	Numerical Prediction Model
NPOESS	National Polar-orbiting Operational Environmental satellite System
NRL	Naval Research Laboratory
NWP	Numerical Weather Prediction
OD	Optical Depth
OI	Optimal Interpolation
OLS	Operational Linescan System
OMIS	Operational Multi-Spectral Imaging Suite
OMPS	Ozone Mapping and Profiler Suite
OSS	Optimal Spectral Sampling
PCA	Principal Component Analysis

PDR	Preliminary Design Review
PSD	Power Spectral Density
POES	Polar Orbiting Environmental Satellite
Psfc	Surface Pressure
PSURF	Surface Pressure
QC	Quality Control
RDR	Raw Data Records
RH	Relative Humidity
RMS	Root Mean Square
RMSE	Root Mean Square Error
RRTM	Rapid Radiative Transfer Model
RT	Radiative Transfer
RTA	Radiative Transfer Algorithm
RTE	Radiative Transfer Equation
RTM	Radiative Transfer Model
S/N	Signal/Noise
SAR	Synthetic Aperture Radar
SDR	Sensor Data Record
SEIT	System Engineering Integrated Product Team
SFR	System Functional Review
SGI	Silicon Graphics, Inc.
SPS	System Performance Simulation
SRD	Sensor Requirement Document
SRR	System Requirements Review
SSM/I	Special Sensor Microwave/Imager
SSM/T	Special Sensor Microwave/Temperature
SSMIS	Special Sensor Microwave Imager Sounder
SST	Sea Surface Temperature
SVD	Single Value Decomposition
SW	Shortwave
T	Temperature
TBD	To Be Determined (by contractor)
TBR	To Be Resolved (by contractor/government)
TBS	To Be Supplied (by government)
TIGR	Thermodynamic Initial Guess Retrieval
TIM	Technical Interchange Meeting
TOA	Top Of Atmosphere
TOD	Time of Day
TOVS	TIROS-N Operational Vertical Sounder
TRD	Technical Requirements Document
TSKIN	Skin Temperature
UA	Upper Atmosphere
UR	Unified Retrieval
USGS	United States Geological Survey
VIIRS	Visible/Infrared Imager/Radiometer Suite
WPTB	Weather Product Test Bed
WV	Water Vapor
WVF	Water Vapor Fraction

11 References

11.1 Government Documents and Communications

Specifications:

ICSRs and Responses:

11.2 BSS Documents

Specifications:

CMIS Performance Specification

Memos:

Calibration Plan submitted as part of PDR documentation

11.3 Technical Literature

SDST-092: MODIS Level 1A Earth Location: Algorithm Theoretical Basis Document
Version 3.0, GSFC / SBRS , SDST-092, Aug. 26, 1997

Fleig 93: Fleig, A., Hubanks, P., Storey, J., Carpenter, L., “ An Analysis of MODIS Earth Location Error”, Version 2.0, MODIS Science Data Support Team (SDST), Sept. 1993

Colton 98: Colton, M., Poe, G., Inter-Sensor Calibration of DMSP SSM/I F-8 to F-14 1987-1997, IEEE trans. On Geoscience, Feb. 1998

Patt 94: Patt, F., Gregg, W., “Exact closed-form geolocation algorithm for Earth Survey Sensors”, Int. J. Remote Sensing, 1994, Vol. 15, No. 18, 3719-3734

Hollinger 89: Hollinger, J., “DMSP Special Sensor Microwave / Imager Calibration / Validation”, Naval Research Laboratory, Final Report, Vol. I, 20 July 1989

WGS84: : DMA TR 8350.2-A, Defense Mapping Agency (DMA) Technical Report (TR), Supplement to Department of Defense World Geodetic System 1984 (WGS84) Technical Report, prepared by the DMA WGS84 Development Committee, Dec. 1, 1987.

APPENDIX A: DERIVATION OF THE ANTENNA TEMPERATURE EQUATIONS FOR ANTENNA CROSS POLARIZATION

A.1 Introduction

In this appendix, we derive expressions for the scene antenna temperatures measured by CMIS in terms of the earth scene polarized brightness temperatures (TBs). We consider antenna cross-polarization only, and not the overall rotation of the TBs by Faraday rotation or CMIS rotation. To simplify the notation, therefore, we drop all primes on the brightness temperatures. However, we do not drop the prime on the antenna temperatures to continually remind the reader that we are writing equations for, and the input to the cross-polarization correction are, the scene components of the antenna temperature (spillover corrected TAs).

In section A.2, we describe the parameters needed to compute the cross-polarization (M) matrix. In section A.3, we derive the antenna temperature (TA) equations for all polarizations as a function of these parameters. In section A.4, we extract close form expressions for the M-matrix elements from the TA equations by assuming the TBs are constant across the spatial integration in the antenna equations. This is a necessary assumption when working with the closed form equations. However, in section A.4.2, we outline a simulation method that allows for a least squares determination of the matrix elements that allows this assumption to be discarded, and that optimized the performance of both the cross-polarization correction as well as the subsequent performance of the EDR algorithms. The heritage of this method is in our determination of the cross-polarization matrix for SSM/I, and the successful retrievals of SSM/I geophysical parameters.

In Appendix B, we show how the antenna equations can be used to specify the M-matrix in the various representations discussed in Section 3.

A.2 Required Inputs for Determination of the M-matrix

There is one cross-polarization matrix for each CMIS frequency. Each row of the M-matrix specifies the cross-polarization for one of two orthogonally polarized TAs measured by a single feedhorn. The data used to compute that row consists of the following parameters:

The co-polarized and cross polarized power gain patterns for the antenna/feedhorn system (i.e. secondary gain patterns). Boeing engineering analysis has shown that the gain patterns should be measured out to 4 and perhaps 5 times the half power beamwidth of the main beam, in order to obtain convergence of the M-matrix and the accuracy required. It is not necessary that the gain functions be referenced to polarization vectors that match earth scene polarization vectors across the entire earth scene. In fact, the common conventions for antenna measurement use a polarization basis that can differ by a few degrees from the earth scene polarization vectors found by projecting the beam onto the earth surface (these will be discussed). But it is necessary (at least assumed in the following derivation of the M-matrix) that the co-pol and cross-pol polarization vectors are orthogonal, and perpendicular to the beam.

The relative phase added to the incoming co-pol and x-pol radiation (E-fields) by the antenna/feed system. Like the gain patterns, this is a function of antenna polar coordinates, and should be measured out to the same angular distance as the gain functions. In the practice of range measurement, the phase added to the co-pol and cross-pol radiation are measured

separately (although M depends only on their difference), and require careful comparison of the phase of the received E-field to that transmitted by a test or “reference” antenna.

For the purpose of defining the EDR performance and sensitivity to knowledge errors in the M-matrix, we have used gain patterns and phases computed by Boeing using a sophisticated antenna/feed model and radiation propagation code. But, the final determination of the gain patterns and phases for the instrument will be obtained from actual measurements utilizing a carefully calibrated reference antenna to transmit radiation toward the CMIS flight antenna.

A.3 Derivation of the Antenna Temperature Equations

The development of the TA equations follows the methodology of Claassen and Fung (1974), with the notable exception that we do not assume that the 3rd and 4th Stokes parameters are zero, and therefore do not discard terms containing them. We will begin by deriving the TA equations for the case of monochromatic radiation, and then expand the derivation to include the finite bandpass of the instrument.

A.3.1 Notation

Each port of each feed horn is meant to measure earth scene radiation of a particular polarization, which will be denoted by the subscript “p”. The orthogonal polarization will be denoted by “q”. The corresponding “co-polarized and cross-polarized” polarizations for the reference antenna will be denoted p’ and q’. The co-pol gain function and phase will be denoted g_{pp} and β_{pp} , and the cross-polarized gain function and phase will be denoted g_{pq} and β_{pq} .

A.3.2 Power Equation for Port p

Consider the radiation entering the antenna system in a beam of solid angle $d\Omega$, centered on antenna polar coordinates (θ, ϕ) . (The antenna polar coordinate $\theta=0$ can be defined as the center of the beam, maximum of the co-pol gain function etc, but generally lies near the boresight for that feed). We express the electric field for this radiation in terms of the orthogonal co-pol and cross-pol polarization vectors ($\hat{e}_{p'}$ and $\hat{e}_{q'}$) of the reference antenna (the “reference polarizations”) as

$$\vec{E} = E_{p'}\hat{e}_{p'} + E_{q'}\hat{e}_{q'} \quad (A1)$$

The receiving properties of the antenna in the p-polarized channel can be described in terms of the vector complex effective height (Ko, 1962; Claassen and Fung, 1974):

$$\vec{I}_p = I_{pp'}\hat{e}_{p'} + I_{pq'}\hat{e}_{q'} \quad (A2)$$

where

$$\begin{aligned} I_{pp'} &= \sqrt{g_{pp'}} e^{ib_{pp}} \\ I_{pq'} &= \sqrt{g_{pq'}} e^{ib_{pq}} \end{aligned} \quad (A3)$$

Again, the gain functions and phase are measured in the polarization basis of the reference antenna, and thus the primes in the second index (the first index simply denotes the earth scene polarization that the port is intended to measure).

Claasen and Fung (1974) show that electric field received by the p-polarized channel (E_r) is the dot product of the incoming E-field with the vector complex effective height:

$$E_p^{rec} = \bar{I}_p \cdot \bar{E} = I_{pp'} E_{p'} + I_{pq'} E_{q'} \quad (A4)$$

The received power in the solid angle $d\Omega$ is then

$$dP_p^{rec} = C \langle |E_p^{rec}|^2 \rangle d\Omega \quad (A5)$$

Now,

$$\begin{aligned} |E_p^{rec}|^2 &= (I_{pp'} E_{p'} + I_{pq'} E_{q'}) (I_{pp'} E_{p'} + I_{pq'} E_{q'})^* \\ &= |I_{pp'}|^2 |E_{p'}|^2 + |I_{pq'}|^2 |E_{q'}|^2 + 2 \operatorname{Re}(I_{pp'} E_{p'} I_{pq'}^* E_{q'}^*) \\ &= |I_{pp'}|^2 |E_{p'}|^2 + |I_{pq'}|^2 |E_{q'}|^2 + 2 \operatorname{Re}(I_{pp'} I_{pq'}^*) \operatorname{Re}(E_{p'} E_{q'}^*) - 2 \operatorname{Im}(I_{pp'} I_{pq'}^*) \operatorname{Im}(E_{p'} E_{q'}^*) \end{aligned} \quad (A7)$$

Plugging in the expressions for the I components and using

$$I_{pp'} I_{pq'}^* = \sqrt{g_{pp'} g_{pq'}} e^{i\mathbf{b}_p} \text{ where } \mathbf{b}_p \equiv \mathbf{b}_{pp'} - \mathbf{b}_{pq'} \quad (A8)$$

yields

$$dP_p^{rec} = C \left[g_{pp'} \langle |E_{p'}|^2 \rangle + g_{pq'} \langle |E_{q'}|^2 \rangle + 2\sqrt{g_{pp'} g_{pq'}} (\cos \mathbf{b}_p \operatorname{Re} \langle E_{p'} E_{q'}^* \rangle - \sin \mathbf{b}_p \operatorname{Im} \langle E_{p'} E_{q'}^* \rangle) \right] d\Omega \quad (A9)$$

This is the master power equation in the polarization basis of the reference antenna. Now we want to put this equation in the polarization basis of the earth (unprimed system). The orthogonal vectors \mathbf{e}_p and \mathbf{e}_q define the polarizations on the earth, that is with respect to the plane of incidence with the Earth. These vectors lie in the same plane as the reference antenna polarizations. Let the rotation angle from \mathbf{e}_p to $\mathbf{e}_{p'}$ be denoted α , measured clockwise from \mathbf{e}_p when looking from the radiometer. It is also assumed that \mathbf{e}_q and $\mathbf{e}_{q'}$ are 90 degree clockwise rotations from \mathbf{e}_p and $\mathbf{e}_{p'}$. A diagram is shown in Figure A1. Then,

$$\begin{aligned} \hat{\mathbf{e}}_p \cdot \hat{\mathbf{e}}_{p'} &= \cos \alpha \\ \hat{\mathbf{e}}_p \cdot \hat{\mathbf{e}}_{q'} &= -\sin \alpha \\ \hat{\mathbf{e}}_q \cdot \hat{\mathbf{e}}_{p'} &= \sin \alpha \\ \hat{\mathbf{e}}_q \cdot \hat{\mathbf{e}}_{q'} &= \cos \alpha \end{aligned} \quad (A10)$$

In the earth polarization basis, the incoming E-field can be represented as

$$\vec{E} = E_p \hat{e}_p + E_q \hat{e}_q \quad (\text{A11})$$

Therefore we can represent the E-field components in the reference basis in terms of the components in the earth basis as

$$E_{p'} = \vec{E} \cdot \hat{e}_{p'} = E_p (\hat{e}_p \cdot \hat{e}_{p'}) + E_q (\hat{e}_q \cdot \hat{e}_{p'}) = E_p \cos \mathbf{a} + E_q \sin \mathbf{a}, \quad (\text{A12})$$

and similarly

$$E_{q'} = -E_p \sin \mathbf{a} + E_q \cos \mathbf{a} \quad (\text{A13})$$

We can now define the master power equation (A9) in terms of the earth polarization basis using equations (A12) and (A13). First we compute the terms in $E_{p'}$ and $E_{q'}$ in (A9) as

$$\begin{aligned} |E_{p'}|^2 &= |E_p|^2 \cos^2 \mathbf{a} + |E_q|^2 \sin^2 \mathbf{a} + \text{Re}(E_p E_q^*) \sin 2\mathbf{a} \\ |E_{q'}|^2 &= |E_p|^2 \sin^2 \mathbf{a} + |E_q|^2 \cos^2 \mathbf{a} - \text{Re}(E_p E_q^*) \sin 2\mathbf{a} \end{aligned} \quad (\text{A14})$$

Additionally,

$$E_{p'} E_{q'}^* = \frac{1}{2} \left(|E_q|^2 - |E_p|^2 \right) \sin 2\mathbf{a} + E_p E_q^* \cos^2 \mathbf{a} - (E_p E_q^*)^* \sin^2 \mathbf{a} \quad (\text{A15})$$

but we will need the real and imaginary parts

$$\begin{aligned} \text{Re}(E_{p'} E_{q'}^*) &= \frac{1}{2} \left(|E_q|^2 - |E_p|^2 \right) \sin 2\mathbf{a} + \text{Re}(E_p E_q^*) (\cos^2 \mathbf{a} - \sin^2 \mathbf{a}) \\ &= \frac{1}{2} \left(|E_q|^2 - |E_p|^2 \right) \sin 2\mathbf{a} + \text{Re}(E_p E_q^*) \cos 2\mathbf{a}, \\ \text{Im}(E_{p'} E_{q'}^*) &= \text{Im}(E_p E_q^*) (\cos^2 \mathbf{a} + \sin^2 \mathbf{a}) = \text{Im}(E_p E_q^*) \end{aligned} \quad (\text{A16})$$

Simply plugging in (A14) and (A16) into (A9) gives the master power equation in the earth polarization basis:

$$dP_p^{rec} = C \left[\begin{aligned} &g_{pp'} \left(\langle |E_p|^2 \rangle \cos^2 \mathbf{a} + \langle |E_q|^2 \rangle \sin^2 \mathbf{a} + \text{Re} \langle E_p E_q^* \rangle \sin 2\mathbf{a} \right) \\ &+ g_{pq'} \left(\langle |E_p|^2 \rangle \sin^2 \mathbf{a} + \langle |E_q|^2 \rangle \cos^2 \mathbf{a} - \text{Re} \langle E_p E_q^* \rangle \sin 2\mathbf{a} \right) \\ &+ 2\sqrt{g_{pp'} g_{pq'}} \cos \mathbf{b}_p \left[\frac{1}{2} \left(\langle |E_q|^2 \rangle - \langle |E_p|^2 \rangle \right) \sin 2\mathbf{a} + \text{Re}(E_p E_q^*) \cos 2\mathbf{a} \right] \\ &- 2\sqrt{g_{pp'} g_{pq'}} \sin \mathbf{b}_p \text{Im} \langle E_p E_q^* \rangle \end{aligned} \right] d\Omega \quad (\text{A17})$$

Grouping like terms, and expressing the power for each polarization in terms of the Stokes parameters for the earth polarization basis gives

$$dP_p^{rec} = C \left\{ \begin{aligned} & \left(g_{pp'} \cos^2 \mathbf{a} + g_{pq'} \sin^2 \mathbf{a} - \sqrt{g_{pp'} g_{pq'}} \cos \mathbf{b}_p \sin 2\mathbf{a} \right) \langle |E_p|^2 \rangle \\ & + \left(g_{pp'} \sin^2 \mathbf{a} + g_{pq'} \cos^2 \mathbf{a} + \sqrt{g_{pp'} g_{pq'}} \cos \mathbf{b}_p \sin 2\mathbf{a} \right) \langle |E_q|^2 \rangle \\ & + \left(\frac{1}{2} (g_{pp'} - g_{pq'}) \sin 2\mathbf{a} + \sqrt{g_{pp'} g_{pq'}} \cos \mathbf{b}_p \cos 2\mathbf{a} \right) (2 \operatorname{Re} \langle E_p E_q^* \rangle) \\ & - \sqrt{g_{pp'} g_{pq'}} \sin \mathbf{b}_p (2 \operatorname{Im} \langle E_p E_q^* \rangle) \end{aligned} \right\} d\Omega \quad (\text{A18})$$

Now, the earth scene radiation is incoherent, meaning that the E-field of the incoming radiation from $d\Omega(\theta, \phi)$ has no phase relationship with that from any other $d\Omega(\theta', \phi')$. Therefore we can simply integrate (A18) over solid angle to find the total power.

$$P_p^{rec} = \int C \left\{ \begin{aligned} & \left(g_{pp'} \cos^2 \mathbf{a} + g_{pq'} \sin^2 \mathbf{a} - \sqrt{g_{pp'} g_{pq'}} \cos \mathbf{b}_p \sin 2\mathbf{a} \right) \langle |E_p|^2 \rangle \\ & + \left(g_{pp'} \sin^2 \mathbf{a} + g_{pq'} \cos^2 \mathbf{a} + \sqrt{g_{pp'} g_{pq'}} \cos \mathbf{b}_p \sin 2\mathbf{a} \right) \langle |E_q|^2 \rangle \\ & + \left(\frac{1}{2} (g_{pp'} - g_{pq'}) \sin 2\mathbf{a} + \sqrt{g_{pp'} g_{pq'}} \cos \mathbf{b}_p \cos 2\mathbf{a} \right) (2 \operatorname{Re} \langle E_p E_q^* \rangle) \\ & - \sqrt{g_{pp'} g_{pq'}} \sin \mathbf{b}_p (2 \operatorname{Im} \langle E_p E_q^* \rangle) \end{aligned} \right\} d\Omega \quad (\text{A19})$$

A.3.3 Antenna Temperature Equation

A.3.3.1 Monochromatic Antenna Temperature Equations

We will now use (A19) to determine the antenna temperature equations for each linear polarization. To do this, we will need to make the identification of p and q for each channel, convert power into brightness temperature, and finally normalize the resulting antenna temperature equation using an isotropy condition.

Case I: The Vertically Polarized Antenna Temperature Equation

We make the identification $p=v$ in (A19). From Figure A1, it should be apparent that $q=h$ (horizontal polarization). Therefore, we can make the following identifications

$$\begin{aligned} \langle |E_p|^2 \rangle &= \langle |E_v|^2 \rangle \rightarrow T_v \\ \langle |E_q|^2 \rangle &= \langle |E_h|^2 \rangle \rightarrow T_h \\ 2 \operatorname{Re} \langle E_p E_q^* \rangle &= 2 \operatorname{Re} \langle E_v E_h^* \rangle \rightarrow T_U \\ 2 \operatorname{Im} \langle E_p E_q^* \rangle &= 2 \operatorname{Im} \langle E_v E_h^* \rangle \rightarrow T_4 \end{aligned} \quad (\text{A20})$$

and

$$P_p^{rec} \rightarrow T'_{Av} \quad (\text{A21})$$

where the T's are the earth scene temperatures, and T_U and T_4 are the 3rd and 4th Stokes parameters, respectively.

Therefore (A19) becomes

$$T'_{Av} = C_v \int \left\{ \begin{aligned} & \left(g_{vv'} \cos^2 \mathbf{a} + g_{vh'} \sin^2 \mathbf{a} - \sqrt{g_{vv'} g_{vh'}} \cos \mathbf{b}_v \sin 2\mathbf{a} \right) T_v \\ & + \left(g_{vv'} \sin^2 \mathbf{a} + g_{vh'} \cos^2 \mathbf{a} + \sqrt{g_{vv'} g_{vh'}} \cos \mathbf{b}_v \sin 2\mathbf{a} \right) T_h \\ & + \left(\frac{1}{2} (g_{vv'} - g_{vh'}) \sin 2\mathbf{a} + \sqrt{g_{vv'} g_{vh'}} \cos \mathbf{b}_v \cos 2\mathbf{a} \right) T_U \\ & - \sqrt{g_{vv'} g_{vh'}} \sin \mathbf{b}_v T_4 \end{aligned} \right\} d\Omega \quad (\text{A22})$$

Finding the normalization constant C_v is a simple matter if we consider the reception of isotropic unpolarized radiation of temperature T. In that case $T_U=T_4=0$, and the antenna temperature should also be T, so equation (A22) becomes

$$T = C_v \int (g_{vv'} + g_{vh'}) T d\Omega \quad (\text{A23})$$

or

$$C_v = \frac{1}{\int (g_{vv'} + g_{vh'}) d\Omega} \quad (\text{A23b})$$

Equations (A22) and (A23b) constitute the monochromatic TA equation for the v-port.

Case II: The Horizontally Polarized Antenna Temperature Equation

The antenna temperature equation for the horizontally polarized channel is derived in much the same way as for the vertically polarized channel. As before, the polarization label “p” in (A19) is given by the label of the earth polarization the channel is intended to measure (here, “h”); in terms of the polarization vectors in Figures A1 $\mathbf{e}_p = \mathbf{e}_h$. However, with reference to the polarization definitions in Figure A2, $\mathbf{e}_q = -\mathbf{e}_v$ (note the minus sign). The following identifications are then made in (A19):

$$\begin{aligned} \langle |E_p|^2 \rangle &= \langle |E_h|^2 \rangle \rightarrow T_h \\ \langle |E_q|^2 \rangle &= \langle |-E_v|^2 \rangle \rightarrow T_v \\ 2 \operatorname{Re} \langle E_p E_q^* \rangle &= 2 \operatorname{Re} \langle E_h (-E_v^*) \rangle = -2 \operatorname{Re} \langle E_v E_h^* \rangle \rightarrow -T_U \\ 2 \operatorname{Im} \langle E_p E_q^* \rangle &= 2 \operatorname{Im} \langle E_h (-E_v^*) \rangle = -2 \operatorname{Im} \langle E_h E_v^* \rangle = 2 \operatorname{Im} \langle E_v E_h^* \rangle \rightarrow T_4 \end{aligned} \quad (\text{A24})$$

and

$$P_p^{rec} = P_h^{rec} \rightarrow T'_{Ah} \quad (\text{A25})$$

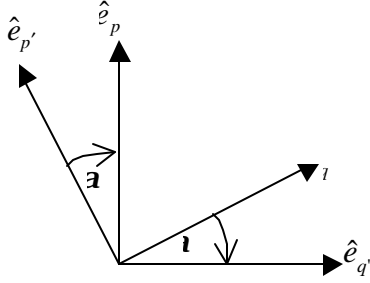


Figure A1

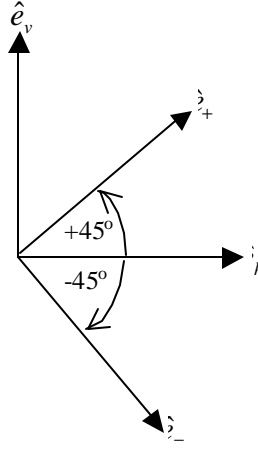


Figure A2

The final parameter to be substituted into (A19) is the phase factor from (A8),

$$\mathbf{b}_p = \mathbf{b}_{pp'} - \mathbf{b}_{pq'} \quad (\text{A26})$$

i.e.,

$$\mathbf{b}_h = \mathbf{b}_{hh'} - \mathbf{b}_{h(-v')} \quad (\text{A27})$$

$\beta_{hh'}$ is the phase added during reception of the E-field of the h' reference antenna polarization (with phase measured with respect to the +h' polarization vector). $\beta_{h(-v')}$ is the same for the E-field of radiation of the v' polarization, with the added phase measured with respect to the -v' reference polarization vector. But the phase added in the latter case is the same whether the absolute phase of the transmitted and received E-fields are both measured with respect to the positive or the negative of the v' polarization vector. Therefore,

$$\mathbf{b}_h = \mathbf{b}_{hh'} - \mathbf{b}_{hv'} \quad (\text{A28})$$

Making these substitutions into (A19) gives the antenna equation for the h-channel as

$$T'_{Ah} = C_h \int \left[\begin{aligned} & \left(g_{hh'} \sin^2 \mathbf{a} + g_{hv'} \cos^2 \mathbf{a} + \sqrt{g_{hh'} g_{hv'}} \cos \mathbf{b}_h \sin 2\mathbf{a} \right) T_v \\ & + \left(g_{hh'} \cos^2 \mathbf{a} + g_{lv'} \sin^2 \mathbf{a} - \sqrt{g_{hh'} g_{lv'}} \cos \mathbf{b}_h \sin 2\mathbf{a} \right) T_h \\ & - \left(\frac{1}{2} (g_{hh'} - g_{lv'}) \sin 2\mathbf{a} + \sqrt{g_{hh'} g_{lv'}} \cos \mathbf{b}_h \cos 2\mathbf{a} \right) T_U \\ & - \sqrt{g_{hh'} g_{lv'}} \sin \mathbf{b}_h T_4 \end{aligned} \right] d\Omega \quad (\text{A29})$$

Again the normalization condition for C_h is that, when the antenna is bathed in isotropic, unpolarized radiation of brightness temperature T, the antenna temperature T'_{Ah} must equal T. From (A29), this yields

$$C_h = \frac{1}{\int (g_{hh'} + g_{hv'}) d\Omega} \cdot \quad (\text{A30})$$

Equations (A29) and (A30) constitute the antenna temperature equation for the horizontally polarized channels.

Case III: The +45 Degree Polarized Antenna Temperature Equation

Using Figures A1 and A2, we make the identification of e_p with e_+ and e_q with e_- , i.e.,

$$\begin{aligned} \hat{e}_p &= \hat{e}_+ = \frac{\hat{e}_h + \hat{e}_v}{\sqrt{2}} \\ \hat{e}_q &= \hat{e}_- = \frac{\hat{e}_h - \hat{e}_v}{\sqrt{2}} \end{aligned} \quad (\text{A31})$$

Analogous relationships hold for the reference antenna polarization vectors. Therefore, we make the following identifications in equation (A19):

$$\begin{aligned} \langle |E_p|^2 \rangle &= \langle |E_+|^2 \rangle \rightarrow T_+ \\ \langle |E_q|^2 \rangle &= \langle |E_-|^2 \rangle \rightarrow T_- \\ 2 \operatorname{Re} \langle E_p E_q^* \rangle &= 2 \operatorname{Re} \langle E_+ E_-^* \rangle \quad (\text{A32}) \\ 2 \operatorname{Im} \langle E_p E_q^* \rangle &= 2 \operatorname{Im} \langle E_+ E_-^* \rangle \\ P_p^{rec} &= P_+^{rec} \rightarrow T_{A+}' \\ \mathbf{b}_p &= \mathbf{b}_+ = \mathbf{b}_{++}' - \mathbf{b}_{+-}' \end{aligned}$$

Now,

$$\begin{aligned} \langle E_+ E_-^* \rangle &= \langle (E_h + E_v)(E_h^* - E_v^*) \rangle / 2 \\ &= \langle |E_h|^2 - |E_v|^2 + E_v E_h^* - (E_v E_h^*)^* \rangle / 2 \end{aligned} \quad (\text{A33})$$

so that

$$\begin{aligned} 2 \operatorname{Re} \langle E_p E_q^* \rangle &= \langle |E_h|^2 - |E_v|^2 \rangle \rightarrow T_h - T_v = -T_Q \\ 2 \operatorname{Im} \langle E_p E_q^* \rangle &= 2 \operatorname{Im} \langle E_v E_h^* \rangle \rightarrow T_4 \end{aligned} \quad (\text{A34})$$

in (A19). Therefore the antenna temperature equation is

$$T'_{A+} = C_+ \int \left[\begin{array}{l} (g_{++'} \cos^2 \mathbf{a} + g_{+-'} \sin^2 \mathbf{a} - \sqrt{g_{++'} g_{+-'}} \cos \mathbf{b}_+ \sin 2\mathbf{a}) T_+ \\ + (g_{++'} \sin^2 \mathbf{a} + g_{+-'} \cos^2 \mathbf{a} + \sqrt{g_{++'} g_{+-'}} \cos \mathbf{b}_+ \sin 2\mathbf{a}) T_- \\ - \left(\frac{1}{2} (g_{++'} - g_{+-'}) \sin 2\mathbf{a} + \sqrt{g_{++'} g_{+-'}} \cos \mathbf{b}_+ \cos 2\mathbf{a} \right) T_\rho \\ - \sqrt{g_{++'} g_{+-'}} \sin \mathbf{b}_+ T_4 \end{array} \right] d\Omega \quad (\text{A35})$$

where the normalization condition given in case I yields

$$C_+ = \frac{1}{\int (g_{++'} + g_{+-'}) d\Omega} \quad (\text{A36}).$$

Case IV: The -45 Degree Polarized Antenna Temperature Equation

By now the reader is familiar with the procedure used to derive the antenna equations for the linear polarizations, and so we state without proof the antenna temperature equation for the -45 degree channel:

$$T'_{A-} = C_- \int \left[\begin{array}{l} (g_{--'} \sin^2 \mathbf{a} + g_{-+'} \cos^2 \mathbf{a} + \sqrt{g_{--'} g_{-+'}} \cos \mathbf{b}_- \sin 2\mathbf{a}) T_+ \\ + (g_{--'} \cos^2 \mathbf{a} + g_{-+'} \sin^2 \mathbf{a} - \sqrt{g_{--'} g_{-+'}} \cos \mathbf{b}_- \sin 2\mathbf{a}) T_- \\ + \left(\frac{1}{2} (g_{--'} - g_{-+'}) \sin 2\mathbf{a} + \sqrt{g_{--'} g_{-+'}} \cos \mathbf{b}_- \cos 2\mathbf{a} \right) T_\rho \\ - \sqrt{g_{--'} g_{-+'}} \sin \mathbf{b}_- T_4 \end{array} \right] d\Omega \quad (\text{A37})$$

where

$$C_- = \frac{1}{\int (g_{--'} + g_{-+'}) d\Omega}. \quad (\text{A38})$$

Case V: The Left Circularly Polarized Antenna Temperature

If the gain functions and phase for the circularly polarized channels were measured with circularly polarized radiation, then the procedure for finding the antenna temperature equations would be analogous to that for the linear polarizations. However, Boeing intends to measure the circularly polarized channels with v' and h' reference antenna polarized radiation. This requires us derive a new expression for the complex effective height vector, and follow through again with the calculation of the power and antenna temperature equations.

Complex Effective Height Vector

The basis vectors for left and right circular polarized radiation are

$$\hat{e}_l = \frac{\hat{e}_h - i\hat{e}_v}{\sqrt{2}} \quad \text{and} \quad \hat{e}_r = \frac{\hat{e}_h + i\hat{e}_v}{\sqrt{2}} \quad (\text{A39})$$

Analogously, the expressions for the left and right circular complex effective height vectors are

$$\begin{aligned}\bar{I}_l &= I_{lh'}\hat{e}_{h'} - iI_{lv'}\hat{e}_{v'} \text{ where } I_{lh'} = \sqrt{g_{lh'}}e^{ib_{lh'}} \text{ and } I_{lv'} = \sqrt{g_{lv'}}e^{ib_{lv'}} \\ \bar{I}_r &= I_{rh'}\hat{e}_{h'} + iI_{rv'}\hat{e}_{v'} \text{ where } I_{rh'} = \sqrt{g_{rh'}}e^{ib_{rh'}} \text{ and } I_{rv'} = \sqrt{g_{rv'}}e^{ib_{rv'}}\end{aligned}\quad (\text{A40})$$

(the square root of 2 factor is not important at this point, due to the normalization condition that will be used at the end). Therefore the effective electric field received in the left polarized channel is expressed as

$$E_l^{rec} = \bar{I}_l \cdot \bar{E} = -iI_{lv'}E_{v'} + I_{lh'}E_{h'} \quad (\text{A41})$$

Power and Antenna Temperature Equations

With a little algebra it is a simple matter to show that

$$\begin{aligned}|E_l^{rec}|^2 &= |I_{lv'}|^2|E_{v'}|^2 + |I_{lh'}|^2|E_{h'}|^2 + 2\text{Im}(I_{lv'}I_{lh'}^*E_{v'}E_{h'}^*) \\ &= |I_{lv'}|^2|E_{v'}|^2 + |I_{lh'}|^2|E_{h'}|^2 + 2\{\text{Re}(I_{lv'}I_{lh'}^*)\text{Im}(E_{v'}E_{h'}^*) + \text{Im}(I_{lv'}I_{lh'}^*)\text{Re}(E_{v'}E_{h'}^*)\}\end{aligned}\quad (\text{A42})$$

Plugging in the definitions for the I's from (A40) yields

$$|E_l^{rec}|^2 = g_{lv'}|E_{v'}|^2 + g_{lh'}|E_{h'}|^2 + 2\sqrt{g_{lv'}g_{lh'}}\{\cos \mathbf{b}_l \text{Im}(E_{v'}E_{h'}^*) + \sin \mathbf{b}_l \text{Re}(E_{v'}E_{h'}^*)\} \quad (\text{A43})$$

where

$$\mathbf{b}_l = \mathbf{b}_{lv'} - \mathbf{b}_{lh'} \quad (\text{A44})$$

In (A43), expressions for the squares and cross-product of the E-fields in the reference basis (primed), in terms of the E-fields in the earth polarization basis (unprimed), can be found using p=v, q=h in equations (A14) and (A16). Plugging these into (A43) without rearrangement gives

$$\begin{aligned}|E_l^{rec}|^2 &= g_{lv'}\left[|E_v|^2 \cos^2 \mathbf{a} + |E_h|^2 \sin^2 \mathbf{a} + \text{Re}(E_vE_h^*)\sin 2\mathbf{a}\right] \\ &\quad + g_{lh'}\left[|E_v|^2 \sin^2 \mathbf{a} + |E_h|^2 \cos^2 \mathbf{a} - \text{Re}(E_vE_h^*)\sin 2\mathbf{a}\right] \\ &\quad + 2\sqrt{g_{lv'}g_{lh'}}\left\{\cos \mathbf{b}_l \text{Im}(E_vE_h^*) \right. \\ &\quad \left. + \sin \mathbf{b}_l \left[\frac{1}{2}(|E_h|^2 - |E_v|^2)\sin 2\mathbf{a} + \text{Re}(E_vE_h^*)\cos 2\mathbf{a}\right]\right\}\end{aligned}\quad (\text{A45})$$

Grouping like terms, and integrating over solid angle gives the power equation, and then making the identifications with the Stokes parameters in (A20) gives the following antenna temperature equation

$$T'_{Al} = C_l \int \left[\begin{aligned} & (g_{lv'} \cos^2 \mathbf{a} + g_{lh'} \sin^2 \mathbf{a} - \sqrt{g_{lv'} g_{lh'}} \sin \mathbf{b}_l \sin 2\mathbf{a}) T_v \\ & + (g_{lv'} \sin^2 \mathbf{a} + g_{lh'} \cos^2 \mathbf{a} + \sqrt{g_{lv'} g_{lh'}} \sin \mathbf{b}_l \sin 2\mathbf{a}) T_h \\ & + \left(\frac{1}{2} (g_{lv'} - g_{lh'}) \sin 2\mathbf{a} + \sqrt{g_{lv'} g_{lh'}} \sin \mathbf{b}_l \cos 2\mathbf{a} \right) T_U \\ & + \sqrt{g_{lv'} g_{lh'}} \cos \mathbf{b}_l T_4 \end{aligned} \right] d\Omega \quad (\text{A46})$$

For reasons that will become apparent in the next appendix, we want to put this expression in terms of the individual left and right circular earth scene temperatures. This is accomplished by expressing the T_v and T_h terms in (A46) in terms of the sum and difference of T_v and T_h , using

$$\sin^2 \mathbf{a} = \frac{1}{2}(1 - \cos 2\mathbf{a})$$

$$\cos^2 \mathbf{a} = \frac{1}{2}(1 + \cos 2\mathbf{a})$$

and then substituting $T_l + T_r$ for $T_v + T_h$, T_Q for $T_v - T_h$, and $T_l - T_r$ for T_4 . These operations result in

$$T'_{Al} = C_l \int \left[\begin{aligned} & \left(\frac{1}{2} (g_{lv'} + g_{lh'}) + \sqrt{g_{lv'} g_{lh'}} \cos \mathbf{b}_l \right) T_l \\ & + \left(\frac{1}{2} (g_{lv'} + g_{lh'}) - \sqrt{g_{lv'} g_{lh'}} \cos \mathbf{b}_l \right) T_r \\ & + \left(\frac{1}{2} (g_{lv'} - g_{lh'}) \cos 2\mathbf{a} - \sqrt{g_{lv'} g_{lh'}} \sin \mathbf{b}_l \sin 2\mathbf{a} \right) T_Q \\ & + \left(\frac{1}{2} (g_{lv'} - g_{lh'}) \sin 2\mathbf{a} + \sqrt{g_{lv'} g_{lh'}} \sin \mathbf{b}_l \cos 2\mathbf{a} \right) T_U \end{aligned} \right] d\Omega \quad (\text{A47})$$

Not surprisingly, the normalization condition derived from (A47) is

$$C_l = \frac{1}{\int (g_{lv'} + g_{lh'}) d\Omega} \quad (\text{A48})$$

Case VI: The Right Circularly Polarized Antenna Temperature

Starting with the definition of the right circular complex effective height vector in (A40), the procedure used in Case V can be followed to derive the antenna temperature equation for right circularly polarized channels. The result is

$$T'_{Ar} = C_r \int \left[\begin{aligned} & \left(\frac{1}{2}(g_{rv'} + g_{rh'}) - \sqrt{g_{rv'}g_{rh'}} \cos \mathbf{b}_r \right) T_l \\ & + \left(\frac{1}{2}(g_{rv'} + g_{rh'}) + \sqrt{g_{rv'}g_{rh'}} \cos \mathbf{b}_r \right) T_r \\ & + \left(\frac{1}{2}(g_{rv'} - g_{rh'}) \cos 2\mathbf{a} + \sqrt{g_{rv'}g_{rh'}} \sin \mathbf{b}_r \sin 2\mathbf{a} \right) T_Q \\ & + \left(\frac{1}{2}(g_{rv'} - g_{rh'}) \sin 2\mathbf{a} - \sqrt{g_{rv'}g_{rh'}} \sin \mathbf{b}_r \cos 2\mathbf{a} \right) T_U \end{aligned} \right] d\Omega \quad (\text{A49})$$

with a normalization factor

$$C_r = \frac{1}{\int (g_{rv'} + g_{rh'}) d\Omega} \quad (\text{A50})$$

and differential phase

$$\mathbf{b}_r = \mathbf{b}_{rv'} - \mathbf{b}_{rh'}. \quad (\text{A51})$$

A.3.3.2 Bandwidth Effects

In Section 3.3.1, we considered gain patterns and phases at a single frequency in deriving the antenna temperature equations; that is they are monochromatic antenna temperature equations. Here we extend the method to include the finite bandwidth of the channels. First, we review the form of the antenna temperature equations and then the normalization issue, which will be of interest once again.

Review of the Monochromatic Antenna Temperature Equations

Inspection of the monochromatic antenna temperature equations in Section A3.3.1 for the 6 channel polarizations reveals that they can all be expressed in similar form. Let p be any of the 6 polarizations, q be the orthogonal polarization, and S₁ and S₂ be the labels of the Stokes parameters formed from all polarizations that are not orthogonal to p. (Note that we have already considered the signs in the last section, so no signs are attached to the channel labels here.) For example if p=v, then q=h, S₁=U, and S₂=”4”. Then the monochromatic antenna temperature equation for the p-polarized channel can be expressed as

$$T'_{Ap} = C_p \int (G_{pp} T_p + G_{pq} T_q + G_{pS_1} T_{S_1} + G_{pS_2} T_{S_2}) d\Omega \quad (\text{A52})$$

where the capital G's are functions of the gain functions g_{pp}', g_{pq}', and the phase β_p. The G's can be found by comparing (A52) with the monochromatic antenna temperature equations, and are shown explicitly in Section A.4.3.

The normalization condition that allowed us to derive C_p in the monochromatic case was that, when the radiometer is bathed in isotropic, unpolarized radiation of temperature T, the antenna temperature must also be T. Isotropic unpolarized radiation of temperature T has

$$\begin{aligned} T_p &= T_q = T \\ T_{S_1} &= T_{S_2} = 0 \end{aligned} \quad (\text{A53, isotropic unpolarized radiation})$$

at all antenna coordinates. Therefore the normalization condition becomes

$$T = C_p T \int (G_{pp} + G_{pq}) d\Omega \quad (\text{A54})$$

and

$$C_p = \frac{1}{\int (G_{pp} + G_{pq}) d\Omega} \quad (\text{A55})$$

Now, $G_{pp} + G_{pq} = g_{pp} + g_{pq}$, so this reduces to the same normalization as found in Section A3.3.1.

We now consider the effect of the finite bandwidth of the channels in determining the final antenna temperature equations, and consider the form of the normalization along the way.

Consideration of Bandwidth in the Antenna Temperature Equations

Let $B_p(\nu)$ be the *power bandpass function* of the p-polarized channel. We assume that $B(\nu)$ has been normalized so that

$$\int_{\nu_1}^{\nu_2} B_p(\mathbf{n}) d\mathbf{n} = 1 \quad (\text{A56})$$

where ν_1 and ν_2 are frequencies below and above the center frequency for the channel, beyond which the bandpass function is negligible.

To form an antenna temperature equation that includes the finite bandwidth of the channel, we need to multiply the monochromatic antenna temperature equation by $B(\nu)$ and integrate over frequency. But the question arises as to whether there is an overall normalization factor for the antenna temperature equation,

$$T'_{Ap} = C_p \int_{\nu_1}^{\nu_2} \left[\int (G_{pp} T_p + G_{pq} T_q + G_{pS_1} T_{S_1} + G_{pS_2} T_{S_2}) d\Omega \right] \cdot B_p(\mathbf{n}) d\mathbf{n} \quad (\text{A57-alternate 1})$$

or if the normalization factor is itself frequency dependent, and belongs inside the frequency integral,

$$T'_{Ap} = \int_{\nu_1}^{\nu_2} \left[C_p \int (G_{pp} T_p + G_{pq} T_q + G_{pS_1} T_{S_1} + G_{pS_2} T_{S_2}) d\Omega \right] \cdot B_p(\mathbf{n}) d\mathbf{n} \quad (\text{A57-alternate 2})$$

To choose, we consider the antenna temperature when the antenna is bathed in isotropic, unpolarized radiation with a temperature $T(\nu)$ that has an arbitrary dependence on frequency (but is not identically zero between ν_1 and ν_2). In this case, the antenna temperature must be

$$T'_{Ap} = \int_{n_1}^{n_2} T(\mathbf{n}) B(\mathbf{n}) d\mathbf{n} \quad (\text{A58})$$

Isotropic and unpolarized again means that

$$\begin{aligned} T_p &= T_q = T(\mathbf{n}) \\ T_{S_1} &= T_{S_2} = 0 \end{aligned} \quad (\text{A59})$$

The two alternate forms of the antenna temperature equation (A57) become

$$T'_{Ap} = C_p \int_{n_1}^{n_2} \left[\int (G_{pp} + G_{pq}) d\Omega \right] T(\mathbf{n}) \cdot B_p(\mathbf{n}) d\mathbf{n} \quad (\text{A60-alternate 1})$$

$$T'_{Ap} = \int_{n_1}^{n_2} \left[C_p \int (G_{pp} + G_{pq}) d\Omega \right] T(\mathbf{n}) \cdot B_p(\mathbf{n}) d\mathbf{n} \quad (\text{A60-alternate 2})$$

But, given that $T(\mathbf{v})$ is an arbitrary function, the only way the right hand sides of (A60) and (A58) can be equal is if the integrands of their frequency integrals are equal at all frequencies

$$C_p \int (G_{pp} + G_{pq}) d\Omega T(\mathbf{n}) \cdot B_p(\mathbf{n}) = T(\mathbf{n}) \cdot B_p(\mathbf{n}) \quad (\text{A61})$$

at all frequencies ν between ν_1 and ν_2 . Thus, once again we find

$$C_p = \frac{1}{\int (G_{pp} + G_{pq}) d\Omega} \quad (\text{A62})$$

But, the gain patterns g and phases β (and therefore the G 's) are functions of frequency. Therefore, C_p is itself a function of frequency, and must be included inside the integral over frequency in computing the final antenna temperature equation, as shown below.

$$T'_{Ap} = \int_{n_1}^{n_2} \left[C_p \int (G_{pp} T_p + G_{pq} T_q + G_{pS_1} T_{S_1} + G_{pS_2} T_{S_2}) d\Omega \right] \cdot B_p(\mathbf{n}) d\mathbf{n} \quad (\text{A63})$$

where C_p is defined implicitly as a function of frequency through equation (A62).

To be more explicit, we can write this out to show that the normalization with respect to the gain patterns occurs at each frequency, and is not an overall normalization:

$$T'_{Ap} = \int_{n_1}^{n_2} \left[\frac{\int (G_{pp} T_p + G_{pq} T_q + G_{pS_1} T_{S_1} + G_{pS_2} T_{S_2}) d\Omega}{\int (G_{pp} + G_{pq}) d\Omega} \right] \cdot B_p(\mathbf{n}) d\mathbf{n} \quad (\text{A64})$$

where the G 's are frequency dependent. **Equation (A64) is the final expression for the integral antenna temperature equation for channel p in terms of the earth scene brightness temperatures; the definitions of the G 's are found in Section A.4.3.**

A4. Conversion of Integral Antenna Temperature Equations to Simultaneous Linear Equations

The required function of the antenna cross polarization correction of the SDR algorithm is to invert the antenna temperature measurements to obtain the earth scene temperatures. In order to accomplish this, the integral expressions for the antenna temperatures of section A3.3.2 need to be converted to simultaneous linear equations that can be solved rapidly in the cross polarization correction. We do this here.

We consider two types of approximations to the antenna temperature equations, which allow them to be expressed in terms of linear combinations of the earth scene brightness temperatures at the feed boresights. The first approximation allows for a closed form expression for the coefficients of the boresight earth scene temperatures (ie., the M -matrix); it is sufficient for producing theoretical, predicted and measured M -matrices useful for determining the cross-polarization performance, and for estimating the cross-polarization knowledge error, where theoretical or predicted M -matrices are compared to those produced from actual measurements.

The second method requires simulated brightness temperature data on a fine grid for many ocean-atmosphere scenes, evaluation of the antenna temperature integrals for each polarization for each scene, and a separate regression for the elements in each row of the M -matrix. This method is man-power intensive to set up, computationally intensive, and is not suited to the day-to-day computation and recomputation of the M -matrices that occurs during antenna design and optimization (i.e, during the risk reduction phase). However, our experience with SSM/I shows that determining the cross-polarization matrix this way reduces knowledge error and offers slightly better performance on orbit. Therefore, this method is most appropriate for a single, final determination of the M -matrices for on-orbit use.

A4.1 First Method: Approximation of Earth Scene TBs as Constant over the Range of Integrations

The simplest way to extract linear equations from the antenna temperature integrals is to assume that the earth scene brightness temperatures are constant over the bandwidth and over the projection of the solid angle integration range onto the earth (i.e. are uniform and equal to the brightness temperature at boresight at the center frequency). This is not an unreasonable assumption for the 6-36 GHz window channels. Insofar as the variation with frequency is linear, and the bandpass function $B(\nu)$ is symmetric around the center frequency, the variation away from the center frequency will cancel out in the integral formulation of the antenna equations.

For even a uniform earth scene, the TBs vary with earth incidence angle, as it changes across the range of the solid angle integration. But the variation with earth incidence angle tends to be very linear. Therefore, to the extent that the measured gain patterns g_{pp} and g_{pq} are symmetric about the boresight for channel p , the variation of the TBs away from boresight will cancel in the integral over solid angle.

If we make this assumption, the TBs factor out of both the frequency and solid angle integrals, and the antenna temperature equation for the p -polarized channel becomes

$$T'_{Ap} = M_{pp}T_p + M_{pq}T_q + M_{pS_1}T_{S_1} + M_{pS_2}T_{S_2} \quad (A65)$$

where, using equation (A63), the expressions for the M's become,

$$M_{px} = \int_{n_1}^{n_2} [C_p \int (G_{px}) d\Omega] \cdot B_p(\mathbf{n}) d\mathbf{n} \quad (A66)$$

where the frequency dependent normalization constant is given in (A62) and “x” is one of “p”, “q”, “S₁”, or “S₂”.

Again, the definitions of q, S₁ and S₂ for each channel p are shown in Table A1 in Section A4.3; also equation (A65) is stated explicitly for all polarizations in equation (B1) of Appendix B.

A4.2 Second Method: Regression for M-matrix Coefficients using Simulated TB and TA Data

One does not have to depend on the assumption of uniform brightness temperatures, across frequency and solid angle integration ranges, in determining the M-coefficients in (A65). But, including the variation of the TBs with frequency and EIA complicates the procedure significantly; the M-coefficients must be determined through regression, so no closed form expressions for the coefficients result.

The basic method is to simulate brightness temperatures for wide variety of earth scenes, in increments of frequency around the center frequency, and on a fine grid in antenna coordinates, using the correct EIA for each grid point. All polarizations are simulated. The integral expressions of Section A4.3 are then used to determine the antenna temperatures for each scene. The set of antenna temperatures is then regressed against the brightness temperatures at the boresight EIA and center frequency, to find the M-coefficients.

The step-by-step description of the method for a p-polarized channel is as follows:

- (1) Create an ensemble of geophysical scenes labeled by S_i, i=1,...N. The distributions of the relevant geophysical parameters in the ensemble should be similar to and span the range of the natural distributions. For ocean scenes, is necessary to create scenes which span the range of SST, wind speed, direction, water vapor and cloud liquid water. (The set relevant geophysical parameters for scene S_i are labeled GPS_i). The scenes are spatially uniform.
- (2) Divide the bandpass for the channel into a set of grid points. Label these frequencies ν_j, j=0,...M, with the center frequency denoted ν₀.
- (3) Grid the antenna coordinates inside the range of solid angle integration. Label the grid points (θ_k, φ_k), k=0,...L, with the k=0 label attached to the antenna electrical boresight (θ=0) for channel p. . By projecting the beam on the earth, compute the EIA, θ_i(k) that corresponds to each of the grid points.
- (4) For each geophysical scene S_i, use the radiative transfer model to simulate the brightness temperatures for all 6 polarizations (denoted u), for each grid point in frequency and antenna coordinates (using the correct EIA for each grid point in antenna coordinates). That is, for each scene S_i, compute

$$T_u^{ijk} = T_u(GPS_i, \mathbf{n}_j, \mathbf{q}_i(k)), j = 0, \dots, M, k = 0, \dots, L, u = v, h, +, -, l, r$$

- (5) For scene S_i use the gridded brightness temperatures, as shown above, in a discrete version of the master antenna temperature equation (A64) to compute the simulated antenna temperature for that channel. Call the result T_{Ap}^i . Do this for all scenes to collect the ensemble of simulated antenna temperatures, $i=1, \dots, N$.
- (6) Find the M-coefficients, M_{px} , in (A65) by performing a regression of the simulated boresight brightness temperatures at the center frequency against simulated antenna temperatures from step 5. That is find the M-coefficients in

$$T_{Ap}^i = M_{pp} T_p^{i00} + M_{pq} T_q^{i00} + M_{pS_1} T_{S_1}^{i00} + M_{pS_2} T_{S_2}^{i00} + \mathbf{e}_i$$

that minimizes the sum-square error

$$\sum_{i=1}^N \mathbf{e}_i^2$$

over the ensemble of scenes.

Since we regress to the TBs for the center frequency and the boresight EIA to determine the M-coefficients, we will be retrieving the best estimate of the boresight scene TBs in the cross-polarization correction based on the M-coefficients computed using this method.

A.4.3 Summary of Linear Antenna Temperature Formulae

For a p-polarized channel, the linearized antenna temperature equation can be expressed as

$$T'_{Ap} = M_{pp} T_p + M_{pq} T_q + M_{pS_1} T_{S_1} + M_{pS_2} T_{S_2} \quad (\text{A100})$$

where S_1 and S_2 are defined by the Stokes parameters corresponding to the real and imaginary parts of $2\langle E_p E_q^* \rangle$, respectively; where q is the orthogonal polarization to p, S_1 and S_2 are the Stokes parameters corresponding to the polarizations that are not orthogonal to p; in Table A1 these are compiled from the antenna equations derived in Section A3.3.1. For the approximation of uniform brightness temperatures across bandwidth and earth scene, we found in Section A3.3.2 that the expressions for the M-coefficients are

$$M_{px} = \int_{n_1}^{n_2} \left[C_p \int (G_{px}) d\Omega \right] \cdot B_p(\mathbf{n}) d\mathbf{n} \quad (\text{A101})$$

B_p is the bandpass function for the p-polarized channel and x is one of p, q, S_1 , or S_2 . In section A3.3.1, we found that the G's for the linear polarizations are given by

$$\begin{aligned}
G_{pp} &= g_{pp'} \cos^2 \mathbf{a} + g_{pq'} \sin^2 \mathbf{a} - \sqrt{g_{pp'} g_{pq'}} \cos \mathbf{b}_p \sin 2\mathbf{a} \\
G_{pq} &= g_{pp'} \sin^2 \mathbf{a} + g_{pq'} \cos^2 \mathbf{a} + \sqrt{g_{pp'} g_{pq'}} \cos \mathbf{b}_p \sin 2\mathbf{a} \\
G_{pS_1} &= \pm \left[\frac{1}{2} (g_{pp'} - g_{pq'}) \sin 2\mathbf{a} + \sqrt{g_{pp'} g_{pq'}} \cos \mathbf{b}_p \cos 2\mathbf{a} \right] \quad (\text{A102})
\end{aligned}$$

$$G_{pS_2} = -\sqrt{g_{pp'} g_{pq'}} \sin \mathbf{b}_p$$

$$\mathbf{b}_p = \mathbf{b}_{pp} - \mathbf{b}_{pq}$$

Although we have not emphasized it, these are the power gain functions with respect to brightness temperatures in the earth polarization basis.

The normalization factor is frequency dependant and is given by

$$C_p = \frac{1}{\int (G_{pp} + G_{pq}) d\Omega} \quad (\text{A103})$$

The G's for the circular polarizations, which are computed from gain functions and phase measured using v' and h' polarized radiation, were found in Section A3.3.1 to be:

$$\begin{aligned}
G_{pp} &= \frac{1}{2} (g_{pv'} + g_{ph'}) + \sqrt{g_{pv'} g_{ph'}} \cos \mathbf{b}_p \\
G_{pq} &= \frac{1}{2} (g_{pv'} + g_{ph'}) - \sqrt{g_{pv'} g_{ph'}} \cos \mathbf{b}_p \\
G_{pS_1} &= \frac{1}{2} (g_{pv'} - g_{ph'}) \cos 2\mathbf{a} \mp \sqrt{g_{pv'} g_{ph'}} \sin \mathbf{b}_p \sin 2\mathbf{a} \quad (\text{A104}) \\
G_{pS_2} &= \frac{1}{2} (g_{pv'} - g_{ph'}) \sin 2\mathbf{a} \pm \sqrt{g_{pv'} g_{ph'}} \sin \mathbf{b}_p \cos 2\mathbf{a} \\
\mathbf{b}_p &= \mathbf{b}_{pv} - \mathbf{b}_{ph}
\end{aligned}$$

All of the g's and β 's, and therefore all the G's, are assumed to be frequency dependent. Polarizations q, S₁, S₂, and the sign of the +/- terms in G_{ps1} and G_{ps2} are given for each polarization p in Table A1. When the sign has already been included in the expression for the matrix element (G_{p4}) the sign is put in parenthesis to denote that it should not be applied again.

p	q	S ₁	Sign G _{ps1}	S ₂	Sign G _{ps2}
v	h	U	+	4	(-)
h	v	U	-	4	(-)
+	-	Q	-	4	(-)
-	+	Q	+	4	(-)
l	r	Q	-	U	+
r	l	Q	+	U	-

Table A1: Stokes parameters q, S₁ and S₂ that correspond to each polarization, p. Sign ambiguity in formulae for G's is also shown.

A.5 Rotation Angle between Reference and Earth Scene Polarization Vector

The angle α was defined in Section 3.3.1 (power equation) as the rotation between the polarization vectors of the reference antenna used in range measurement of the gain functions

and phases, and the corresponding polarization vectors on the earth. To determine the latter, we project the antenna spherical polar coordinates on the earth, with origin of the polar coordinate centered on the nominal nadir angle for that frequency, and find the earth polarization vectors as a function of antenna coordinates. Thus, α is a function of antenna coordinates and the nominal nadir angle.

The form of the expression for α will depend upon the choice of the reference antenna polarization vectors. There are several conventions used for the reference polarization vectors, which are defined in Ludwig (Ludwig 73). While the measurements of gain functions and phase will be measured in the near field, the measurements will be translated to the far field, with reference polarizations that are consistent with Ludwig's third definition of polarization vectors.

We give without derivation the expression for α for this definition of the far field reference polarization vectors:

$$\mathbf{a} = \mathbf{h} - \mathbf{j}$$

Where:

$$\sin \mathbf{h} = \frac{AC \cos \mathbf{q}_n \sin \mathbf{j} - BC \cos \mathbf{j} - (A^2 + B^2) \sin \mathbf{q}_n \sin \mathbf{j}}{\sqrt{A^2 + B^2}}$$

$$\cos \mathbf{h} = \frac{B \cos \mathbf{q}_n \sin \mathbf{j} + A \sin \mathbf{j}}{\sqrt{A^2 + B^2}}$$

$$\begin{pmatrix} A \\ B \\ C \end{pmatrix} = \begin{pmatrix} \cos \mathbf{q}_n \sin \mathbf{q} \cos \mathbf{j} + \sin \mathbf{q}_n \cos \mathbf{q} \\ \sin \mathbf{q} \sin \mathbf{j} \\ \sin \mathbf{q}_n \sin \mathbf{q} \cos \mathbf{j} - \cos \mathbf{q}_n \cos \mathbf{q} \end{pmatrix}$$

The azimuthal antenna coordinate ϕ is measured from counter-clockwise from the plane of incidence at boresight. θ is the polar antenna coordinate. θ_n is the nominal nadir angle at the boresight ($\theta=0$).

Appendix A references:

Ludwig 73: Ludwig, A. "The Definition of Cross Polarization", IEEE Trans. Antenna Propagat., Vol. AP-21, pp116-119, June 1973

APPENDIX B: REPRESENTATIONS OF THE CROSS-POLARIZATION MATRIX

B.1 Introduction

In this appendix, we derive expressions for the M-matrix representations (channel, Stokes, and mixed) discussed in the body of this document. We also consider the properties of the cross-polarization corrections based on each representation.

There are several properties that are important for a cross-polarization correction:

1. The cross-polarization correction should be robust with respect to spurious noise, or a problem with the TA from a single channel. That is the problem should not be propagated in a significant way to the derived brightness temperatures for other polarizations (the problem should be largely confined to the derived TB for the corresponding polarization).
2. The cross-polarization correction should minimize correlation of the noise in the derived TBs; the SST algorithm, whose performance at high SST is very close to the measurement uncertainty requirement, is especially sensitive to correlated noise in the TBs.
3. The cross-polarization correction should be robust with respect to single channel failure. By this we mean that a single channel failure should not corrupt the derived TBs for all polarizations.

Considerations (1) and (2) require that the correction should not mix the antenna temperatures any more than is necessary to derive the scene brightness temperatures. That is, the SDR derived TB for polarization p should depend to the maximum extent on the p-polarized antenna temperature.

Consideration (3) also implies that the mixing of TAs in the correction should be minimized. However, this is not in itself sufficient; one cannot simply zero out the TA for the failed channel and presume that the correction will work. Therefore, it is necessary for robustness in the face of single channel failure that the cross-polarization correction can be easily modified to take into account the missing channel, and provide accurate results for the TBs of all other polarizations.

Therefore, after concluding the discussion of the various representations, we assess the robustness of the SDR algorithms for each representation, and select the algorithm that best meets these criteria.

B.2 Form of the Cross-Polarization Equations

In Section A4, we showed that the equations for the scene components of the antenna temperatures can be put in the form

$$\begin{aligned}
T'_{Av} &= [M_{vv}T_v + M_{vh}T_h] + M_{vU}T_U + M_{v4}T_4 \\
T'_{Ah} &= [M_{hv}T_v + M_{hh}T_h] + M_{hU}T_U + M_{h4}T_4 \\
T'_{A+} &= M_{+Q}T_Q + [M_{++}T_+ + M_{+-}T_-] + M_{+4}T_4 \\
T'_{A-} &= M_{-Q}T_Q + [M_{-+}T_+ + M_{--}T_-] + M_{-4}T_4 \\
T'_{Al} &= M_{lQ}T_Q + M_{lU}T_U + [M_{ll}T_l + M_{lr}T_r] \\
T'_{Ar} &= M_{rQ}T_Q + M_{rU}T_U + [M_{rl}T_l + M_{rr}T_r]
\end{aligned} \tag{B1}$$

As in appendix A, we are considering the effect of antenna cross polarization alone (no CMIS or Faraday Rotation) and therefore drop the double prime that appears on the scene brightness temperatures in Section 6. However, we do not drop the prime on the antenna temperatures; we want to continually remind the reader that we are writing equations for, and the input to the cross-polarization correction are, the scene components of the antenna temperature (spillover corrected TAs).

The purpose of the brackets in (B1) is simply to show that, for any two orthogonal polarizations p,q, the antenna temperature equations for T_{Ap} and T_{Aq} involve the p and q polarized brightness temperatures (individual polarizations), and the two scene Stokes parameters that can be made from the polarizations that are not orthogonal to p and q (denoted S_1 and S_2 in appendix A, and listed in Table A1).

Also, the bracketed M-coefficients for each row sum to one.

$$M_{pp} + M_{pq} = 1. \tag{B1-b}$$

Using the assumption of uniform brightness temperatures in Section A4.1, this is apparent from combining equations (A66) and (A62). However (B-1b) must be true however one defines the M-coefficients (Section A4.1 or A4.2). It is just a reflection of the requirement that the antenna temperatures be T when the antenna is bathed in isotropic unpolarized blackbody radiation of temperature T.

The traditional TA equations for a v,h polarized instrument consists of the bracketed terms in the first two equations of (B1); cross-polarization from the third and forth Stokes parameters are neglected; no measurements of the +,-,l,r polarizations are made, so cross-polarization from them into the v, h measurements cannot be corrected. Because T_U and T_4 are small (a few K or less) compared to the v and h TBs, the residual cross-polarization from T_U and T_4 does not significantly affect the TBs derived from inverting the traditional TA equations. In fact, for CMIS frequencies 6 and 23 GHz, the column-elimination method described in Section 6.3.2.3 results in the traditional v,h TA equations.

However, for polarimetric channels it would be perilous to assert by analogy that only the bracketed terms be used; T_Q is not small for ocean scenes (typically 85K), and ignoring the T_Q terms in the third through sixth equations in (B1) is certain to add a large biases to the derived scene TBs. Fortunately, we measure the v, h polarizations at all frequencies so the T_Q terms are never discarded.

When the gain functions for the linear (circular) polarizations are measured with linear (circular) polarized radiation from a test antenna, the antenna equations naturally come out in the form of

(B1). However, as in our case, when the circularly polarized channels are measured using linearly polarized test radiation, a little re-arrangement is necessary to make the l and r TA equations come out in this form.

B.3 The Channel Representation for the M-matrix

TA equations in the form of (B1) cannot be inverted to obtain the scene TBs, because the variables on the right hand side are different for each pair of antenna temperatures. The simplest way to write (B1) so that it can be inverted is to expand the equations in terms of the individual polarized brightness temperatures by substituting in the definitions of the scene Stokes parameters

$$\begin{aligned} T_Q &= T_v - T_h \\ T_U &= T_+ - T_- \\ T_4 &= T_l - T_r \end{aligned} \quad (\text{B2})$$

which yields

$$\begin{pmatrix} T'_{Av} \\ T'_{Ah} \\ T'_{A+} \\ T'_{A-} \\ T'_{Al} \\ T'_{Ar} \end{pmatrix} = \begin{pmatrix} M_{vv} & M_{vh} & M_{vU} & -M_{vU} & M_{v4} & -M_{v4} \\ M_{hv} & M_{hh} & M_{hU} & -M_{hU} & M_{h4} & -M_{h4} \\ M_{+Q} & -M_{+Q} & M_{++} & M_{+-} & M_{+4} & -M_{+4} \\ M_{-Q} & -M_{-Q} & M_{-+} & M_{--} & M_{-4} & -M_{-4} \\ M_{lQ} & -M_{lQ} & M_{lU} & -M_{lU} & M_{ll} & M_{lr} \\ M_{rQ} & -M_{rQ} & M_{rU} & -M_{rU} & M_{rl} & M_{rr} \end{pmatrix} \begin{pmatrix} T_v \\ T_h \\ T_+ \\ T_- \\ T_l \\ T_r \end{pmatrix} \quad (\text{B3, Master 6x6})$$

We call the matrix on the right hand side the 6x6 M-matrix for obvious reasons, even when TAs are not measured for all 6 polarizations.

We call the matrix in (B3) the master 6x6 M-matrix, for reasons that will become apparent in a moment. The representation of the 6x6 M-matrix in Equation (B3) is not unique. This is because of the relationship between the scene TBs

$$T_v + T_h = T_+ + T_- = T_l + T_r. \quad (\text{B4})$$

Therefore, for a given row in the M-matrix of (B3), one can subtract a constant C from the matrix elements for any two orthogonal polarizations and add C to the matrix elements for any other two polarizations, and obtain another M-matrix that is also a valid representation of the M-matrix (i.e. is equivalent to the description in (B3)). For example

$$\begin{pmatrix} T'_{Av} \\ T'_{Ah} \\ T'_{A+} \\ T'_{A-} \\ T'_{Al} \\ T'_{Ar} \end{pmatrix} = \begin{pmatrix} M_{vv} & M_{vh} & M_{vU} & -M_{vU} & M_{v4} & -M_{v4} \\ M_{hv} & M_{hh} & M_{hU} & -M_{hU} & M_{h4} & -M_{h4} \\ M_{+Q} & -M_{+Q} & M_{++} & M_{+-} & M_{+4} & -M_{+4} \\ M_{-Q} & -M_{-Q} & M_{-+} & M_{--} & M_{-4} & -M_{-4} \\ M_{lQ} + \frac{1}{2} & -M_{lQ} + \frac{1}{2} & M_{lU} & -M_{lU} & M_{ll} - \frac{1}{2} & M_{lr} - \frac{1}{2} \\ M_{rQ} + \frac{1}{2} & -M_{rQ} + \frac{1}{2} & M_{rU} & -M_{rU} & M_{rl} - \frac{1}{2} & M_{rr} - \frac{1}{2} \end{pmatrix} \begin{pmatrix} T_v \\ T_h \\ T_+ \\ T_- \\ T_l \\ T_r \end{pmatrix} \quad (\text{B5})$$

is an equivalent expression of (B3). (In fact, a little algebra shows that the transformation on the circularly polarized TA equations used in Appendix A to put them in the form of (B1) is really a transformation of (B5) to (B3).)

But, the importance of representation (B3) is that the M-matrix that results is nearly diagonal. This can be seen by using a rearrangement of (B-1b)

$$M_{pp} = 1 - M_{pq} \quad (\text{B6})$$

to put (B3) in a more suggestive form:

$$M^{66} = \begin{pmatrix} 1 - M_{vh} & M_{vh} & M_{vU} & -M_{vU} & M_{v4} & -M_{v4} \\ M_{hv} & 1 - M_{hv} & M_{hU} & -M_{hU} & M_{h4} & -M_{h4} \\ M_{+Q} & -M_{+Q} & 1 - M_{+-} & M_{+-} & M_{+4} & -M_{+4} \\ M_{-Q} & -M_{-Q} & M_{-+} & 1 - M_{-+} & M_{-4} & -M_{-4} \\ M_{lQ} & -M_{lQ} & M_{lU} & -M_{lU} & 1 - M_{lr} & M_{lr} \\ M_{rQ} & -M_{rQ} & M_{rU} & -M_{rU} & M_{rl} & 1 - M_{rl} \end{pmatrix} \quad (\text{B7, alt of (B3)})$$

This puts each row of the M-matrix in terms of the three independent parameters, corresponding to the three parameters (2 gain functions and 1 relative phase) used to compute the row.” But, the point of writing (B3) in form (B7) is that the off diagonal elements, M_{pq} , M_{pS1} , and M_{pS2} , are much less than one (as borne out by the M-matrices shown in Section 6.5.3).

The solution of (B3) for the scene TBs is

$$\vec{T}_B = (M^{66})^{-1} \vec{T}_A \quad (\text{B8})$$

i.e., the cross-polarization correction based on the 6x6 M-matrix uses the inverse of the 6x6 M-matrix. Since M^{66} in equation (B3) differs from the identity matrix by small quantities, the inverse of M^{66} will differ from the identity matrix by only small quantities. In other words, because M^{66} is nearly the identity matrix, its inverse is nearly the identity matrix.

Thus, the use of M^{66} in the form of (B3) in the cross-polarization correction minimizes the mixing of the antenna temperatures of different polarizations and maximizes the contribution of the co-pol TA's in the solution for the TBs.

Additionally, our simulations of the SDR algorithm show that the inverted matrix has the same symmetry properties as (B7); that is the elements of a given row of the inverted matrix sum to 1, and the matrix elements of row p that correspond to two orthogonal polarizations that are not orthogonal to p are of equal magnitude and opposite sign. This means that only the difference of the + and – and l and r TAs appear in the solution for T_v and T_h , the difference of the v and h and the + and – channels appear in the solution for T_+ and T_- , etc.

Another reason for using the representation (B3) for the 6x6 M-matrix is convenience in performing the knowledge error sensitivity analyses. We can also use (B6) to obtain another equivalent expression of the matrix in (B3) as

$$M^{66} = \begin{pmatrix} M_{vv} & 1 - M_{vv} & M_{vU} & -M_{vU} & M_{v4} & -M_{v4} \\ M_{hv} & 1 - M_{hv} & M_{hU} & -M_{hU} & M_{h4} & -M_{h4} \\ M_{+Q} & -M_{+Q} & M_{++} & 1 - M_{++} & M_{+4} & -M_{+4} \\ M_{-Q} & -M_{-Q} & M_{-+} & 1 - M_{-+} & M_{-4} & -M_{-4} \\ M_{lQ} & -M_{lQ} & M_{lU} & -M_{lU} & M_{ll} & 1 - M_{ll} \\ M_{rQ} & -M_{rQ} & M_{rU} & -M_{rU} & M_{rl} & 1 - M_{rl} \end{pmatrix}. \quad (\text{B9, alt of (B3)})$$

Equation B7 makes it clear that the knowledge error matrix can be represented as

$$\Delta M^{66} = \begin{pmatrix} \Delta M_{vv} & -\Delta M_{vv} & \Delta M_{vU} & -\Delta M_{vU} & \Delta M_{v4} & -\Delta M_{v4} \\ \Delta M_{hv} & -\Delta M_{hv} & \Delta M_{hU} & -\Delta M_{hU} & \Delta M_{h4} & -\Delta M_{h4} \\ \Delta M_{+Q} & -\Delta M_{+Q} & \Delta M_{++} & -\Delta M_{++} & \Delta M_{+4} & -\Delta M_{+4} \\ \Delta M_{-Q} & -\Delta M_{-Q} & \Delta M_{-+} & -\Delta M_{-+} & \Delta M_{-4} & -\Delta M_{-4} \\ \Delta M_{lQ} & -\Delta M_{lQ} & \Delta M_{lU} & -\Delta M_{lU} & \Delta M_{ll} & -\Delta M_{ll} \\ \Delta M_{rQ} & -\Delta M_{rQ} & \Delta M_{rU} & -\Delta M_{rU} & \Delta M_{rl} & -\Delta M_{rl} \end{pmatrix}. \quad (\text{B10})$$

In other words, we can simulate a set of knowledge errors for the 1st, 3rd and 5th columns, and the knowledge errors for the 2nd, 4th, and 6th columns are just the negative of the previously mentioned columns, respectively.

B.4 The Mixed Representation for the M-Matrix

Given that only 4 Stokes parameters are required to completely specify any polarization state of radiation, it is possible to express the antenna cross-pol equation using the scene Stokes parameters. This can be accomplished, for example, by simply substituting the results of combining equation (B2) and (B4) to obtain

$$\begin{aligned} T_+ &= \frac{T_v + T_h}{2} + \frac{T_U}{2} & T_- &= \frac{T_v + T_h}{2} - \frac{T_U}{2} \\ T_l &= \frac{T_v + T_h}{2} + \frac{T_4}{2} & T_r &= \frac{T_v + T_h}{2} - \frac{T_4}{2} \end{aligned} \quad (\text{B11})$$

and then substituting these definitions of the polarized TBs into (B3) to obtain

$$\begin{pmatrix} T'_{Av} \\ T'_{Ah} \\ T'_{A+} \\ T'_{A-} \\ T'_{Al} \\ T'_{Ar} \end{pmatrix} = \begin{pmatrix} M_{vv} & M_{vh} & M_{vU} & M_{v4} \\ M_{hv} & M_{hh} & M_{hU} & M_{h4} \\ M_{+Q} + \frac{1}{2} & \frac{1}{2} - M_{+Q} & \frac{1}{2} - M_{+-} & M_{+4} \\ M_{-Q} + \frac{1}{2} & \frac{1}{2} - M_{-Q} & M_{-+} - \frac{1}{2} & M_{-4} \\ M_{lQ} + \frac{1}{2} & \frac{1}{2} - M_{lQ} & M_{lU} & \frac{1}{2} - M_{lr} \\ M_{rQ} + \frac{1}{2} & \frac{1}{2} - M_{rQ} & M_{rU} & M_{rl} - \frac{1}{2} \end{pmatrix} \begin{pmatrix} T_v \\ T_h \\ T_U \\ T_4 \end{pmatrix} \equiv \mathbf{M}^{64} \begin{pmatrix} T_v \\ T_h \\ T_U \\ T_4 \end{pmatrix} \quad (\text{B12})$$

We have also used (B5) to simplify factors leading with $\frac{1}{2}$. The TA equations then represent 4 unknowns (TBs) in 6 equations. If there were no NEDTs, and the elements of the 6x6 M-matrix had not knowledge error, then we could state that these equations were exact. But due to the presence of noise in the TAs, they are not exact, and require solution by least squares.

For the sake of simplification, let's assume that the NEDTs for the six antenna temperatures all come from the same distribution (actually we know for ocean scenes, the h-pol NEDT is smaller than v-pol NEDT, and the NEDTs for the other antenna temperatures are about the average of the NEDTs for v- and h-pol). In that case, the solution for the scene TBs is

$$\begin{pmatrix} T_v \\ T_h \\ T_U \\ T_4 \end{pmatrix} = \left(\mathbf{M}_{64}^T \mathbf{M}_{64} \right)^{-1} \mathbf{M}_{64}^T \begin{pmatrix} T'_{Av} \\ T'_{Ah} \\ T'_{A+} \\ T'_{A-} \\ T'_{Al} \\ T'_{Ar} \end{pmatrix} \quad (\text{B13})$$

To get some idea of the behavior of a cross-polarization correction based on (B13), let's assume for the moment that there is no cross-polarization in any of the channels. Then the 6x6 M-matrix defined by (B3) is equal to the identity matrix, and from (B12) the 6x4 M-matrix is

$$\mathbf{M}^{64} = \begin{pmatrix} 1 & 0 & 0 & 0 \\ 0 & 1 & 0 & 0 \\ \frac{1}{2} & \frac{1}{2} & \frac{1}{2} & 0 \\ \frac{1}{2} & \frac{1}{2} & -\frac{1}{2} & 0 \\ \frac{1}{2} & \frac{1}{2} & 0 & \frac{1}{2} \\ \frac{1}{2} & \frac{1}{2} & 0 & -\frac{1}{2} \end{pmatrix} \quad (\text{B13, 6x4 for no cross-pol})$$

and the “inverse” is then

$$(M_{64}^T M_{64})^{-1} M_{64}^T = \begin{pmatrix} \frac{2}{3} & -\frac{1}{3} & \frac{1}{6} & \frac{1}{6} & \frac{1}{6} & \frac{1}{6} \\ -\frac{1}{3} & \frac{2}{3} & \frac{1}{6} & \frac{1}{6} & \frac{1}{6} & \frac{1}{6} \\ 0 & 0 & 1 & -1 & 0 & 0 \\ 0 & 0 & 0 & 0 & 1 & -1 \end{pmatrix} \quad (\text{B14, inverse of B13})$$

All polarizations are mixed significantly in the least squares solution for T_v and T_h , even though the simplest solution is just

$$\begin{aligned} T_v &= T'_{Av} \\ T_h &= T'_{Ah} \end{aligned} \quad (\text{B15})$$

The solution for T_U and T_4 is the same as the simplest solution. However, the mixing of antenna temperatures in the solution for the T_v and T_h is to be expected: least squares tries to minimize the RMS error in the product, which it does by minimizing the sum-square of the coefficients in the first two rows (the noise in the least square solution is $\sqrt{2/3}$ *NEDT, whereas the noise in the simplest solution is just NEDT). In doing this, it maximizes the mixing of the channels in the cross-pol correction. When one considers the normal equations for the least squares solution for actual NEDTs, the solution for T_v makes even more use of the other polarizations (the mixing becomes more pronounced).

B.5 The Stokes Representation for the M-matrix

Equations (B12) can be considered as exact in the case of zero NEDTs. Given that there are four unknowns in 6 equations, either there is one solution or no solution. In the case of a solution, two of the TA equations must be dependent on the others; then, just as T_v , T_h , $T_U = T_+ - T_-$, and $T_4 = T_l - T_r$ form an independent basis from which any polarized TB can be computed, T_{Av} , T_{Ah} , $T_{AU} = T_{A+} - T_{A-}$, and $T_{A4} = T_{Al} - T_{Ar}$ form an independent basis from which any polarized TA can be computed. Therefore, we can replace both the T_{A+} and T_{A-} equation with their difference, and replace the T_{Al} and T_{Ar} equations by their difference to form a new set of equivalent equations:

$$\begin{pmatrix} T'_{Av} \\ T'_{Ah} \\ T'_{AU} \\ T'_{A4} \end{pmatrix} = \begin{pmatrix} 1 - M_{vh} & M_{vh} & M_{vU} & M_{v4} \\ M_{hv} & 1 - M_{hv} & M_{hU} & M_{h4} \\ M_{+Q} - M_{-Q} & -(M_{+Q} - M_{-Q}) & 1 - (M_{++} + M_{--}) & M_{+4} - M_{-4} \\ M_{lQ} - M_{rQ} & -(M_{lQ} - M_{rQ}) & M_{lU} - M_{rU} & 1 - (M_{lr} + M_{rl}) \end{pmatrix} \begin{pmatrix} T_v \\ T_h \\ T_U \\ T_4 \end{pmatrix} \quad (\text{B16})$$

$$\equiv M^{44} \begin{pmatrix} T_v \\ T_h \\ T_U \\ T_4 \end{pmatrix}$$

We have used (B5) again to put the diagonal elements of the first two rows in terms of matrix elements much less than 1. As all of the matrix elements in (B16) are small compared to 1, this matrix is nearly diagonal (in fact, nearly the 4x4 identity matrix). As the 6x4 matrix was unique, so is the 4x4. The beginning of the SDR algorithm that corresponds to (B16) is simple matrix inversion:

$$\begin{pmatrix} T_v \\ T_h \\ T_U \\ T_4 \end{pmatrix} = M_{44}^{-1} \begin{pmatrix} T'_{Av} \\ T'_{Ah} \\ T'_{AU} \\ T'_{A4} \end{pmatrix} \quad (\text{B17})$$

Since the matrix is nearly the identity matrix, one does not expect mixing of the TAs in the solution beyond what is necessary, unlike the 6x4 algorithm.

However, all algorithms require as input the individually polarized TBs, and not the Stokes parameters (the only place where the Stokes parameters are used is in the wind direction ambiguity search, but even there, the model function is filled in with regression values of parameters determined using individual polarizations). Therefore it is necessary to convert the Stokes parameters back to individual polarizations using equations (B11). This results in extreme mixing of the v and h TAs into the solution for each of the polarimetric TBs.

B.6 Selection of the M-matrix Representation for the Cross-polarization Correction

The mixed (6x4) representation of the M-matrix results in a cross-polarization correction that does not meet our robustness criteria, due to the extreme mixing of the TAs in the solution for T_v and T_h , and therefore will not be considered further.

The Stokes (4x4) representation results in a cross-polarization correction that does not mix the TAs significantly in the solution for T_v , T_h , T_U , or T_4 . However, since the conversion back to individual channels is required, any problem in the T_v and T_h channels is propagated at the 50% level into the derived polarimetric TBs. Furthermore, if one polarimetric channel fails, the inputs to the SDR algorithm (difference of polarimetric channels) cannot be computed. One could eliminate the equation (row) and column corresponding to the missing channel, similar to the elimination method described in the main text, but then one cannot correct for the cross-polarization from what are now 2 missing TBs. We will show below a way to fix this problem, but it requires that the M-matrix be written in the 6x6 form in order to perform the fix.

Testing of the cross-polarization correction algorithm bases on the 4x4 M-matrix shows that the SST algorithm performs 0.02-0.04K worse than using the correction based on the 6x6 M-matrix. We attribute this to the correlation of the NEDTs between the derived v,h and polarimetric channels. While better than the 6x4 algorithm, the 4x4 algorithm doesn't meet the robustness or noise correlation criteria.

The cross-polarization correction based on the form (B3) of the channel representation (6x6) M-matrix is the most robust algorithm. It minimizes the mixing of the TAs in the solution for each TB, and therefore does not propagate spurious noise or other problems with a single channel into the derived TBs for other polarizations in a significant way. Nor does it correlate the NEDTs in the derived TBs significantly.

A single channel failure can be handled in two ways. Lets assume that it is the + channel that fails. Since the solution for the v,h,l,r TBs only use the difference of the + and – channels, it is possible to give up on trying to derive T_+ and T_- , and eliminate those rows and columns from the M-matrix, resulting in a square matrix that can be inverted to obtain T_v , T_h , T_r , and T_l . However, the cross-polarization from the difference of the + and – channels will not be removed in the process. We find this unsatisfactory, because a single channel failure results in not being able to obtain 2 polarized TBs.

However, there is another solution. Since $T_v + T_h = T_+ + T_-$, one can substitute

$$T_+ = T_v + T_h - T_- \quad (\text{B18})$$

into (B3) to obtain another set of TA equations in terms of all TBs other than T_+ . Then, one eliminates the equation for T_{A+} from set resulting of equations, making the system a set of 5x5 equations that can be inverted to solve for all TBs other than T_+ .

The resulting equations are

$$\begin{pmatrix} T'_{Av} \\ T'_{Ah} \\ T'_{A-} \\ T'_{Al} \\ T'_{Ar} \end{pmatrix} = \begin{pmatrix} M_{vv} + M_{vU} & M_{vh} + M_{vU} & -2M_{vU} & M_{v4} & -M_{v4} \\ M_{hv} + M_{hU} & M_{hh} + M_{hU} & -2M_{hU} & M_{h4} & -M_{h4} \\ M_{-Q} + M_{-+} & M_{-+} - M_{-Q} & M_{-+} - M_{-Q} & M_{-4} & -M_{-4} \\ M_{lQ} + M_{lU} & M_{lU} - M_{lQ} & -2M_{lU} & M_{ll} & M_{lr} \\ M_{rQ} + M_{rU} & M_{rU} - M_{rQ} & -2M_{rU} & M_{rl} & M_{rr} \end{pmatrix} \begin{pmatrix} T_v \\ T_h \\ T_- \\ T_l \\ T_r \end{pmatrix} \quad (\text{B19})$$

Recall that the matrix elements M_{pp} are near 1 and all others are $\ll 1$. Therefore, we have preserved the near-diagonal nature of the M-matrix in this transformation, and its inverse will also be nearly diagonal, i.e., result in only a little more mixing of the TAs in the solution for the TBs than the original equations (B3).

Additionally, and estimate of the missing T_+ can be found from (B18), although one has to accept that the noise in T_+ will be highly correlated with that in T_v and T_h and T_- .

Therefore, one can recover all 6 polarized TBs if one is willing to accept some correlation in the noise between the synthesized TB corresponding to the missing TA and the noise in the other TBs. Regardless of the missing channel, it is always possible to do this, as long as at least two sets of orthogonal polarizations is measured, as the following Table shows

Missing or Degraded Channel	If T_{A+} and T_{A-} measured, substitute into (B3)	If T_{Al} and T_{Ar} are measured, substitute into (B3)
T_v	$T_v = T_+ + T_- - T_h$	$T_v = T_l + T_r - T_h$
T_h	$T_h = T_+ + T_- - T_v$	$T_h = T_l + T_r - T_v$
T_+	--	$T_+ = T_v + T_h - T_-$ or $T_+ = T_l + T_r - T_-$
T_-	--	$T_- = T_v + T_h - T_+$ or $T_- = T_l + T_r - T_+$
T_l	$T_l = T_v + T_h - T_r$ or $T_l = T_+ + T_- - T_r$	--
T_r	$T_r = T_v + T_h - T_l$ or	--

	$T_r = T_+ + T_- - T_l$	
--	-------------------------	--

Most important is the fact that these are simple substitutions, and in the event of single channel degradation or failure, the algebra can be done quickly, and the SDR cross-polarization correction algorithm for that frequency can be modified in short order. In fact it may be possible to automate the entire process of accommodating a missing channel. This could be done by using a set of channel use switches (1's and 0's) to describe what channels are to be used. The algorithm could automatically detect difference between the channel use switches and the nominal channel set. The above transformations can each be expressed as a matrix (call it N) which multiplies the M in (B3) on the right, and then the equation for the missing channel can be removed automatically as well. After the cross-polarization correction, it is possible to obtain a good estimate of the missing TB by multiplying the vector of derived TBs by N on the left.

B.7 Conclusion

The M-matrix in the channel representation was selected for the cross-polarization correction, because:

it is robust with respect to spurious noise or degradation in a single channel. It does not add significant correlation to the noise in the SDR derived TBs, as required by the SST EDR algorithm.

It is also a trivial matter to alter a cross-polarization correction based on the channel representation to accommodate a single channel failure, and still obtain TBs for all desired polarizations.

Furthermore, the process of accommodating a single channel failure can be automated in the cross-polarization correction.

It is important to note that we do not in any way expect a channel to fail during the sated life of the CMIS instruments. However, carefully considering the event of channel failure as we have done here may allow the life of the instrument to be extended in a way that is more or less transparent to the users of the SDR product.

APPENDIX C: LINEARITY: PLANCK VERSUS BRIGHTNESS TEMPERATURE

An ideal radiometer responds linearly to input radiative power. That power can be expressed as radiance, so the ideal radiometer response can be expressed as $V=a+bL$, where V is output voltage and L is input radiance.

For calibration, we measure the radiometer output voltages for views of two scenes (V_1 and V_2). If we know the brightness temperature of each scene (T_{B1} and T_{B2}) and the frequency, we can compute each scene's radiance (L_1 and L_2) from the Planck function. When radiometer linearity is assumed, the measurements V_1 , V_2 , L_1 , and L_2 can be used to solve for a and b , and those coefficients can then be used to convert any other measured V into a radiance. The inverse of the Planck function can then be used to compute the temperature of a blackbody that would emit that radiance: the brightness temperature T_B .

Alternatively, calibration can be done under the assumption that the radiometer responds linearly to the input brightness temperature. In this case, it is assumed that $V=c+dT_B$ and V_1 , V_2 , T_{B1} , and T_{B2} are used to solve for c and d .

Say that we are given a pair of calibration targets and use the measurements to solve for a , b , c , and d . Then, given a measurement V , we can determine the radiance and brightness temperature

from $L = \frac{V-a}{b}$ and $T_B = B^{-1}(L, \mathbf{n})$, where $B(T, \mathbf{n})$ is the Planck function and $B^{-1}(L, \mathbf{n})$ is its

inverse and \mathbf{n} is the frequency. We can also compute an estimate of the brightness temperature

from $\hat{T}_B = \frac{V-c}{d}$. The difference $\hat{T}_B - T_B$ is the error, in terms of brightness temperature, that

comes about from assuming the radiometer response is linear with respect to brightness temperature instead of radiance.

This error is illustrated in Fig. C-1b for the case where $T_{B1} = 3$ K and $T_{B2} = 300$ K. The error is less than 0.1 K for all values of T_B , for frequencies 37 GHz and lower. At 183 GHz, the error is as large as 1.5 K. Note that the error varies roughly linearly among brightness temperatures greater than about 60 K, which indicates that the nonlinearity is concentrated at temperatures below 60 K. Fig. C-1a illustrates the errors for the case where the calibration targets have temperatures $T_{B1} = 80$ K and $T_{B2} = 300$ K. In this case, the errors are very small at all frequencies.

The case of Fig. C-1b is characteristic of in-flight calibration for CMIS. The graphs indicate that the nonlinearity of the brightness temperature with respect to radiance must be accounted for in the CMIS calibration, at least for the higher frequency channels.

From Fig. C-1a, we can see that this nonlinearity is not apparent when the cold calibration target is at a temperature more typical of pre-flight calibration test conditions. If, on the other hand, pre-flight tests use a lower value of T_{B1} , then linearity tests must account for this aspect of nonlinearity; that is, nonlinearity in the relationship between brightness temperature and radiance must not be confused with non-ideal behavior of the radiometer.

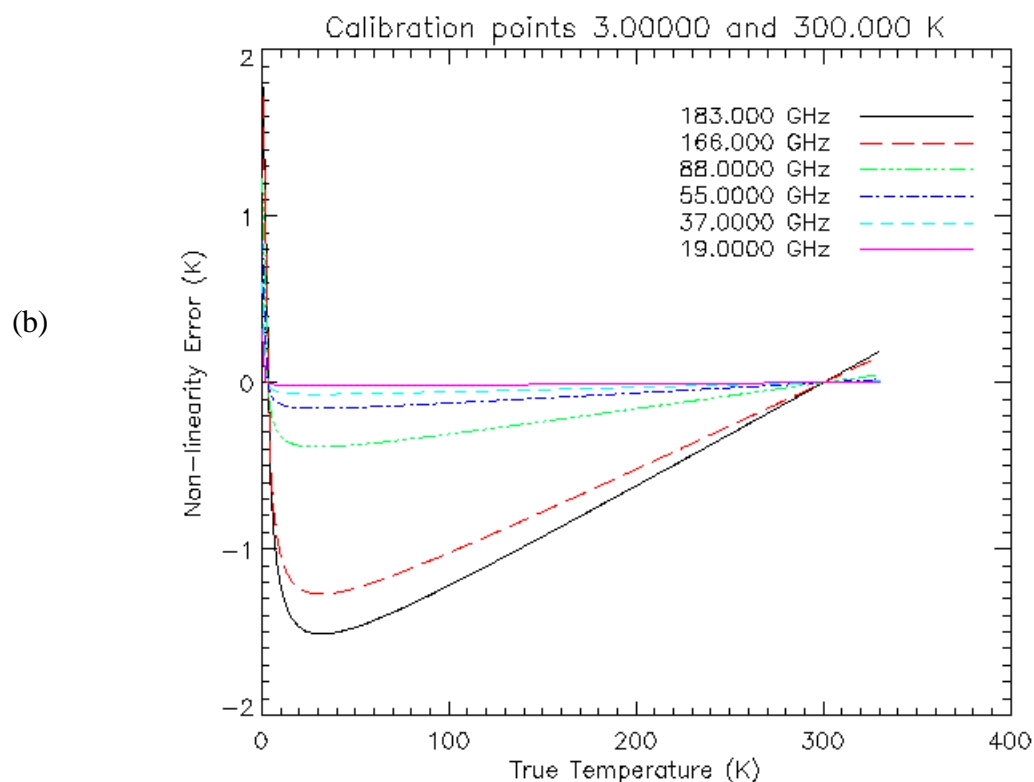
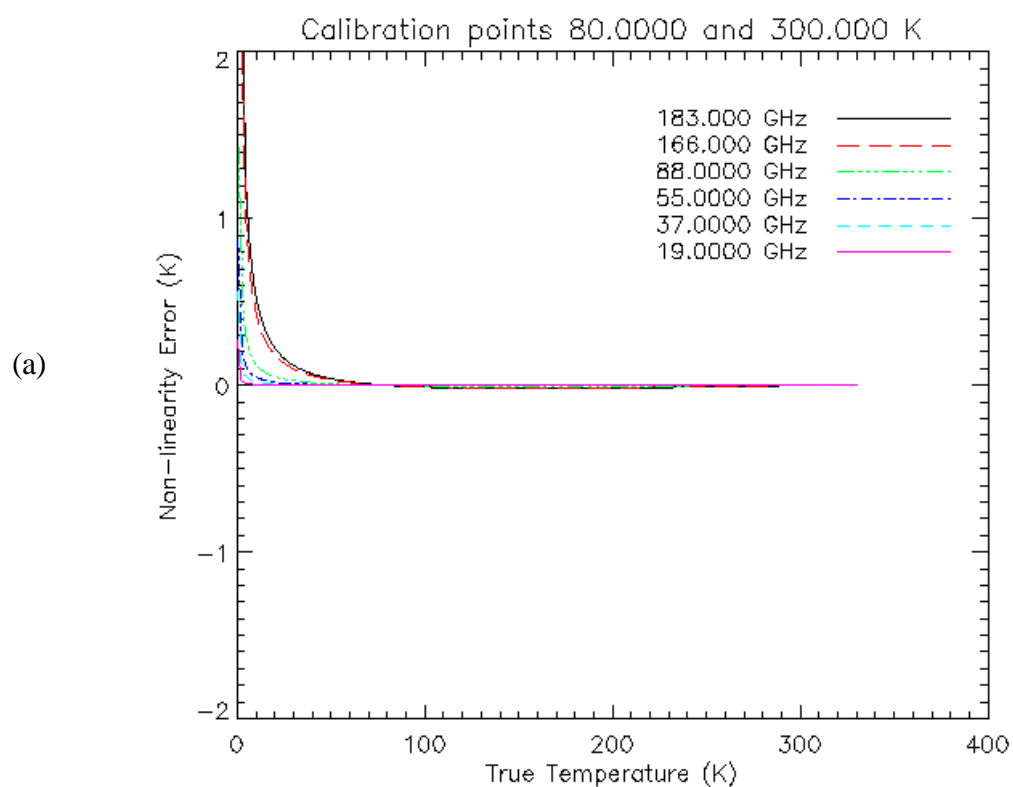


Figure C-1. The non-linearity error $\hat{T}_B - T_B$ due to the assumption that the radiometer responds linearly to brightness temperature, plotted as a function of T_B .

APPENDIX D: DERIVATION OF TDR / SDR EQUATIONS FROM CALIBRATION BUDGET ANALYSIS

There are 3 embedded excel worksheets in this appendix: one each for the active scan analysis, cold load analysis, and warm load analysis. Only the summary portions of the excel worksheets are visible. Opening either the indicated file or embedded excel worksheet allows access to the complete analysis.

Active Scan Analysis from worksheet "calibration_atbd_active.xls"

Excel worksheet for calibration_atbd_active

Antenna Temperature Equation

$$TA = A1T1 + A2T2 + A3T3 + A4T4 + A5T5 + A6T6 + A7T7 + A8T8 + A9T9 + A10T10 + A11T11$$

Solve for Earth Scene Temperature (T1) from Antenna Temperature (TA)

$$TA' = (TA - A2T2 + A3T3 + A4T4 + A5T5 + A6T6 + A7T7 + A8T8 + A9T9 + A10T10 + A11T11)/A1$$

Subscene Descriptions for the components of the energy

Scene(n)	An Coefficient Equation	Tn Temperature	Subscene (n) description
1	$Fr*(1-Er)*(1-Vs-Vsc)$	Te	Reflector Scene (earth for primary/secondary, Tcos for colc
2	$Fr*Er$	Tr	Reflector emission
3	$Fr*(1-Er)*Vs*Evs$	Tvs	Sensor emission viewed through reflector
4	$Fr*(1-Er)*Vs*(1-Evs)$	Tcos	Sensor reflection viewed through reflector
5	$Fr*(1-Er)*Vsc*Evsc$	Tvsc	Spacecraft emission viewed through reflector
6	$Fr*(1-Er)*Vsc*(1-Evsc)$	Tcos	Spacecraft reflection viewed through reflector
7	$(1-Fr)*(1-Ss-Ssc)$	Tcos	Spillover directly from space
8	$(1-Fr)*Ss*Ess$	Tss	Spillover emission from sensor
9	$(1-Fr)*Ss*(1-Ess)*Qsc$	Tqsc	Spillover reflected off sensor from spacecraft
10	$(1-Fr)*Ss*(1-Ess)*(1-Qsc)$	Tcos	Spillover reflected off sensor from space
11	$(1-Fr)*Ssc$	Tssc	Spillover emission from spacecraft
Sum	1		The Sum of all the coefficients equals 1

Equations for derivatives of T1 with respect to all terms in equation for T1

Param	Partial Derivative of TA equation with respect to T1 (earth scene component of TA)
Er	$(-Ta - (-1 + Fr)*(1 + Ess*(-1 + Qsc)*Ss - Qsc*Ss - Ssc)*Tcos + (-1 + Ess)*(-1 + Fr)*Qsc*Ss*Tqsc + Ess*Ss*Tss + Ssc*Tssc + Fr*(Tr - Ess*Ss*Tss - Ssc*Tssc))/(Power(-1 + Er,2)*Fr*(-1 + Vs + Vsc))$
Ess	$((-1 + Fr)*Ss*((-1 + Qsc)*Tcos - Qsc*Tqsc + Tss))/((-1 + Er)*Fr*(-1 + Vs + Vsc))$
Evs	$((-Tcos + Tvs)*Vs)/(-1 + Vs + Vsc)$
Evsc	$((-Tcos + Tvsc)*Vsc)/(-1 + Vs + Vsc)$
Fr	$(-Ta + (1 + Ess*(-1 + Qsc)*Ss - Qsc*Ss - Ssc)*Tcos - (-1 + Ess)*Qsc*Ss*Tqsc + Ess*Ss*Tss + Ssc*Tssc)/((-1 + Er)*Power(Fr,2)*(-1 + Vs + Vsc))$
Qsc	$((-1 + Ess)*(-1 + Fr)*Ss*(Tcos - Tqsc))/((-1 + Er)*Fr*(-1 + Vs + Vsc))$
Ss	$((-1 + Fr)*(Qsc*(-Tcos + Tqsc) + Ess*((-1 + Qsc)*Tcos - Qsc*Tqsc + Tss)))/((-1 + Er)*Fr*(-1 + Vs + Vsc))$
Ssc	$-(((1 + Fr)*(Tcos - Tssc))/((-1 + Er)*Fr*(-1 + Vs + Vsc)))$
Tcos	$(-1 + (Ess + Qsc - Ess*Qsc)*Ss + Ssc + Fr*(1 + Ess*(-1 + Qsc)*Ss - Qsc*Ss - Ssc + (-1 + Er + Evs - Er*Evs)*Vs - (-1 + Er)*(-1 + Evsc)*Vsc))/((-1 + Er)*Fr*(-1 + Vs + Vsc))$
Te	0
Tqsc	$-(((1 + Ess)*(-1 + Fr)*Qsc*Ss))/((-1 + Er)*Fr*(-1 + Vs + Vsc))$
Tr	$-(Er)/((-1 + Er)*(-1 + Vs + Vsc))$
Tss	$(Ess*(-1 + Fr)*Ss)/((-1 + Er)*Fr*(-1 + Vs + Vsc))$
Tssc	$((-1 + Fr)*Ssc)/((-1 + Er)*Fr*(-1 + Vs + Vsc))$
Tvs	$(Evs*Vs)/(-1 + Vs + Vsc)$
Tvsc	$(Evsc*Vsc)/(-1 + Vs + Vsc)$
Vs	$(-Ta + (-1 + Ess)*(-1 + Fr)*Qsc*Ss*Tqsc + Ess*Ss*Tss + Ssc*Tssc + Fr*(Er*Tr - Ess*Ss*Tss - Ssc*Tssc + Evs*Tvs - Er*Evs*Tvs + (-1 + Er)*(Evs*Tvs - Evsc*Tvsc)*Vsc) + Tcos*(1 - Ess*Ss + Ess*Fr*Ss - Qsc*Ss + Ess*Qsc*Ss + Fr*Qsc*Ss - Ess*Fr*Qsc*Ss - Ssc + Fr*Ssc + Evs*Fr*(-1 + Vsc) - Evsc*Fr*Vsc + Er*Fr*(-1 + Evs - Evs*Vsc + Evsc*Vsc)))/((-1 + Er)*Fr*Power(-1 + Vs + Vsc,2))$
Vsc	$(-Ta + (-1 + Ess)*(-1 + Fr)*Qsc*Ss*Tqsc + Ess*Ss*Tss + Ssc*Tssc + Tcos*(1 - Er*Fr - Evsc*Fr + Er*Evsc*Fr - Ess*Ss + Ess*Fr*Ss - Qsc*Ss + Ess*Qsc*Ss + Fr*Qsc*Ss - Ess*Fr*Qsc*Ss - Ssc + Fr*Ssc + (-1 + Er)*(Evs - Evsc)*Fr*Vs) + Fr*(Er*Tr - Ess*Ss*Tss - Ssc*Tssc + Evsc*Tvsc - Er*Evsc*Tvsc + (-1 + Er)*(-1 + Evs)*Vsc + Evsc*Vsc))/((-1 + Er)*Fr*Power(-1 + Vs + Vsc,2))$

Description of all parameters

Param	Parameter Description
Er	emissivity of reflector
Ess	emissivity of the part of the sensor viewed in spillover
Evs	emissivity of the part of the sensor viewed through the reflector
Evsc	emissivity of the part of the spacecraft viewed through the reflector
Fr	fraction from reflector, viewed from feedhorn (1 - spillover)
Qsc	fraction from spacecraft, among spillover reflected off sensor
Ss	fraction from sensor, among spillover
Ssc	fraction from spacecraft, among spillover
Tcos	Cosmic brightness temperature
Te	True Earth scene brightness temperature
Tqsc	Temperature of spacecraft viewed in spillover reflected off sensor
Tr	Antenna reflector physical temperature
Tss	temperature of the part of the sensor viewed in spillover
Tssc	temperature of the part of spacecraft viewed in direct spillover
Tvs	temperature of the part of the sensor viewed through the reflector
Tvsc	temperature of the part of the spacecraft viewed through the reflector
Vs	fraction from sensor, viewed through reflector
Vsc	fraction from spacecraft, viewed through reflector

Nominal Values for all Parameters as a function of channel

shading indicates varies by channel from 6 Gz									
	6 GHZ	10	18	23	36	50-60	89	166	183
Param	Nominal	Nominal	Nominal	Nominal	Nominal	Nominal	Nominal	Nominal	Nominal
Er	0.00027	0.00036	0.00047	0.00053	0.00066	0.00085	0.001	0.0014	0.0015
Ess	0.1	0.1	0.1	0.1	0.1	0.1	0.1	0.1	0.1
Evs	0.1	0.1	0.1	0.1	0.1	0.1	0.1	0.1	0.1
Evsc	0.5	0.5	0.5	0.5	0.5	0.5	0.5	0.5	0.5
Fr	0.967	0.954	0.986	0.992	0.99	0.998	0.999	0.994	0.995
Qsc	0.01	0.01	0.01	0.01	0.01	0.01	0.01	0.01	0.01
Ss	0.2	0.2	0.2	0.2	0.2	0.2	0.2	0.2	0.2
Ssc	0.005	0.005	0.005	0.005	0.005	0.005	0.005	0.005	0.005
Tcos	2.7	2.7	2.7	2.7	2.7	2.7	2.7	2.7	2.7
Te	300	300	300	300	300	300	300	300	300
Tqsc	300	300	300	300	300	300	300	300	300
Tr	350	350	350	350	350	350	350	350	350
Tss	300	300	300	300	300	300	300	300	300
Tssc	300	300	300	300	300	300	300	300	300
Tvs	300	300	300	300	300	300	300	300	300
Tvsc	300	300	300	300	300	300	300	300	300
Vs	0	0	0.0008	0.0011	0	0	0	0	0
Vsc	0.0005	0.0005	0.0005	0.0005	0.0005	0.0005	0.0005	0.0005	0.0005

Measurement Uncertainty (1 sigma) for all Parameters as a function of channel

shading indicates varies by channel from 6 Gz									
	6 GHZ	10	18	23	36	50-60	89	166	183
Param	Uncert.								
dEr	0.00005	0.00005	0.00005	0.00005	0.00005	0.00005	0.00005	0.00005	0.00005
dEss	0.05	0.05	0.05	0.05	0.05	0.05	0.05	0.05	0.05
dEvs	0.05	0.05	0.05	0.05	0.05	0.05	0.05	0.05	0.05
dEvsc	0.1	0.1	0.1	0.1	0.1	0.1	0.1	0.1	0.1
dFr	0.002	0.002	0.002	0.002	0.002	0.002	0.001	0.002	0.002
dQsc	0.005	0.005	0.005	0.005	0.005	0.005	0.005	0.005	0.005
dSs	0.02	0.02	0.02	0.02	0.02	0.02	0.02	0.02	0.02
dSsc	0.001	0.001	0.001	0.001	0.001	0.001	0.001	0.001	0.001
dTcos	0.1	0.1	0.1	0.1	0.1	0.1	0.1	0.1	0.1
dTe	0	0	0	0	0	0	0	0	0
dTqsc	20	20	20	20	20	20	20	20	20
dTr	20	20	20	20	20	20	20	20	20
dTss	20	20	20	20	20	20	20	20	20
dTssc	20	20	20	20	20	20	20	20	20
dTvs	50	50	50	50	50	50	50	50	50
dTvsc	50	50	50	50	50	50	50	50	50
dVs	0.0001	0.0001	0.0001	0	0	0	0	0	0
dVsc	0.0001	0.0001	0.0001	0.0001	0.0001	0.0001	0.0001	0.0001	0.0001

Numerical values for derivatives of T1. using nominal values

	6 GHZ		10		18		23		36 50-60		89		166		183	
Param	Partial	Partial	Partial	Partial	Partial	Partial	Partial	Partial	Partial	Partial	Partial	Partial	Partial	Partial	Partial	Partial
Er	-50.11291	-50.11742	-50.37751843	-50.47612	-50.1325	-50.142	-50.14952	-50.16961	-50.1746							
Ess	-2.010398	-2.840816	-0.837298545	-0.475734	-0.59529	-0.118126	-0.059013	-0.356	-0.2964							
Evs	0	0	-0.238149594	-0.327554	0	0	0	0	0							
Evsc	-0.148724	-0.148724	-0.148843497	-0.148888	-0.14872	-0.148724	-0.148724	-0.148724	-0.14872							
Fr	-299.3738	-303.4853	-293.6916777	-291.9426	-292.552	-290.2721	-290.0326	-291.6285	-291.37							
Qsc	-1.827635	-2.58256	-0.761180496	-0.432485	-0.54117	-0.107387	-0.053648	-0.323637	-0.26945							
Ss	-1.106734	-1.563884	-0.460937078	-0.261894	-0.32771	-0.065029	-0.032487	-0.19598	-0.16317							
Ssc	-10.15353	-14.34756	-4.228780532	-2.402696	-3.00652	-0.596597	-0.298045	-1.797982	-1.49696							
Tcos	-0.033487	-0.047216	-0.014814011	-0.009107	-0.01009	-0.002203	-0.001226	-0.006136	-0.00515							
Te	0	0	0	0	0	0	0	0	0							
Tqsc	-6.15E-05	-8.69E-05	-2.56031E-05	-1.45E-05	-1.8E-05	-3.61E-06	-1.8E-06	-1.09E-05	-9.1E-06							
Tr	-0.00027	-0.00036	-0.000470833	-0.000531	-0.00066	-0.000851	-0.001002	-0.001403	-0.0015							
Tss	-0.000683	-0.000965	-0.000284479	-0.000162	-0.0002	-4.01E-05	-2.01E-05	-0.000121	-0.0001							
Tssc	-0.000171	-0.000241	-7.11198E-05	-4.04E-05	-5.1E-05	-1E-05	-5.01E-06	-3.02E-05	-2.5E-05							
Tvs	0	0	-8.01041E-05	-0.00011	0	0	0	0	0							
Tvsc	-0.00025	-0.00025	-0.000250325	-0.00025	-0.00025	-0.00025	-0.00025	-0.00025	-0.00025							
Vs	267.7039	267.7039	267.9182938	267.9988	267.7039	267.70385	267.70385	267.70385	267.7039							
Vsc	148.7244	148.7244	148.8434965	148.88822	148.7244	148.72436	148.72436	148.72436	148.7244							

Numerical error (derivative x measurement uncertainty) in Earth Scene (Te) for each parameter

	6 GHZ		10		18		23		36 50-60		89		166		183	
Param	Error	Error	Error	Error	Error	Error	Error	Error	Error	Error	Error	Error	Error	Error	Error	Error
Er	-0.002506	-0.002506	-0.002518876	-0.002524	-0.00251	-0.002507	-0.002507	-0.002507	-0.002508	-0.00251						
Ess	-0.10052	-0.142041	-0.041864927	-0.023787	-0.02976	-0.005906	-0.002951	-0.0178	-0.01482							
Evs	0	0	-0.01190748	-0.016378	0	0	0	0	0							
Evsc	-0.014872	-0.014872	-0.01488435	-0.014889	-0.01487	-0.014872	-0.014872	-0.014872	-0.014872							
Fr	-0.598748	-0.606971	-0.587383355	-0.583885	-0.5851	-0.580544	-0.290033	-0.583257	-0.58274							
Qsc	-0.009138	-0.012913	-0.003805902	-0.002162	-0.00271	-0.000537	-0.000268	-0.001618	-0.00135							
Ss	-0.022135	-0.031278	-0.009218742	-0.005238	-0.00655	-0.001301	-0.00065	-0.00392	-0.00326							
Ssc	-0.010154	-0.014348	-0.004228781	-0.002403	-0.00301	-0.000597	-0.000298	-0.001798	-0.0015							
Tcos	-0.003349	-0.004722	-0.001481401	-0.000911	-0.00101	-0.00022	-0.000123	-0.000614	-0.00052							
Te	0	0	0	0	0	0	0	0	0							
Tqsc	-0.001229	-0.001737	-0.000512062	-0.000291	-0.00036	-7.22E-05	-3.61E-05	-0.000218	-0.00018							
Tr	-0.005404	-0.007206	-0.009416662	-0.010623	-0.01322	-0.017023	-0.02003	-0.028053	-0.03006							
Tss	-0.013661	-0.019304	-0.00568958	-0.003233	-0.00405	-0.000803	-0.000401	-0.002419	-0.00201							
Tssc	-0.003415	-0.004826	-0.001422395	-0.000808	-0.00101	-0.000201	-0.0001	-0.000605	-0.0005							
Tvs	0	0	-0.004005207	-0.005509	0	0	0	0	0							
Tvsc	-0.012506	-0.012506	-0.012516271	-0.01252	-0.01251	-0.012506	-0.012506	-0.012506	-0.01251							
Vs	0.02677	0.02677	0.026791829	0	0	0	0	0	0							
Vsc	0.014872	0.014872	0.01488435	0.0148888	0.014872	0.0148724	0.0148724	0.0148724	0.014872							

Assume all parameters contributing to error are uncorrelated so that result can be Root Sum Squared

Sum	-0.755994	-0.833586	-0.669179812	-0.67027	-0.66179	-0.622217	-0.329903	-0.655316	-0.65196
Sum(Abs)	0.83928	0.916872	0.75253217	0.700048	0.691539	0.6519617	0.3596478	0.6850608	0.681701
RSS	0.608967	0.625887	0.590335902	0.5852824	0.586593	0.581347	0.2917785	0.5847439	0.584237

The RSS values get entered into the calibration budget

An Coefficients using nominal values

	6 GHZ	10	18	23	36	50-60	89	166	183
A1	0.966256	0.95318	0.984255382	0.9898879	0.988852	0.9966531	0.997502	0.9921121	0.993011
A2	0.000261	0.000343	0.00046342	0.0005258	0.000653	0.0008483	0.000999	0.0013916	0.001493
A3	0	0	7.88429E-05	0.0001091	0	0	0	0	0
A4	0	0	0.000709586	0.0009816	0	0	0	0	0
A5	0.000242	0.000238	0.000246384	0.0002479	0.000247	0.0002493	0.0002495	0.0002482	0.000248
A6	0.000242	0.000238	0.000246384	0.0002479	0.000247	0.0002493	0.0002495	0.0002482	0.000248
A7	0.026235	0.03657	0.01113	0.00636	0.00795	0.00159	0.000795	0.00477	0.003975
A8	0.00066	0.00092	0.00028	0.00016	0.0002	0.00004	0.00002	0.00012	0.0001
A9	5.94E-05	8.28E-05	0.0000252	0.0000144	0.000018	0.0000036	0.0000018	0.0000108	9E-06
A10	0.005881	0.008197	0.0024948	0.0014256	0.001782	0.0003564	0.0001782	0.0010692	0.000891
A11	0.000165	0.00023	7E-05	0.00004	0.00005	0.00001	0.000005	0.00003	0.000025
Sum(An)	1	1	1	1	1	1	1	1	1

Tn		6 GHZ	10	18	23	36	50-60	89	166	183
Te	A1xT1	289.8767	285.9539	295.2766147	296.96636	296.6556	298.99594	299.2506	297.63363	297.9032
Tr	A2xT2	0.091382	0.120204	0.162197	0.184016	0.22869	0.296905	0.34965	0.48706	0.522375
Tvs	A3xT3	0	0	0.023652878	0.0327186	0	0	0	0	0
Tcos	A4xT4	0	0	0.001915883	0.0026502	0	0	0	0	0
Tvsc	A5xT5	0.072505	0.071524	0.073915244	0.0743606	0.074201	0.0747864	0.0748501	0.0744456	0.074513
Tcos	A6xT6	0.000653	0.000644	0.000665237	0.0006692	0.000668	0.0006731	0.0006737	0.00067	0.000671
Tcos	A7xT7	0.070835	0.098739	0.030051	0.017172	0.021465	0.004293	0.0021465	0.012879	0.010733
Tss	A8xT8	0.198	0.276	0.084	0.048	0.06	0.012	0.006	0.036	0.03
Tqsc	A9xT9	0.01782	0.02484	0.00756	0.00432	0.0054	0.00108	0.00054	0.00324	0.0027
Tcos	A10xT10	0.015878	0.022132	0.00673596	0.0038491	0.004811	0.0009623	0.0004811	0.0028868	0.002406
Tssc	A11xT11	0.0495	0.069	0.021	0.012	0.015	0.003	0.0015	0.009	0.0075
Ta	Sum(AnTn)	290.3932	286.637	295.6883079	297.34612	297.0658	299.38964	299.68644	298.25981	298.5541

Based on sensitivity analysis of errors in T_a' as a function of uncertainties in spacecraft & sensor temperatures
 Use a slight approximation to the expression for earth scene component by combining like terms

Let $T_s = (T_{vs} + T_{ss})/2$ [average sensor temperature for all views]

Let $T_{sc} = (T_{vsc} + T_{qsc} + T_{ssc})/3$ [Average spacecraft temperature for all views]

then rewrite T_a' as shown below to solve for the earth scene component

$$T_a' = A_{sp} T_a - A_r T_r - A_s T_s - A_{sc} T_{sc} - A_{cos} T_{cos}$$

where

$A_{sp} = (1/A_1)$	spillover coefficient	T_a	Antenna Temperature
$A_r = (A_2/A_1)$	reflector coefficient	T_r	Reflector Temperature
$A_s = (A_3 + A_8)/A_1$	sensor coefficient	T_s	Average Sensor Temperature
$A_{sc} = (A_5 + A_9 + A_{11})/A_1$	spacecraft coefficient	T_{sc}	Average Spacecraft temperature
$A_{cos} = (A_4 + A_6 + A_7 + A_{10})/A_1$	cosmic background coefficient	T_{cos}	Cosmic Temperature

Note that $A_{sp} - (A_r + A_s + A_{sc} + A_{cos})$ should always equal 1

	6 GHZ	10	18	23	36	50-60	89	166	183
A_{sp}	1.034923	1.04912	1.015996476	1.0102154	1.011274	1.0033581	1.0025043	1.0079506	1.007038
A_r	0.00027	0.00036	0.000470833	0.0005311	0.000661	0.0008511	0.0010015	0.0014027	0.001503
A_s	0.000683	0.000965	0.000364583	0.0002718	0.000202	4.013E-05	2.005E-05	0.000121	0.000101
A_{sc}	0.000482	0.000578	0.000347048	0.0003054	0.000319	0.0002638	0.0002569	0.0002912	0.000284
A_{cos}	0.033487	0.047216	0.014814011	0.0091071	0.010092	0.0022031	0.0012258	0.0061358	0.00515

Check that $A_{sp} - (A_r + A_s + A_{sc} + A_{cos}) = 1$

	6 GHZ	10	18	23	36	50-60	89	166	183
A_{sp}	1.034923	1.04912	1.015996476	1.0102154	1.011274	1.0033581	1.0025043	1.0079506	1.007038
A_r	0.00027	0.00036	0.000470833	0.0005311	0.000661	0.0008511	0.0010015	0.0014027	0.001503
A_s	0.000683	0.000965	0.000364583	0.0002718	0.000202	4.013E-05	2.005E-05	0.000121	0.000101
A_{sc}	0.000482	0.000578	0.000347048	0.0003054	0.000319	0.0002638	0.0002569	0.0002912	0.000284
A_{cos}	0.033487	0.047216	0.014814011	0.0091071	0.010092	0.0022031	0.0012258	0.0061358	0.00515
$A_{sp} - (A_r + A_s + A_{sc} + A_{cos})$	1	1	1	1	1	1	1	1	1

	6 GHZ	10	18	23	36	50-60	89	166	183
T_a	290.3932	286.637	295.6883079	297.34612	297.0658	299.38964	299.68644	298.25981	298.5541
T_r	350	350	350	350	350	350	350	350	350
T_s	300	300	300	300	300	300	300	300	300
T_{sc}	300	300	300	300	300	300	300	300	300
T_{cos}	2.7	2.7	2.7	2.7	2.7	2.7	2.7	2.7	2.7

$A_{sp} T_a$	300.5346	300.7166	300.4182788	300.38364	300.4149	300.39502	300.43693	300.63116	300.6555
$A_r T_r$	0.094573	0.126108	0.16479158	0.1858958	0.231268	0.297902	0.3505256	0.4909324	0.526052
$A_s T_s$	0.204915	0.289557	0.109374945	0.0815432	0.060676	0.0120403	0.006015	0.0362862	0.030211
$A_{sc} T_{sc}$	0.144709	0.173487	0.104114486	0.0916069	0.095668	0.0791312	0.0770826	0.0873748	0.085309
$A_{cos} T_{cos}$	0.090416	0.127484	0.039997831	0.0245892	0.027248	0.0059483	0.0033096	0.0165665	0.013906

Now recover the earth scene component from each by applying the equation for T_a'

T_a'	300	300	300	300	300	300	300	300	300
--------	-----	-----	-----	-----	-----	-----	-----	-----	-----

Cold Load Analysis from worksheet “calibration_atbd_cold.xls”

Excel worksheet for calibration_atbd_cold

Note: the majority of the analysis is identical to active, except some of the term change and $T_1 = T_{cos}$ instead of T_e
 T_e is still carried in the equations since it was easier to cut and past the equations but T_e was set to $T_{cos} = 2.7$ nominal
 We also change T_a to T_{cold} since the antenna temperature is now for cold sky

Antenna Temperature Equation for Tcold

$$T_{cold} = T_A = A1T1 + A2T2 + A3T3 + A4T4 + A5T5 + A6T6 + A7T7 + A8T8 + A9T9 + A10T10 + A11T11$$

Subscene Descriptions for the components of the energy

Scene(n)	An Coefficient Equation	Tn Temperature	Subscene (n) description
1	$Fr*(1-Er)*(1-Vs-Vsc)$	T_e	Reflector Scene (earth for primary/secondary, T_{cos} for colc
2	$Fr*Er$	T_r	Reflector emission
3	$Fr*(1-Er)*Vs*Evs$	T_{vs}	Sensor emission viewed through reflector
4	$Fr*(1-Er)*Vs*(1-Evs)$	T_{cos}	Sensor reflection viewed through reflector
5	$Fr*(1-Er)*Vsc*Evs$	T_{vsc}	Spacecraft emission viewed through reflector
6	$Fr*(1-Er)*Vsc*(1-Evsc)$	T_{cos}	Spacecraft reflection viewed through reflector
7	$(1-Fr)*(1-Ss-Ssc)$	T_{cos}	Spillover directly from space
8	$(1-Fr)*Ss*Ess$	T_{ss}	Spillover emission from sensor
9	$(1-Fr)*Ss*(1-Ess)*Qsc$	T_{qsc}	Spillover reflected off sensor from spacecraft
10	$(1-Fr)*Ss*(1-Ess)*(1-Qsc)$	T_{cos}	Spillover reflected off sensor from space
11	$(1-Fr)*Ssc$	T_{ssc}	Spillover emission from spacecraft
Sum	1		The Sum of all the coefficients equals 1

Equations for derivatives of T1 with respect to all terms in equation for T1

Param	Partial Derivative of TA equation with respect to T1 (reflector scene component of TA)
Er	$(-Ta - (-1 + Fr)*(1 + Ess*(-1 + Qsc)*Ss - Qsc*Ss - Ssc)*Tcos + (-1 + Ess)*(-1 + Fr)*Qsc*Ss*Tqsc + Ess*Ss*Tss + Ssc*Tssc + Fr*(Tr - Ess*Ss*Tss - Ssc*Tssc))/(Power(-1 + Er,2)*Fr*(-1 + Vs + Vsc))$
Ess	$((-1 + Fr)*Ss*(-1 + Qsc)*Tcos - Qsc*Tqsc + Tss)/((-1 + Er)*Fr*(-1 + Vs + Vsc))$
Evs	$((-Tcos + Tvs)*Vs)/(-1 + Vs + Vsc)$
Evsc	$((-Tcos + Tvsc)*Vsc)/(-1 + Vs + Vsc)$
Fr	$(-Ta + (1 + Ess*(-1 + Qsc)*Ss - Qsc*Ss - Ssc)*Tcos - (-1 + Ess)*Qsc*Ss*Tqsc + Ess*Ss*Tss + Ssc*Tssc)/((-1 + Er)*Power(Fr,2)*(-1 + Vs + Vsc))$
Qsc	$((-1 + Ess)*(-1 + Fr)*Ss*(Tcos - Tqsc))/((-1 + Er)*Fr*(-1 + Vs + Vsc))$
Ss	$((-1 + Fr)*(Qsc*(Tcos + Tqsc) + Ess*(-1 + Qsc)*Tcos - Qsc*Tqsc + Tss))/((-1 + Er)*Fr*(-1 + Vs + Vsc))$
Ssc	$-(((1 + Fr)*(Tcos - Tssc))/((-1 + Er)*Fr*(-1 + Vs + Vsc)))$
Tcos	$(-1 + (Ess + Qsc - Ess*Qsc)*Ss + Ssc + Fr*(1 + Ess*(-1 + Qsc)*Ss - Qsc*Ss - Ssc + (-1 + Er + Evs - Er*Evs)*Vs - (-1 + Er)*(-1 + Evsc)*Vsc))/((-1 + Er)*Fr*(-1 + Vs + Vsc))$
Te	0
Tqsc	$-(((1 + Ess)*(-1 + Fr)*Qsc*Ss)/((-1 + Er)*Fr*(-1 + Vs + Vsc)))$
Tr	$-(Er)/((-1 + Er)*(-1 + Vs + Vsc))$
Tss	$(Ess*(-1 + Fr)*Ss)/((-1 + Er)*Fr*(-1 + Vs + Vsc))$
Tssc	$((-1 + Fr)*Ssc)/((-1 + Er)*Fr*(-1 + Vs + Vsc))$
Tvs	$(Evs*Vs)/(-1 + Vs + Vsc)$
Tvsc	$(Evsc*Vsc)/(-1 + Vs + Vsc)$
Vs	$(-Ta + (-1 + Ess)*(-1 + Fr)*Qsc*Ss*Tqsc + Ess*Ss*Tss + Ssc*Tssc + Fr*(Er*Tr - Ess*Ss*Tss - Ssc*Tssc + Evs*Tvs - Er*Evs*Tvs + (-1 + Er)*(Evs*Tvs - Evsc*Tvsc)*Vsc) + Tcos*(1 - Ess*Ss + Ess*Fr*Ss - Qsc*Ss + Ess*Qsc*Ss + Fr*Qsc*Ss - Ess*Fr*Qsc*Ss - Ssc + Fr*Ssc + Evs*Fr*(-1 + Vsc) - Evsc*Fr*Vsc + Er*Fr*(-1 + Evs - Evs*Vsc + Evsc*Vsc)))/((-1 + Er)*Fr*Power(-1 + Vs + Vsc,2))$
Vsc	$(-Ta + (-1 + Ess)*(-1 + Fr)*Qsc*Ss*Tqsc + Ess*Ss*Tss + Ssc*Tssc + Tcos*(1 - Er*Fr - Evsc*Fr + Er*Evsc*Fr - Ess*Ss + Ess*Fr*Ss - Qsc*Ss + Ess*Qsc*Ss + Fr*Qsc*Ss - Ess*Fr*Qsc*Ss - Ssc + Fr*Ssc + (-1 + Er)*(Evs - Evsc)*Fr*Vs) + Fr*(Er*Tr - Ess*Ss*Tss - Ssc*Tssc + Evsc*Tvsc - Er*Evsc*Tvsc + (-1 + Er)*(-1 + Evs - Evs*Vsc + Evsc*Vsc)*Vs))/((-1 + Er)*Fr*Power(-1 + Vs + Vsc,2))$

Description of all parameters

Param	Parameter Description
Er	emissivity of reflector
Ess	emissivity of the part of the sensor viewed in spillover
Evs	emissivity of the part of the sensor viewed through the reflector
Evsc	emissivity of the part of the spacecraft viewed through the reflector
Fr	fraction from reflector, viewed from feedhorn (1 - spillover)
Qsc	fraction from spacecraft, among spillover reflected off sensor
Ss	fraction from sensor, among spillover
Ssc	fraction from spacecraft, among spillover
Tcos	Cosmic brightness temperature
Te	True Earth scene brightness temperature or Tcos for cold sky analysis
Tqsc	Temperature of spacecraft viewed in spillover reflected off sensor
Tr	Antenna reflector physical temperature
Tss	temperature of the part of the sensor viewed in spillover
Tssc	temperature of the part of spacecraft viewed in direct spillover
Tvs	temperature of the part of the sensor viewed through the reflector
Tvsc	temperature of the part of the spacecraft viewed through the reflector
Vs	fraction from sensor, viewed through reflector
Vsc	fraction from spacecraft, viewed through reflector

Nominal Values for all Parameters as a function of channel

shading indicates varies by channel from 6 Gz									
	6 GHZ	10	18	23	36	50-60	89	166	183
Param	Nominal	Nominal	Nominal	Nominal	Nominal	Nominal	Nominal	Nominal	Nominal
Er	0.00027	0.00036	0.00047	0.00053	0.00066	0.00085	0.001	0.0014	0.0015
Ess	0.1	0.1	0.1	0.1	0.1	0.1	0.1	0.1	0.1
Evs	0.1	0.1	0.1	0.1	0.1	0.1	0.1	0.1	0.1
Evsc	0.5	0.5	0.5	0.5	0.5	0.5	0.5	0.5	0.5
Fr	0.994	0.9995	0.993	0.998	0.998	0.999	1	0.999	0.999
Qsc	0.01	0.01	0.01	0.01	0.01	0.01	0.01	0.01	0.01
Ss	0.2	0.2	0.2	0.2	0.2	0.2	0.2	0.2	0.2
Ssc	0	0	0	0	0	0	0	0	0
Tcos	2.7	2.7	2.7	2.7	2.7	2.7	2.7	2.7	2.7
Te	2.7	2.7	2.7	2.7	2.7	2.7	2.7	2.7	2.7
Tqsc	300	300	300	300	300	300	300	300	300
Tr	350	350	350	350	350	350	350	350	350
Tss	300	300	300	300	300	300	300	300	300
Tssc	300	300	300	300	300	300	300	300	300
Tvs	300	300	300	300	300	300	300	300	300
Tvsc	300	300	300	300	300	300	300	300	300
Vs	0.0014	0.0012	0.0008	0.0005	0.0014	0.0015	0.0001	0.0003	0.0003
Vsc	0.0005	0.0012	0.0008	0.0005	0.0014	0.0015	0.0001	0.0003	0.0003

Measurement Uncertainty (1 sigma) for all Parameters as a function of channel

shading indicates varies by channel from 6 Gz									
	6 GHZ	10	18	23	36	50-60	89	166	183
Param	Uncert.								
dEr	0.00005	0.00005	0.00005	0.00005	0.00005	0.00005	0.00005	0.00005	0.00005
dEss	0.05	0.05	0.05	0.05	0.05	0.05	0.05	0.05	0.05
dEvs	0.05	0.05	0.05	0.05	0.05	0.05	0.05	0.05	0.05
dEvsc	0.1	0.1	0.1	0.1	0.1	0.1	0.1	0.1	0.1
dFr	0.002	0.002	0.002	0.002	0.002	0.001	0.001	0.002	0.002
dQsc	0.005	0.005	0.005	0.005	0.005	0.005	0.005	0.005	0.005
dSs	0.02	0.02	0.02	0.02	0.02	0.02	0.02	0.02	0.02
dSsc	0.001	0.001	0.001	0.001	0.001	0.001	0.001	0.001	0.001
dTcos	0.1	0.1	0.1	0.1	0.1	0.1	0.1	0.1	0.1
dTe	0	0	0	0	0	0	0	0	0
dTqsc	20	20	20	20	20	20	20	20	20
dTr	20	20	20	20	20	20	20	20	20
dTss	20	20	20	20	20	20	20	20	20
dTssc	20	20	20	20	20	20	20	20	20
dTvs	50	50	50	50	50	50	50	50	50
dTvsc	50	50	50	50	50	50	50	50	50
dVs	0.0001	0.0001	0.0001	0.0001	0.0001	0.0001	0.0001	0.0001	0.0001
dVsc	0.0001	0.0001	0.0001	0.0001	0.0001	0.0001	0.0001	0.0001	0.0001

Numerical values for derivatives of T1 using nominal values

	6 GHZ		10		18		23		36 50-60		89		166		183	
Param	Partial	Partial	Partial	Partial	Partial	Partial	Partial	Partial	Partial	Partial	Partial	Partial	Partial	Partial	Partial	Partial
Er	-347.9389	-348.0463	-347.8771401	-347.7427	-348.255	-348.3728	-347.6993	-347.9421	-347.977							
Ess	-0.356097	-0.029529	-0.415822979	-0.118147	-0.11838	-0.059152	0	-0.059042	-0.05905							
Evs	-0.417012	-0.357618	-0.238221154	-0.148799	-0.41739	-0.447292	-0.029736	-0.089244	-0.08924							
Evsc	-0.148933	-0.357618	-0.238221154	-0.148799	-0.41739	-0.447292	-0.029736	-0.089244	-0.08924							
Fr	6.323027	6.162208	6.231698627	6.2298974	6.035254	5.9473993	6.1233667	5.959342	5.925106							
Qsc	-0.323724	-0.026844	-0.37802089	-0.107407	-0.10761	-0.053774	0	-0.053675	-0.05368							
Ss	-0.196033	-0.016256	-0.22891265	-0.065041	-0.06517	-0.032563	0	-0.032503	-0.03251							
Ssc	-1.798469	-0.149136	-2.100116054	-0.596704	-0.59786	-0.298747	0	-0.298194	-0.29822							
Tcos	-0.00743	-0.002175	-0.008031763	-0.002664	-0.00393	-0.003089	-0.00014	-0.001401	-0.0014							
Te	0	0	0	0	0	0	0	0	0							
Tqsc	-1.09E-05	-9.03E-07	-1.27151E-05	-3.61E-06	-3.6E-06	-1.81E-06	0	-1.81E-06	-1.8E-06							
Tr	-0.000271	-0.000361	-0.000470975	-0.000531	-0.00066	-0.000853	-0.001001	-0.001403	-0.0015							
Tss	-0.000121	-1E-05	-0.000141279	-4.01E-05	-4E-05	-2.01E-05	0	-2.01E-05	-2E-05							
Tssc	0	0	0	0	0	0	0	0	0							
Tvs	-0.00014	-0.00012	-8.01282E-05	-5.01E-05	-0.00014	-0.00015	-1E-05	-3E-05	-3E-05							
Tvsc	-0.00025	-0.000601	-0.000400641	-0.00025	-0.0007	-0.000752	-5E-05	-0.00015	-0.00015							
Vs	-29.78659	-29.80152	-29.77764423	-29.75976	-29.8135	-29.81946	-29.73595	-29.74785	-29.7478							
Vsc	-148.933	-149.0076	-148.8882212	-148.7988	-149.067	-149.0973	-148.6797	-148.7392	-148.739							

Numerical error (derivative x measurement uncertainty) in Earth Scene (Te) for each parameter

	6 GHZ		10		18		23		36 50-60		89		166		183	
Param	Error	Error	Error	Error	Error	Error	Error	Error	Error	Error	Error	Error	Error	Error	Error	Error
Er	-0.017397	-0.017402	-0.017393857	-0.017387	-0.01741	-0.017419	-0.017385	-0.017397	-0.0174							
Ess	-0.017805	-0.001476	-0.020791149	-0.005907	-0.00592	-0.002958	0	-0.002952	-0.00295							
Evs	-0.020851	-0.017881	-0.011911058	-0.00744	-0.02087	-0.022365	-0.001487	-0.004462	-0.00446							
Evsc	-0.014893	-0.035762	-0.023822115	-0.01488	-0.04174	-0.044729	-0.002974	-0.008924	-0.00892							
Fr	0.012646	0.012324	0.012463397	0.0124598	0.012071	0.0059474	0.0061234	0.0119187	0.01185							
Qsc	-0.001619	-0.000134	-0.001890104	-0.000537	-0.00054	-0.000269	0	-0.000268	-0.00027							
Ss	-0.003921	-0.000325	-0.004578253	-0.001301	-0.0013	-0.000651	0	-0.00065	-0.00065							
Ssc	-0.001798	-0.000149	-0.002100116	-0.000597	-0.0006	-0.000299	0	-0.000298	-0.0003							
Tcos	-0.000743	-0.000217	-0.000803176	-0.000266	-0.00039	-0.000309	-1.4E-05	-0.00014	-0.00014							
Te	0	0	0	0	0	0	0	0	0							
Tqsc	-0.000218	-1.81E-05	-0.000254303	-7.23E-05	-7.2E-05	-3.62E-05	0	-3.61E-05	-3.6E-05							
Tr	-0.005412	-0.00722	-0.009419491	-0.010616	-0.01325	-0.017066	-0.020024	-0.028056	-0.030006							
Tss	-0.00242	-0.000201	-0.002825585	-0.000803	-0.0008	-0.000402	0	-0.000401	-0.0004							
Tssc	0	0	0	0	0	0	0	0	0							
Tvs	-0.007013	-0.006014	-0.00400641	-0.002503	-0.00702	-0.007523	-0.0005	-0.001501	-0.0015							
Tvsc	-0.012524	-0.030072	-0.020032051	-0.012513	-0.0351	-0.037613	-0.002501	-0.007505	-0.0075							
Vs	-0.002979	-0.00298	-0.002977764	-0.002976	-0.00298	-0.002982	-0.002974	-0.002975	-0.00297							
Vsc	-0.014893	-0.014901	-0.014888822	-0.01488	-0.01491	-0.01491	-0.014868	-0.014874	-0.01487							

Assume all parameters contributing to error are uncorrelated so that result can be Root Sum Squared

Sum	-0.111839	-0.122429	-0.125230859	-0.080218	-0.15083	-0.163581	-0.056602	-0.078521	-0.0806
Sum(Abs)	0.137131	0.147078	0.150157653	0.1051373	0.174971	0.1754761	0.0688489	0.1023587	0.104299
RSS	0.04393	0.057265	0.048721282	0.0357502	0.065973	0.0695916	0.0314348	0.0403676	0.041769

The RSS values get entered into the calibration budget

An Coefficients using nominal values

	6 GHZ	10	18	23	36	50-60	89	166	183
A1	0.991844	0.996742	0.990945237	0.9964736	0.994549	0.9951564	0.9988002	0.9970028	0.996903
A2	0.000268	0.00036	0.00046671	0.0005289	0.000659	0.0008492	0.001	0.0013986	0.001499
A3	0.000139	0.00012	7.94027E-05	4.987E-05	0.00014	0.0001497	9.99E-06	2.993E-05	2.99E-05
A4	0.001252	0.001079	0.000714624	0.0004489	0.001257	0.0013475	8.991E-05	0.0002694	0.000269
A5	0.000248	0.000599	0.000397013	0.0002494	0.000698	0.0007486	4.995E-05	0.0001496	0.00015
A6	0.000248	0.000599	0.000397013	0.0002494	0.000698	0.0007486	4.995E-05	0.0001496	0.00015
A7	0.0048	0.0004	0.0056	0.0016	0.0016	0.0008	0	0.0008	0.0008
A8	0.00012	1E-05	0.00014	0.00004	0.00004	0.00002	0	0.00002	0.00002
A9	1.08E-05	9E-07	0.0000126	0.0000036	3.6E-06	0.0000018	0	0.0000018	1.8E-06
A10	0.001069	8.91E-05	0.0012474	0.0003564	0.000356	0.0001782	0	0.0001782	0.000178
A11	0	0	0	0	0	0	0	0	0
Sum(An)	1	1	1	1	1	1	1	1	1

Tn		6 GHZ	10	18	23	36	50-60	89	166	183
Te	A1xT1	2.677978	2.691204	2.675552139	2.6904787	2.685282	2.6869223	2.6967605	2.6919077	2.691638
Tr	A2xT2	0.093933	0.125937	0.1633485	0.185129	0.230538	0.2972025	0.35	0.48951	0.524475
Tvs	A3xT3	0.041737	0.035969	0.023820799	0.0149621	0.041888	0.0449168	0.002997	0.0089784	0.008978
Tcos	A4xT4	0.003381	0.002913	0.001929485	0.0012119	0.003393	0.0036383	0.0002428	0.0007273	0.000727
Tvsc	A5xT5	0.07453	0.179845	0.119103995	0.0748103	0.209442	0.2245839	0.014985	0.0448921	0.044888
Tcos	A6xT6	0.000671	0.001619	0.001071936	0.0006733	0.001885	0.0020213	0.0001349	0.000404	0.000404
Tcos	A7xT7	0.01296	0.00108	0.01512	0.00432	0.00432	0.00216	0	0.00216	0.00216
Tss	A8xT8	0.036	0.003	0.042	0.012	0.012	0.006	0	0.006	0.006
Tqsc	A9xT9	0.00324	0.00027	0.00378	0.00108	0.00108	0.00054	0	0.00054	0.00054
Tcos	A10xT10	0.002887	0.000241	0.00336798	0.0009623	0.000962	0.0004811	0	0.0004811	0.000481
Tssc	A11xT11	0	0	0	0	0	0	0	0	0
Ta	Sum(AnTn)	2.947315	3.042078	3.049094834	2.9856276	3.19079	3.2684662	3.0651202	3.2456006	3.28029

Based on sensitivity analysis of errors in T_a as a function of uncertainties in spacecraft & sensor temperatures
 Use a slight approximation to the expression for earth scene component by combining like terms

Let $T_s = (T_{vs} + T_{ss})/2$ [average sensor temperature for all views]

Let $T_{sc} = (T_{vsc} + T_{qsc} + T_{ssc})/3$ [Average spacecraft temperature for all views]

then rewrite T_{cold} as shown below to combine terms

$$T_{cold} = C_{cos} T_{cos} + C_r T_r + C_s T_s + C_{sc} T_{sc}$$

where

$C_r = A_2$	Cold reflector coefficient	T_r	Cold Reflector Temperature
$C_s = A_3 + A_8$	sensor coefficient	T_s	Average Sensor Temperature
$C_{sc} = A_5 + A_9 + A_{11}$	spacecraft coefficient	T_{sc}	Average Spacecraft temperature
$C_{cos} = A_1 + A_4 + A_6 + A_7 + A_{10}$	cosmic background coefficient	T_{cos}	Cosmic Temperature

Note that $(C_r + C_s + C_{sc} + C_{cos})$ should always equal 1

	6 GHZ	10	18	23	36	50-60	89	166	183
C_r	0.000268	0.00036	0.00046671	0.0005289	0.000659	0.0008492	0.001	0.0013986	0.001499
C_s	0.000259	0.00013	0.000219403	8.987E-05	0.00018	0.0001697	9.99E-06	4.993E-05	4.99E-05
C_{sc}	0.000259	0.0006	0.000409613	0.000253	0.000702	0.0007504	4.995E-05	0.0001514	0.000151
C_{cos}	0.999213	0.99891	0.998904274	0.9991282	0.99846	0.9982307	0.9989401	0.9984	0.9983

Check that $(C_r + C_s + C_{sc} + C_{cos}) = 1$

	6 GHZ	10	18	23	36	50-60	89	166	183
T_r	350	350	350	350	350	350	350	350	350
T_s	300	300	300	300	300	300	300	300	300
T_{sc}	300	300	300	300	300	300	300	300	300
T_{cos}	2.7	2.7	2.7	2.7	2.7	2.7	2.7	2.7	2.7
$C_r T_r$	0.093933	0.125937	0.1633485	0.185129	0.230538	0.2972025	0.35	0.48951	0.524475
$C_s T_s$	0.077737	0.038969	0.065820799	0.0269621	0.053888	0.0509168	0.002997	0.0149784	0.014978
$C_{sc} T_{sc}$	0.07777	0.180115	0.122883995	0.0758903	0.210522	0.2251239	0.014985	0.0454321	0.045428
$C_{cos} T_{cos}$	2.697876	2.697057	2.69704154	2.6976462	2.695842	2.6952229	2.6971382	2.6956801	2.69541

Now recover the T_{cold} corresponding to the measured antenna temperature

T_{cold}	2.947315	3.042078	3.049094834	2.9856276	3.19079	3.2684662	3.0651202	3.2456006	3.28029
------------	----------	----------	-------------	-----------	---------	-----------	-----------	-----------	---------

Warm Load Analysis from worksheet “calibration_atbd_warm.xls”

Excel worksheet for calibration_atbd_warm

Note the notation used in this spreadsheet is hot for the warm load

Antenna Temperature Equation for Thot

$$Thot = H1T1 + H2T2 + H3T3 + H4T4 + H5T5 + H6T6$$

Scene(n)	Hn Coefficient Equation	Tn Temperature	Subscene (n) description
1	$F_h * E_h$	$T_k + dT_{kf}$	Hot load emission
2	$F_h * (1 - E_h) * W_i$	T_{si}	Internal sensor emission, reflected by hot load
3	$F_h * (1 - E_h) * (1 - W_i)$	T_{se}	External sensor emission, reflected by hot load
4	$(1 - F_h) * X_s * E_x$	T_{xs}	Spillover emission from sensor
5	$(1 - F_h) * X_s * (1 - E_x)$	T_{cos}	Spillover reflection from sensor
6	$(1 - F_h) * (1 - X_s)$	T_{cos}	Spillover directly from space
Sum	1		

Param	Partial Derivative of Thot w.r.t. parameter
T_k	$E_h * F_h$
dT_{kf}	$E_h * F_h$
F_h	$-T_{cos} + E_h * (dT_{kf} + T_k - T_{se}) + T_{se} + (-1 + E_h) * (T_{se} - T_{si}) * W_i + E_x * (T_{cos} - T_{xs}) * X_s$
E_h	$F_h * (dT_{kf} + T_k + T_{se} * (-1 + W_i) - T_{si} * W_i)$
W_i	$(-1 + E_h) * F_h * (T_{se} - T_{si})$
T_{si}	$-((-1 + E_h) * F_h * W_i)$
T_{se}	$(-1 + E_h) * F_h * (-1 + W_i)$
X_s	$E_x * (-1 + F_h) * (T_{cos} - T_{xs})$
E_x	$(-1 + F_h) * (T_{cos} - T_{xs}) * X_s$
T_{xs}	$-(E_x * (-1 + F_h) * X_s)$
T_{cos}	$(-1 + F_h) * (-1 + E_x * X_s)$

Description of all parameters

Param	
T_k	PRT temp at back of hot load
dT_{kf}	temp diff between front and back
F_h	frac of hot load viewed by feed
E_h	emissivity of hot load
W_i	frac of internal sensor temp reflected by hot load
T_{si}	temp of internal sensor viewed by hot load
T_{se}	temp of external sensor viewed by hot load
X_s	frac of sensor viewed in spillover of feed
E_x	emiss of sensor viewed by feed
T_{xs}	temp of sensor viewed by spillover of feed
T_{cos}	temp of cold space

Nominal Values for all Parameters as a function of channel

	6 GHZ	10	18	23	36	50-60	89	166	183
Param	Nominal	Nominal	Nominal	Nominal	Nominal	Nominal	Nominal	Nominal	Nominal
Tk	300	300	300	300	300	300	300	300	300
dTkf	0.2	0.2	0.2	0.2	0.2	0.2	0.2	0.2	0.2
Fh	0.998	0.995	0.999	0.999	0.999	0.999	0.999	0.999	0.999
Eh	0.999	0.9999	0.9999	0.9999	0.9999	0.9999	0.9999	0.9999	0.9999
Wi	0.5	0.5	0.5	0.5	0.5	0.5	0.5	0.5	0.5
Tsi	275	275	275	275	275	275	275	275	275
Tse	265	265	265	265	265	265	265	265	265
Xs	0.1	0.1	0.1	0.1	0.1	0.1	0.1	0.1	0.1
Exs	0.1	0.1	0.1	0.1	0.1	0.1	0.1	0.1	0.1
Txs	350	350	350	350	350	350	350	350	350
Tcos	2.7	2.7	2.7	2.7	2.7	2.7	2.7	2.7	2.7

Measurement Uncertainty (1 sigma) for all Parameters as a function of channel

	6 GHZ	10	18	23	36	50-60	89	166	183
	delta	delta	delta	delta	delta	delta	delta	delta	delta
uTk	0.1	0.1	0.1	0.1	0.1	0.1	0.1	0.1	0.1
udTkf	0.02	0.02	0.02	0.02	0.02	0.02	0.02	0.02	0.02
uFh	0.0005	0.0005	0.0005	0.0005	0.0005	0.0005	0.0005	0.0005	0.0005
uEh	0.0005	0.0005	0.0005	0.0005	0.0005	0.0005	0.0005	0.0005	0.0005
uWi	0.1	0.1	0.1	0.1	0.1	0.1	0.1	0.1	0.1
uTsi	10	10	10	10	10	10	10	10	10
uTse	20	20	20	20	20	20	20	20	20
uXs	0.05	0.05	0.05	0.05	0.05	0.05	0.05	0.05	0.05
uExs	0.05	0.05	0.05	0.05	0.05	0.05	0.05	0.05	0.05
uTxs	50	50	50	50	50	50	50	50	50
uTc	0.1	0.1	0.1	0.1	0.1	0.1	0.1	0.1	0.1

Numerical values for derivatives of Thot, using nominal values

	6 GHZ	10	18	23	36	50-60	89	166	183
Param	Partial	Partial	Partial	Partial	Partial	Partial	Partial	Partial	Partial
Tk	0.997002	0.994901	0.9989	0.9989	0.9989	0.9989	0.9989	0.9989	0.9989
dTkf	0.997002	0.994901	0.9989	0.9989	0.9989	0.9989	0.9989	0.9989	0.9989
Fh	293.9968	294.024	294.024	294.024	294.024	294.024	294.024	294.024	294.024
Eh	30.1396	30.049	30.1698	30.1698	30.1698	30.1698	30.1698	30.1698	30.1698
Wi	0.00998	0.000995	0.000999	0.000999	0.000999	0.000999	0.000999	0.000999	0.000999
Tsi	0.000499	4.97E-05	4.99E-05	4.99E-05	4.99E-05	4.99E-05	4.99E-05	4.99E-05	4.99E-05
Tse	0.000499	4.97E-05	4.99E-05	4.99E-05	4.99E-05	4.99E-05	4.99E-05	4.99E-05	4.99E-05
Xs	0.06946	0.17365	0.03473	0.03473	0.03473	0.03473	0.03473	0.03473	0.03473
Exs	0.06946	0.17365	0.03473	0.03473	0.03473	0.03473	0.03473	0.03473	0.03473
Txs	0.00002	0.00005	0.00001	0.00001	0.00001	0.00001	0.00001	0.00001	0.00001
Tcos	0.00198	0.00495	0.00099	0.00099	0.00099	0.00099	0.00099	0.00099	0.00099

Numerical error (derivative * measurement uncertainty) in Thot for each parameter

	6 GHZ	10	18	23	36	50-60	89	166	183
Param	Error	Error	Error	Error	Error	Error	Error	Error	Error
Tk	0.0997	0.09949	0.09989	0.09989	0.09989	0.09989	0.09989	0.09989	0.09989
dTkf	0.01994	0.019898	0.019978	0.019978	0.019978	0.019978	0.019978	0.019978	0.019978
Fh	0.146998	0.147012	0.147012	0.147012	0.147012	0.147012	0.147012	0.147012	0.147012
Eh	0.01507	0.015025	0.015085	0.015085	0.015085	0.015085	0.015085	0.015085	0.015085
Wi	0.000998	9.95E-05	9.99E-05	9.99E-05	9.99E-05	9.99E-05	9.99E-05	9.99E-05	9.99E-05
Tsi	0.00499	0.000497	0.000499	0.000499	0.000499	0.000499	0.000499	0.000499	0.000499
Tse	0.00998	0.000995	0.000999	0.000999	0.000999	0.000999	0.000999	0.000999	0.000999
Xs	0.003473	0.008683	0.001737	0.001737	0.001737	0.001737	0.001737	0.001737	0.001737
Exs	0.003473	0.008683	0.001737	0.001737	0.001737	0.001737	0.001737	0.001737	0.001737
Txs	0.001	0.0025	0.0005	0.0005	0.0005	0.0005	0.0005	0.0005	0.0005
Tcos	0.000198	0.000495	9.9E-05	9.9E-05	9.9E-05	9.9E-05	9.9E-05	9.9E-05	9.9E-05
Sum	0.30582	0.303377	0.287635	0.287635	0.287635	0.287635	0.287635	0.287635	0.287635
Sum(Abs)	0.30582	0.303377	0.287635	0.287635	0.287635	0.287635	0.287635	0.287635	0.287635
RSS	0.179789	0.179697	0.179513	0.179513	0.179513	0.179513	0.179513	0.179513	0.179513

The RSS values get entered into the calibration budget

Hn Coefficients using nominal values

	6 GHZ	10	18	23	36	50-60	89	166	183
H1	0.997002	0.994901	0.9989	0.9989	0.9989	0.9989	0.9989	0.9989	0.9989
H2	0.000499	4.97E-05	4.99E-05	4.99E-05	4.99E-05	4.99E-05	4.99E-05	4.99E-05	4.99E-05
H3	0.000499	4.97E-05	4.99E-05	4.99E-05	4.99E-05	4.99E-05	4.99E-05	4.99E-05	4.99E-05
H4	0.00002	0.00005	0.00001	0.00001	0.00001	0.00001	0.00001	0.00001	0.00001
H5	0.00018	0.00045	9E-05	9E-05	9E-05	9E-05	9E-05	9E-05	9E-05
H6	0.0018	0.0045	0.0009	0.0009	0.0009	0.0009	0.0009	0.0009	0.0009
Sum	1	1	1	1	1	1	1	1	1

Tin Eq	6 GHZ	10	18	23	36	50-60	89	166	183
Tk + dTkf H1xT1	299.3	298.6691	299.8698	299.8698	299.8698	299.8698	299.8698	299.8698	299.8698
Tsi H2xT2	0.137225	0.013681	0.013736	0.013736	0.013736	0.013736	0.013736	0.013736	0.013736
Tse H3xT3	0.132235	0.013184	0.013237	0.013237	0.013237	0.013237	0.013237	0.013237	0.013237
Txs H4xT4	0.007	0.0175	0.0035	0.0035	0.0035	0.0035	0.0035	0.0035	0.0035
Tcos H5xT5	0.000486	0.001215	0.000243	0.000243	0.000243	0.000243	0.000243	0.000243	0.000243
Tcos H6xT6	0.00486	0.01215	0.00243	0.00243	0.00243	0.00243	0.00243	0.00243	0.00243
Thot Sum(HnTn)	299.5818	298.7269	299.903	299.903	299.903	299.903	299.903	299.903	299.903

Based on sensitivity anlysis of errors in Twarm as a function of uncertanties in temperatures
Rewrite expression for Twarm by combining similar terms

$$Twarm = Wload (Tpirt + dTpirt) + Wws Tws + Wcos Tcos$$

where

Tws = (Tsi + Tse)/2 , ignore error from Tws not the same as Txs since H4 is very small

Tprt = average PRT temperature on warm load

dTpirt is constant value for front/ back delta temperature

Tcos is cosmic background

Wload = H1	Warm load coefficient	Tprt + dTpri	PRT temperature + front/back d
Wws = (H2+H3+H4)	Sesnor Coefficient	Tws	Temp of sensor seen by warm l
Wcos = (H5+H6)	Cosmic Background Coef	Tcos	Cosmic temperature

	6 GHZ	10	18	23	36	50-60	89	166	183
Wload	0.997002	0.994901	0.9989	0.9989	0.9989	0.9989	0.9989	0.9989	0.9989
Wws	0.001018	0.000149	0.00011	0.00011	0.00011	0.00011	0.00011	0.00011	0.00011
Wcos	0.00198	0.00495	0.00099	0.00099	0.00099	0.00099	0.00099	0.00099	0.00099

Check that Wload + Wws + Wcos = 1

	1	1	1	1	1	1	1	1	1
Tprt + dTpirt	300.2	300.2	300.2	300.2	300.2	300.2	300.2	300.2	300.2
Tws	270	270	270	270	270	270	270	270	270
Tcos	2.7	2.7	2.7	2.7	2.7	2.7	2.7	2.7	2.7

Wload (Tprt + dTpirt)	299.3	298.6691	299.8698	299.8698	299.8698	299.8698	299.8698	299.8698	299.8698
Wws Tws	0.27486	0.040365	0.029673	0.029673	0.029673	0.029673	0.029673	0.029673	0.029673
Wcos Tcos	0.005346	0.013365	0.002673	0.002673	0.002673	0.002673	0.002673	0.002673	0.002673

Now recover the Twarm corresponding to the measured antenna temperature

Twarm	299.5802	298.7229	299.9022	299.9022	299.9022	299.9022	299.9022	299.9022	299.9022
-------	----------	----------	----------	----------	----------	----------	----------	----------	----------

APPENDIX E: SENSOR CONSTANTS FILE

The specific layout of the sensor constant file will be provided in the next phase. This appendix is just a placeholder for general items that must be included. A partial list is also included in the performance specification.

Data	Algorithm / Usage
SCF file version, Antenna Pattern Files version	Version Control
Sensor S/N and Software version	Version Control
Channel Passband Characteristics & NEDT	RTM in EDR processing
Beam Angles in Table 5-2	Geolocation
Constants in Tables 4-3, 4-5, and 4-7	TSR/SDR Correction terms for extraneous energy terms
Thermocouple and PRT constants	TDR/SDR temperature conversion
Sync pulse scan angle	Geo-location
CFOV footprint weights	Computed CFOV from antenna patterns
Cross-Polarization Matrices	SDR cross-polarization algorithm
Timing Information (e.g. τ_T , τ_I)	Geo-location
Bias correction terms	Calibration to RTM
Sensor / spacecraft alignment	Geolocation transformation matrices
Reflector / Sensor Alignment	Geolocation transformation matrices
T_{cos}	Estimate of Cosmic temperature
Channel Flags	Identify channel as not working
Thermistor / thermocouple flags	Identify as not working

APPENDIX F: SAMPLE RESULTS FROM ANTENNA / TIMING ANALYSIS

PDSR Baseline Antenna 14 July 00

81 " Dia, 70 " focal length
FE = 36.6 deg, Hx = 47.48 '

Hom	Antenna Boresight	Freq	feed coord X	feed coord Y	feed coord Z	Radius to Focus	Feed Physical angle to boresight	Beam Position AZ	Beam Position EL	Approximate alpha (using AZ)
1	46.6	6.63	-0.376	-8.411	-1.558	21.000	-22.19	6.05	0.08	8.17
2	46.6	10.70	-2.943	-2.000	0.011	21.000	-6.32	1.41	2.06	1.88
3	46.6	10.70	-2.943	2.000	0.011	21.000	6.32	-1.46	2.06	-1.95
4	46.6	18.70	1.686	-3.993	-0.805	21.000	-9.98	2.82	-1.26	-3.96
6	46.6	18.70	1.639	-1.284	-0.492	21.000	-3.25	0.90	-1.20	-1.26
6	46.6	18.70	1.642	1.284	-0.478	21.000	3.25	-0.90	-1.20	1.26
5	46.6	23.50	1.668	3.830	-0.903	21.000	9.59	-2.77	-1.23	3.89
7	46.6	37.00	-0.515	-3.533	-0.620	21.000	-9.79	2.55	0.32	3.48
8	46.6	37.00	-0.498	3.533	-0.521	21.000	9.78	-2.55	0.32	-3.48
9	46.6	56.90	-0.495	-1.600	-0.217	21.000	-4.46	1.18	0.36	1.60
9	46.6	56.90	-0.495	1.600	-0.217	21.000	4.46	-1.18	0.36	-1.60
10	46.6	89.00	-0.510	0.000	-0.012	21.000	0.00	0.00	0.36	0.00

Hom	Active Scan	Beam turn on	Beam at +X S/C coord	Beam turn off	approx. cold sky position	Feed on under cold sky	Feed nominal under cold sky	Feed off under cold sky	approx. warm load position	Feed on under warm load	Feed nominal under warm load	Feed off under warm load
1	126.8	-71.6	-8.17	55.23	135	155.19	157.19	159.18692	-131	-110.81	-108.81	-106.8131
2	112.6	-58.2	-1.88	54.42	135	139.32	141.32	143.32035	-131	-126.68	-124.68	-122.6797
3	112.6	-54.4	1.95	58.25	135	126.68	128.68	130.67965	-131	-139.32	-137.32	-135.3203
4	145.0	-68.5	3.96	76.46	135	142.98	144.98	146.98248	-131	-123.02	-121.02	-119.0175
6	145.0	-71.2	1.26	73.76	135	136.25	138.25	140.24613	-131	-129.75	-127.75	-125.7539
6	145.0	-73.8	-1.26	71.25	135	129.75	131.75	133.7543	-131	-136.25	-134.25	-132.2457
5	145.0	-76.4	-3.89	68.61	135	123.41	125.41	127.40983	-131	-142.59	-140.59	-138.5902
7	127.0	-67.0	-3.48	60.02	135	142.79	144.79	146.78541	-131	-123.21	-121.21	-119.2146
8	127.0	-60.0	3.48	66.98	135	123.22	125.22	127.22254	-131	-142.78	-140.78	-138.7775
9	132.0	-67.6	-1.60	64.40	135	137.46	139.46	141.46174	-131	-128.54	-126.54	-124.5383
9	132.0	-64.4	1.60	67.60	135	128.54	130.54	132.53826	-131	-137.46	-135.46	-133.4617
10	127.0	-63.5	0.00	63.50	135	133.00	135.00	137	-131	-133.00	-131.00	-129

PDSR Baseline Antenna 14 July 00

Dx=19" Dy=28" Dia, 20" focal length
FE = 29.9 deg, Hx = 12"

Hom	Antenna Boresight	Freq	feed coord X	feed coord Y	feed coord Z	Radius to Focus	Feed Physical angle to boresight	Beam Position AZ	Beam Position EL	Approximate alpha (using AZ)
13	46.6	166	-0.019	-1.300	0.006	21.000	-3.55	-3.10	0.10	4.26
14	46.6	166	-0.018	1.292	0.006	21.000	3.52	3.10	0.10	-4.26
15	46.6	183	-0.058	-0.459	0.018	21.000	-1.26	-1.13	0.17	1.55
17	46.6	183	-0.057	0.455	0.018	21.000	1.24	1.13	0.17	-1.55

Hom	Active Scan	Beam turn on	Beam at +X S/C coord	Beam turn off	approx. cold sky position	Feed on under cold sky	Feed nominal under cold sky	Feed off under cold sky	approx. warm load position	Feed on under warm load	Feed nominal under warm load	Feed off under warm load
13	133.9	108.8	-184.26	-117.31	135	-43.45	-41.45	-39.45	-131	50.55	52.55	54.55
14	133.9	117.3	-175.74	-108.79	135	-50.52	-48.52	-46.52	-131	43.48	45.48	47.48
15	133.9	111.5	178.45	-114.60	135	-45.74	-43.74	-41.74	-131	48.26	50.26	52.26
17	133.9	114.6	181.55	-111.50	135	-48.24	-46.24	-44.24	-131	45.76	47.76	49.76